3-Phenylpyrazino[1,2-*a*]indol-1(2*H*)-ones as dual cholinesterase and amyloid aggregation inhibitors

by

Sarbjeet Singh Gujral

A thesis

presented to the University Of Waterloo

in fulfillment of the

thesis requirement for the degree of

Master of Science

in

Pharmacy

Waterloo, Ontario, Canada, 2017

Author's declaration

I hereby declare that I am the sole author of this thesis. This is a true copy of the thesis, including any required final revisions, as accepted by my examiners.

I understand that my thesis may be made electronically available to the public.

Abstract

The year 2017, marks the 110th anniversary of the discovery of Alzheimer's disease (AD)- a devastating neurodegenerative disease. Regardless of the significant advances made in the past century on the pathology of AD, the current pharmacotherapy options for AD remains woefully low and provide symptomatic relief only. Inhibitors of cholinesterase enzymes such as donepezil (Aricept®), rivastigmine (Exelon®) and galantamine (Razadyne®) which represents the primary class of agents used in the management of AD targets one of the many pathological routes of AD. Our study aims at discovering novel small hybrid molecules based on 3-phenylpyrazino[1,2-*a*]indol-1(2*H*)-one (*PPI*) ring system which can potentially exhibit multiple activities toward various factors involved in AD pathophysiology including (i) the inhibition of cholinesterase enzymes such as acetyl (AChE) and butyrylcholinesterases (BuChE); (ii) preventing the aggregation of the neurotoxic amyloid beta (Aβ) peptide and (iii) antioxidant properties. Initial modeling studies suggested that the tricyclic *PPI* template fits in the catalytic site of AChE and the C3 phenyl can orient toward the peripheral anionic subsite (PAS) in the AChE enzyme. In addition, C3-position provides opportunities to incorporate Aβ binding pharmacophores.

With this goal, we synthesized the *PPI* compound library by coupling ethyl indole-2-carboxylates esters with 2-bromoacetophenones to obtain ethyl-1-(2-oxo-2-phenylethyl)-1*H*-indole-2-carboxylates which underwent an intramolecular cyclization in the presence of ammonium acetate to afford *PPI* derivatives (**5a-n**). The compounds were characterized by analytical methods including NMR and LCMS. The cholinesterase inhibition was evaluated using Ellman's protocol by UV-Vis spectroscopy. The anti-Aβ-aggregation property was evaluated by fluorescence spectroscopy using thioflavin- T (ThT) assays. Antioxidant activity of the *PPI* derivatives was

assessed using DPPH assay method. Transmission electron microscopic imaging (TEM imaging) were also performed to support the in vitro data obtained from ThT based fluorescence assays. The Discovery Studio (DS) software, Structure-Based-Design program (4.0) from BIOVIA Inc. was used to determine the binding interactions of the *PPI* derivatives for SAR optimization.

Our results indicate that several compounds in the series exhibit dual cholinesterase inhibition properties; one such compound is **5h** (3-(2-methoxyphenyl)pyrazino[1,2-*a*]indol-1(2*H*)-one) with IC_{50} AChE = 7.3 μM , IC_{50} BuChE = 1.9 μM. Compound **5h** was found to be much more potent than reference agents donepezil and rivastigmine toward BuChE inhibition. Several other compounds such as **5d** (3-(3,4-dimethoxyphenyl)pyrazino[1,2-*a*]indol-1(2*H*)-one) and **5h** (- 3-(2-methoxyphenyl)pyrazino[1,2-*a*]indol-1(2*H*)-one exhibited excellent of $A\beta_{40/42}$ inhibition (% inhibition of $A\beta_{40}$ = 83.3% and 67.7% at 25 μM respectively, and % inhibition of $A\beta_{42}$ = 90% and 94% at 25 μM respectively). Compound **5d** and **5h** were found to be more potent than curcumin and resveratrol towards $A\beta_{42}$ inhibition. The *PPI* derivatives were also found to exhibit antioxidant activities. Unsubstituted *PPI* compound **5a** exhibited good antioxidant activity (~33% DPPH radical scavenging at 50 μM), while, compound **5k** (3-(4-hydroxy-3-methoxyphenyl)pyrazino[1,2-*a*]indol-1(2*H*)-one) exhibited excellent antioxidant activity (~ 84% DPPH radical scavenging at 50 μM). This proves the multi-targeted activities of *PPI* derivatives.

Our results indicate that the fused tricyclic phenylpyrazino[1,2-*a*]indo-1(2*H*)-ones (*PPI*) represent a novel class of compounds which can be modified chemically to design and develop multi-targeting agents aimed at the cholinergic, amyloid cascade and oxidative stress hypothesis of AD.

Acknowledgements

I would like to thank the all the members of the School of Pharmacy, the University of Waterloo for providing me the opportunity to be a part of this great institution and the financial support needed to complete the presented work. Special thanks to Dr. Praveen Nekkar Rao to believe in me and accepted me as one of his international graduate students. I would not have found a better supervisor than you, Sir. You are simply the best!

Also, the support, comments, concerns and encouragement by Dr. Gary Dmitrienko and Dr. Michael Beazley is highly appreciated. A special note of thanks for Jan Vann for the support provided on NMR data acquisition.

I would also like to thank the staff of the School Pharmacy especially, Dr. Shawn Wettig, Sarah Rae, Penny Pudifin, and Gail Bender for their support and suggestions not just professionally, but personally as well.

The guidance and friendship provided by all my fellow current/ ex-graduate students will always be remembered. A special vote of thanks goes to Dr. Tarek Mohamed, Dr. Aula Al-muslim, Arash Shakari, Nyasha Gondora and Amy Pham for helping me in my project in some way or the other throughout my time as a master's candidate at the school of Pharmacy.

Lastly, my parents, Mr. Narinder Singh Gujral and Mrs. Surinder Kaur Gujral, for supporting me throughout my life. I would not have been here without your constant support, guidance, and believing in me.

Dedication

This thesis is dedicated to Waheguru- The Almighty, my parents, Dr. Nekkar and all the loved once- friends and family.

Table of Contents

List of Figures

List of Tables

List of Schemes

List of abbreviations

Aβ = Amyloid-β

ACh = Acetylcholine

AChE= Acetylcholinesterase

AChEI = Acetylcholinesterase inhibitor

AICD = APP intracellular domain

AcOH= Acetic acid

ATCh= Acetylthiocholine

AD = Alzheimer's disease

ADAM = A disintegrin and metalloprotrease

Apo ε4 = Apolpoprotein ε4

APP = Amyloid precursor protein

BACE = Beta-site APP cleaving enzyme

BBB = Blood brain barrier

BuCh = Butyrylcholinesterase

BuChEI = Butyrylcholinesterase inhibitor

BuOH = Butanol

CADD = Computer aided drug design

CAS= cationic active site

ChAT = Choline acetyltransferase

ChE = Cholinesterase

ChEI = Cholinesterase inhibitor

ClogP = Partition coefficient; Calculated empirically via “group contribution” method

CT = Catalytic triad

DCM = Dichloromethane

DMSO = Dimethylsulfoxide

DPPH = 2,2-Diphenyl-1-picrylhydrazyl radical

DTNB = Dithiobis-(2-nitrobenzoic acid)

EtOAc = Ethyl acetate

EtOH = Ethanol

HPLC = High performance liquid chromatography

IC_{50} = Concentration required for 50% inhibition of activity of an enzyme/ protein.

LCMS = Liquid chromatography mass spectroscopy

MeOH = Methanol

$MgSO_4$ = Magnesium sulphate

MV = Molecular volume

NDD = Neurodegenerative disorder

NTB = 2-Nitro-5-thiobenzoic acid

PAS= Peripheral anionic site

PV = Pressure vial

PPI- 3-Phenylpyrazino[1,2-*a*]indol-1(2*H*)-one

r.t. = Room temperature

$sAPP_{\alpha/\beta}$ = Soluble APP fragments of α/β

ThT = Thioflavin T

TLC = Thin layer chromatography

Chapter 1. Introduction

1.1 Dementia

"Dementia" as a medical term is in use to describe the overall decline in the mental, behavioral and task completion activities of an individual. Patients with dementia find it tough to perform everyday activities such as making meals, traveling, to name a few. Moreover, a sharp decline in the behavior of a person along with impairments associated with speech, memory, recognition of the language, ability of a person to judge the situation wisely, can be observed easily.[1] Dementia can be caused by various associated diseases such as Alzheimer's disease (AD), vascular dementia, dementia with Lewy bodies, mixed dementia, frontotemporal lobar degeneration, Parkinson's disease, Jacobs's disease and Normal pressure hydrocephalus.[2]

According to a recent survey for 2016, in Canada, there are about 564,000 Canadians who are suffering from dementia. These numbers have been estimated to elevate to 937,000 by the year 2030.[3] An evaluation of the statistics reveals that the Canadian government spends about CDN$ 10.4 billion each year to take care of the patients suffering from various forms of dementia[3]

Medically to determine if a patient has dementia, physicians usually refers to a manual known as *Diagnostic and Statistical Manual of mental disorder (DSM)*. According to DSM, dementia is categorized as a prime *Neurogenerative Disorder* (NDD) as it impairs the cognitive functions as well as performing everyday activities of the patient.[4] Assessing whether a patient has dementia is a lengthy and expensive process and usually, involves two different approaches for assessment of the dementia prevalence. The first one being the early process of evaluation which includes questionnaires based on family history of dementia, change in behavior, mental state examinations to name a few.[5] Neuropathological lab testing- autopsy, being the another confirmatory and classifying test which is used to distinguish between the various types of dementias.[6] Proper evaluation of a patient who has dementia is critical as for each type of dementia, a different kind of treatment is used. In many cases, a patient can be misdiagnosed for dementia for having dementia type symptoms. Misdiagnosis is very common in patients suffering from depression, delirium, thyroid problem, and alcohol toxicity[2] as the symptoms mimic dementia. In a national survey, it has been estimated that misdiagnosis of dementia (Alzheimer's disease in particular) can be as high as 67.1% with 18.2% of the misdiagnosed patients receiving inappropriate medications.[6] Hence, in brief, we can say that dementia is a multifaceted neurodegenerative disorder which causes adverse effects on memory, emotions and daily activity.

1.2 Neurodegenerative Disorder (NDD)

Neurodegenerative disorder (NDD) is the pathological condition of the brain in which there is an extensive dysfunction of the nervous system, leading to the death of the neuronal cells.[7,8] The reason for such a catastrophic destruction of the neurons can be:

- sporadic- may be due to infection.
- Stroke – e.g. vascular dementia.

- Protein misfolding and aggregation- the induced defect in the structure and function of the neurons caused by misfolded and aggregated proteins leading the cells to disrupt and rupture.

The misfolding, accumulation and aggregation of certain detached surface proteins, such as amyloid beta(Aβ) protein and tau protein in Alzheimer's disease; alpha-synuclein in dementia with Lewy bodies and Parkinson's disease and so forth, are the examples of misfolded and aggregated proteins causing neurodegeneration. These proteins, which under normal conditions, are present as an integral part of the neurons and whose detachment and aggregation causes the cells to undergo neuronal death accelerates the progression of NDD.[9] More discussion of the individual proteins (amyloid beta and tau protein) and how these proteins cause progression of neurodegeneration in presented in appropriate segments of this thesis.

1.3 Alzheimer's disease (AD)

Alzheimer's disease is considered to be the most prevalent form of NDD and accounts for about 80% of all the registered cases associated with NDD and the leading cause of death associating dementia.[2] AD was first identified in 1907 by Alois Alzheimer, a German neurologist, and psychiatrist.[10] Even after around 110 years of its discovery, little is known about AD's inception[2] even though, there have been many theories which explain the progression of the disease. We will be discussing the individual theories in appropriate sections in this thesis.

1.3.1 Detection of AD: According to the DSM criteria, the changes in the brain morphology of the patient suffering from AD initiates much before the actual symptoms start to appear. Hence, it is believed that to prevent, slow or stop the disease, early detection is crucial[4] which till now is not possible to detect. Currently, for the detection of AD, no single and straightforward test is

available. Usually, a doctor along with a neurologist assess the patient using a variety of tools to help make a diagnosis. Tools which are often utilized for the determination are as follows:

- Evaluate the family history of the patient for AD.
- Psychiatric history and behavioral changes estimation.
- Evaluation of mental state by conducting cognitive and behavioral tests.
- Laboratory tests: by performing blood tests and brain imaging.

Even after using an array of diagnosis, it will take lots of time before a physician can make any diagnosis.[2]

1.3.2 Diagnosis: Early symptoms of AD varies among individuals, though, difficult to remember newer information being the most common among the patients. This is because the neuronal and synapses loss starts in the cerebral cortex and subcortical regions of the brain, which is associated with processing newer information.[11,12] Other initial symptoms of AD are as follows:

- Confusion with the place, time and face recognition.
- Understanding in language recognition.
- Mood swings and initiation of split personality behavior.
- The decline in situation judgment.
- Elevation in anxiety and agitation.
- Poor control over sleep.

1.3.3 Changes in brain morphology: A healthy brain of an adult contains approx. 100 billion neurons connected to each other by more than 100 trillion synapses. This secure interconnection between the neurons helps the brain to function properly by allowing the neurotransmitters to pass through the neurons efficiently. In the case of AD, due to the progression of neuronal death, a

decline in the mental ability occurs which can be compiled by the individual effects of Aβ accumulation, reduction in the levels of neurotransmitters in the brain, generation of neurofibrillary tangles (NFTs) by dead neurons, and a decrease in the number of synapses (Fig. 1-1). The overall effect of neuronal death causes an average decline of brain volume by 5.3% (decline in gray matter volume only) over a period of at least one year.[13]

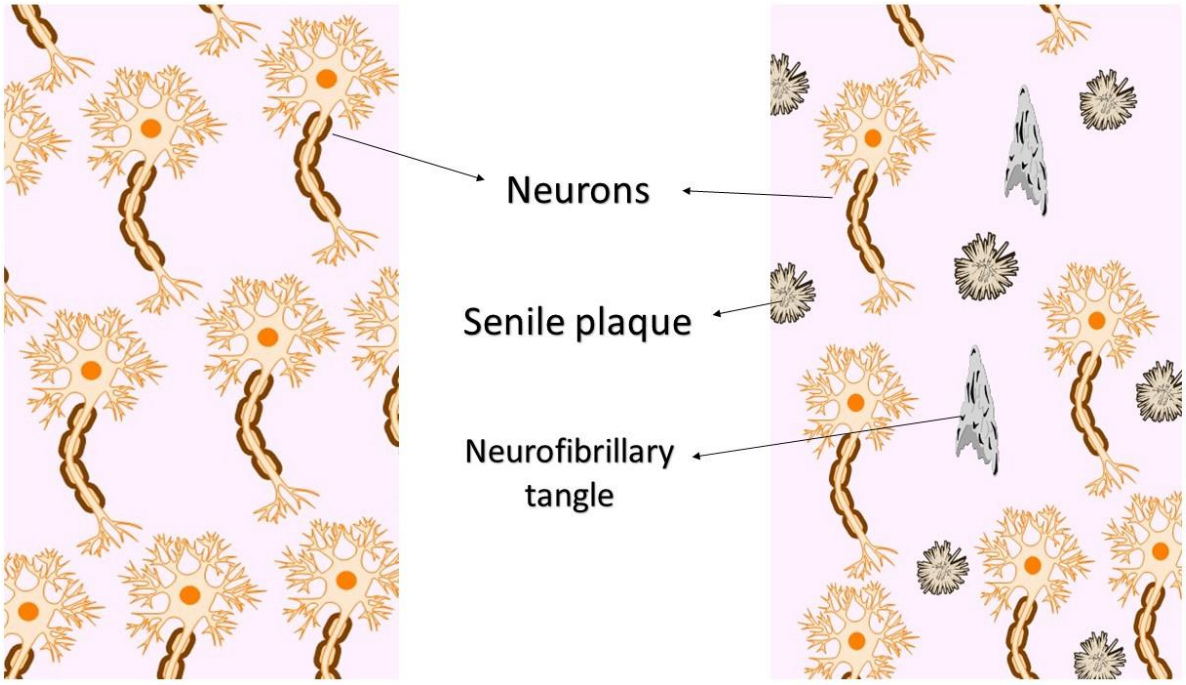

Figure 1-1: Comparison between the microscopy of (a) healthy brain (b) Brain of an AD patient- one can see the accumulation of Aβ plaques and NFTs.

1.4 Initiation of AD

Although AD has been categorized as an age-dependent progressing disorder, genetic abnormalities have found to play a significant role in determining the susceptibility of a patient to develop AD. Based on these observations, AD can be categorized into

- Sporadic AD – This type of AD progression is the most common form of AD and accounts for almost 99% of the cases. The progression of the disease state is dependent on various physical and environment factors.
- Familial AD – AD progression is based on the genetic factors such as down syndrome, genetic mutations, etc.

1.4.1 Familial AD: Alzheimer's disease progression due to genetic variations

It has been estimated that less than 1% of all the cases of AD are linked to genetic changes, causing the progression of AD.[2] Three specific genes have been linked with AD progression. Any abnormal mutations in the genes linked to Amyloid precursor protein (APP), presenilin-1 and presenilin-2, increase the risk of development of AD by 90-95%. It has been observed that patients with such mutations tend to develop the disease at an early age, which can be as early as 30 years.[2]

Down syndrome (DS): This syndrome is caused by the presence of an additional copy of chromosome no. 21 in the genome of a person. Individuals with DS has been reported to have higher chances of developing AD-like pathophysiologies at an early age of around 40 years. Statistically, more than 75% of the people with DS suffer from AD. A clear link has yet to be identified but, researchers assume that the presence of an additional copy of chromosome 21, which also is the locus of the gene encoding for APP, could double the hydrolysis of APP and thus, elevates the risk for developing AD.[2]

1.4.2 Sporadic factors leading to AD:

Chronic type initiation of AD is considered to be the most common form of AD among patients, and experts believe that this can be due to the combined effect of various related/ interrelated effects. Sporadic effects can be divided into two different categories:

- Controllable factors
    - Cardiovascular disease risk factors
    - Education
    - Social and cognitive engagement
    - Traumatic brain injury
- Uncontrollable factors
    - Age
    - Family history
    - Activation of APOε4 gene

1.4.2.1 Controllable Factors: Controllable factors, as the name suggests, can slow down the progression of AD. As we know that AD is an age-dependent disease; aging cannot be stopped. Thus, it would be much easier to control the health-related factors such as diabetes, obesity, cardiovascular diseases, etc. to delay the onset of AD. A recent study aimed to find a link between physical activity and cognition/dementia. Not much of a surprise, it was observed that regular physical activity not only helped manage the cardiovascular risk factors such as hypertension, obesity, diabetes and smoking, it also significantly contributes to reducing the risk of cognitive decline and dementia[2].

Having an active social life have also been linked to a healthy brain function. Isolation of an individual not only hinders personal growth, but it can also affect one's brain in a negative way. Such people are at higher risk of developing dementia. The exact mechanism and a scientifically valid reason are yet to be explained. Similarly, education level of an individual has been proportionally linked to the modified risk of dementia. According to the *cognitive reserve hypothesis*, continuous stimulation of the brain through reading and logical thinking- tasks

involved in formal education, can compensate for the modifications caused by AD and can trick the neurons in making alternate routes for interneuronal communication required for cognitive functions. This can lead to a decline in the symptoms of AD as the aging progesses.[2]

Uncontrollable factors: Uncontrollable factors such as age, family history, and apolipoprotein E-ε4 (APOE4) gene activation are some of the uncontrollable factors which possess the greatest risk factor for the delayed onset of the AD in more than 95% of the reported cases.

Age: Even though aging is one of the most significant risk factors for the development of AD, it is not the standalone for causing the disease. Also, AD is not a common outcome of aging as well. People with sporadic AD lie in the age bracket of 65 and older, and as the age increases, so are the chances of developing AD. That is why AD is considered as an age-dependent disease.[2]

Family history: It has been observed that first degree relatives with similar heredity conditions, similar and shared environmental and lifestyle conditions and whose at least one family member is suffering from AD have higher chances of developing AD in the later stages of their life. The family history may or may not be linked to the activation of the APOE4 gene as explained by some researchers.[2]

Inheritance of APOE4 gene: The APOE4 gene, is located on chromosome 19 and is responsible for the production of cholesterol transportation protein APOE. Isoforms of APOE gene are known to regulate Aβ aggregation and clearance in the parenchyma of the brain. APOE genes are also known to play a role in the regulation of glucose metabolism, lipid transportation in and out of the brain, mitochondrial function, neuron signaling and neuroinflammation.[14] Three very common forms of APOE genes are ε2, ε3, and ε4 are known and one of them is inherited to the offspring by each of the parents. The genetic abundance of each gene is in the order ε3, ε4, and ε2 and forms

six possible APOE forms which are ε2/ ε2, ε2/ ε3, ε2/ ε4, ε3/ ε3, ε3/ ε4, ε4/ ε4. Out of all the possible APOE forms, people who inherit ε4/ ε4 allele are at 8 to 12 fold higher risk than the one with ε3/ ε3 gene and are more prone to develop AD at early stages of life. While it is noticed that people with ε2/ ε2 gene have reduced the risk of developing AD at later stages of life as compared to people with ε3/ ε3 gene. Though these speculations are just observation and no precise mechanism between APOE genes and AD risk is not clear.[2]

1.5 Biomarkers for AD detection

As the number of patients suffering from AD is increasing every passing day, and due to the non-availability of any preventive and curing regime, it is important to delay the progression of the disease as soon as the condition is detected. As, the symptoms of AD starts at a very late age, sometimes as late as when more than 40% neurons have already been degraded, it is important to get a hold on to the disease as early as possible. To do so, biomarker detection for AD at early stages can be an excellent option to hinder the progression of the disease.[15,16]

Biomarkers, as we know, when present in a concentration higher than the standard concentration can be associated with the disease. Diagnosis of such biomarkers helps in monitoring and progression of the illness. For a particular condition, there are specific biomarkers which have been recognized, detected and biochemically evaluated.[17] Similarly, for AD, various imaging techniques- used for direct visualization of brain function, and peptide biomarkers- present in plasma, cerebrospinal fluid (CSF) and urine, can help in evaluating the disease progression.[15,18]

Currently, there are three classes of biomarker detection methods which are available (imaging techniques), and some are still under development (biochemical peptide detection) which can be categorized as follows (Fig. 1-2):

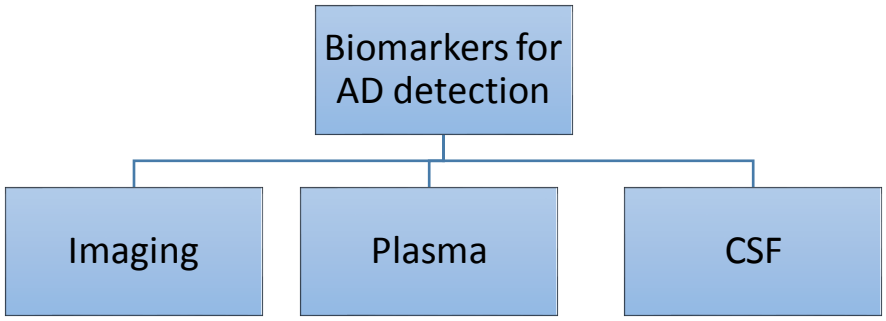

Figure 1-2*:*Classification of biomarkers used in AD detection.

1.5.1 Imaging: Imaging techniques such as CT scan, PET scan, PIB-PET scan and MRI scan can help in estimating changes in the morphology of any region of the brain .[18] A simple visual comparison between CT/ PET scan of an AD patient with a healthy brain scan can be used in evaluating the stage of AD.[19]

Biochemical estimation of a particular peptide or a specific factor (a specific type of peptides) can also be used in evaluating the AD progression. For such assessment, plasma and CSF are used, and via series of biological laboratory tests, the concentration of such biomarkers can be estimated which can be correlated with the imaging biomarkers to make a concrete decision about the stage of the disease, and also to determine the type of dementia, the patient is suffering. E.g. one can clearly distinguish between a patient suffering from AD and Parkinson disease by comparing the imaging and clinical examination.[15,19,20]

1.5.2 Plasma: Biomarkers present in plasma which is specific for AD are α-macroglobulin, component factor H, α_1-antitrypsin, α_1-antichymotrypsin and Aβ species. Even though the estimation of such biomarkers can be performed relatively quickly, the success of such estimates

has limited value as various laboratories use different techniques for determining such markers and thus, lacks specificity, sensitivity, and reproducibility. The Aβ species present in blood plasma can readily be determined using ELISA, and clinical correlation of such data cannot be made to an actual disease state as Aβ in plasma is derived from peripheral tissues which are not correlated with brain Aβ load and no assessment can be done with brain Aβ production.[15,18]

1.5.3 CSF biomarkers: CSF or cerebrospinal fluid is a semi-viscous fluid which is present in the subarachnoid space and ventricular system and acts as a cushion against mechanical injuries to the brain. Because of the direct contact of the CSF to the brain, the presence of any proteins in CSF could be directly related to the brain activity and can thus CSF could be expected to serve as an excellent source of biomarkers for AD.[15] However, in various studies performed by different groups, it was observed that levels of $A\beta_{42}$ change according to the type of protocol used for assay. In most of the reports, a slight decrease in the levels of $A\beta_{42}$ has been observed, and this can be explained by the accumulation of $A\beta_{42}$ to form plaques (known as amyloid sinks)[18], and thus, a decline in the $A\beta_{42}$ concentration in the CSF can be seen. This observation was further supported by an increase in the plaque burden as observed by positron emission tomography (PET) imaging. In the case of $A\beta_{40}$, no such change in the concentration was observed. It has also been noticed that a decrease in the ratio of $A\beta_{42}$/ $A\beta_{40}$ could be more statistically relevant observation than studying the reduction of $A\beta_{42}$ alone. Thus, to conclude, we can say that biomarkers can become a source of early detection of AD progression and the methods are yet to be standardized so as to provide a reliable and reproducible data which can be clinically correlated with AD.[15]

1.6 Currently available treatment for AD

In the present scenario, AD treatment is challenging as currently approved medications only provide symptomatic relief to the patients[9]. None of the drugs can prevent the neuronal destruction

in the brain[2] or cure AD. Presently, there are only four FDA-approved drugs which can be used in the management of AD[2], and those are (Fig. 1.3):

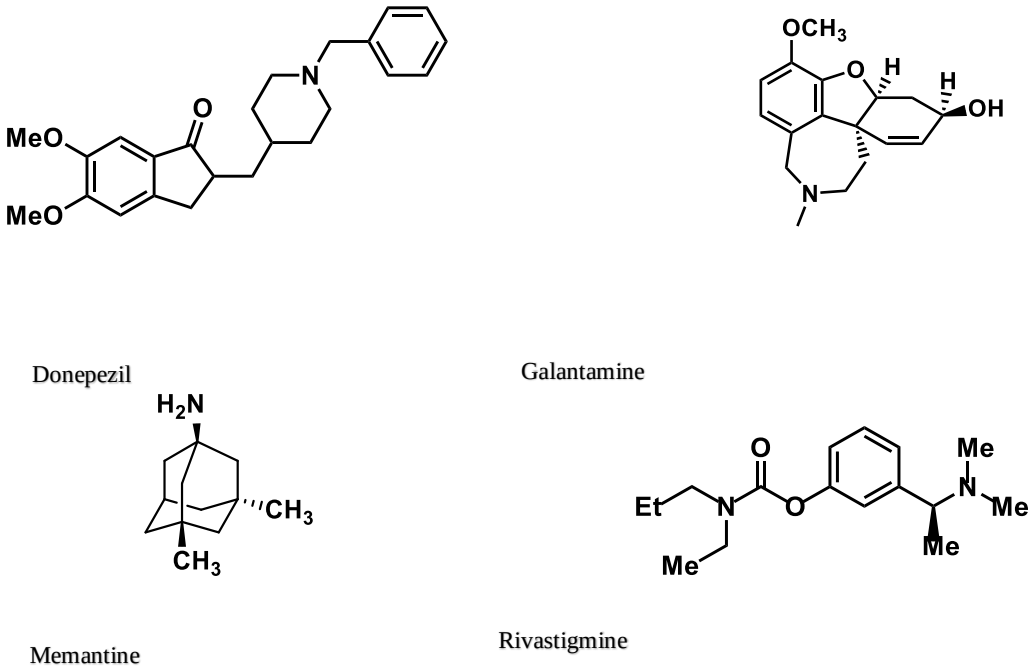

Figure 1-3*:* Molecular structures of (a) Donepezil (b) Galantamine (c) Memantine (d) Rivastigmine.

All the medications mentioned above, except for memantine, targets cholinesterase enzymes; acetylcholinesterase (AChE) and butyrylcholinesterase (BuChE) and provide symptomatic relief to the patients by maintaining the levels of a neurotransmitter known as acetylcholine (ACh) in the brain. These medications are either used alone or in combination with other drugs to provide symptomatic relief to the patients.[2,9] Some of the treatments currently in use for AD patients are as follows:

1.6.1 Monotherapy by AChE and BuChE inhibitors: Monotherapy by one of the approved FDA drugs such as donepezil, galantamine, and rivastigmine are usually used in the management of mild to moderate AD. These agents are known to inhibit both AChE and BuChE activity in a dose-

dependent manner.[21] Initiation of treatment with cholinesterase inhibitors (ChE) inhibitors at early stages of AD with drugs such as Aricept® also known as donepezil or Razadyne® also known as galantamine prevents rapid onset of symptoms associated with AD. Donepezil, a potent benzylpiperidine compound, exhibits high selectivity towards AChE with its IC_{50} value for AChE ~9 nM while for BuChE the IC_{50} value is ~1000 nM. Galantamine, on the other hand, is an alkaloid which was first isolated from flowers and bulbs of plant known as *Galanthus*. Similar to donepezil, galantamine also exhibits selectivity towards AChE with an IC_{50} value of ~0.2 μM. Galantamine is 50-times more selective for AChE compared to BuChE. The in vivo half-life ($t_{1/2}$) for both donepezil and galantamine are 70 h and ~ 6 h respectively. As half-life for donepezil is around three days, this gives an edge over galantamine by reducing the dose frequency and thus, fewer side effects and hence, is used in all stages of AD, while, Galantamine is used in mild to moderate AD because of higher dosing frequencies.[9]

1.6.2 NMDA receptor antagonists: N-methyl-D-aspartate receptors (NMDA) can be categorized as ionotropic glutamate receptors and are ligand-gated ion channels present on the surface of neurons. Overexcitation of these receptors is known to have calcium ion induced toxic effects which lead to the death of the neuron.[22] Normal activation of NMDA receptors is essential for maintaining the proper activity of the brain. However, overactivation of NMDA receptors, as observed in AD, is associated with excess intake of Ca^{2+} ions in the intracellular region. This overburden of calcium ions triggers a cascade of downstream events which results in neurodegeneration. NMDA receptor antagonists such as memantine have been reported to be useful in the treatment of AD.[23,24]

1.6.3 Combination therapy: Namzaric®, which contains a mixture of donepezil HCl (10 mg) and memantine HCl (28 mg) is an approved FDA treatment for moderate to severe AD.

Unfortunately, this is the only combination therapy available for AD management. [2,25] The superiority of this type of therapy was supported by a randomized, double-blind placebo-controlled study which took over a period of 24 weeks. This clinical study concluded that an added advantage is achieved over single drug administration of either donepezil or memantine. A definite improvement in cognition and behavioral aspects of the patients was observed when donepezil and memantine were given as a combination therapy as compared to patients receiving donepezil or memantine alone.[26]

1.7 AD hypothesis

AD initiation and progression has been explained by various hypotheses.[9,27] Among these, the cholinergic hypothesis is the earliest known theory which was put forward in mid-1970's.[28] Amyloid beta (Aβ) hypothesis, was presented in 1991[29]; Tau hypothesis and mitochondrial dysfunction are among others.[27,30] Because all these theories help to explain the different pathological observations in AD, these hypotheses are considered as a primary hypothesis for AD. For example, the cholinergic hypothesis helps account for the role of acetylcholine (ACh); one of the neurotransmitters in the brain in learning and memory.The deficits of ACh (frequent observations in AD patients) is responsible for memory loss in AD patients[28] while the Aβ hypothesis explains the accumulation of senile plaques in both extracellular as well as intracellular regions of the brain. [31] Tau hypothesis, on the other hand, explains the presence of neurofibrillary tangles (NFT's) in intracellular regions of the brain.[30] There are other theories which have been put forward and helps account for the correlation of pathological observations as secondary hypotheses. The examples of secondary hypotheses are oxidative stress, inflammation, cholesterol hypothesis and Aβ pore formation (Fig. 1-4). Relationship between Primary and secondary hypothesis can be explained by the following example: Formation of NFT's (primary hypothesis)

can be described by caspase-mediated cell death which can be initiated by oxidative stress (secondary hypothesis).

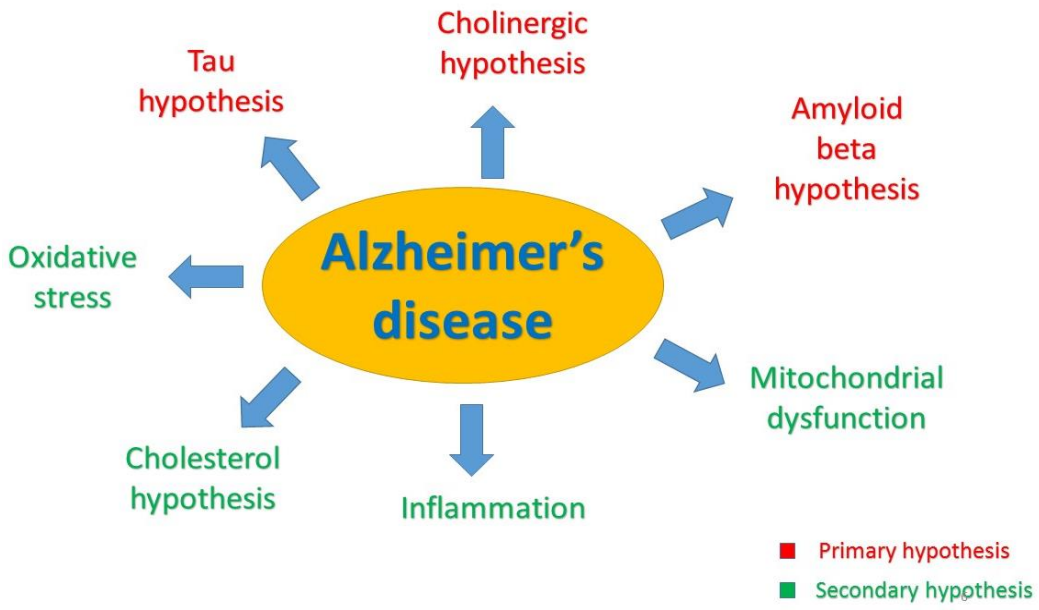

Figure 1-4: Various hypotheses for AD. Hypothesis marked in red (viz. cholinergic, tau, amyloid beta and oxidative stress) are considered as a primary hypothesis for AD. While, hypotheses given in green (viz. mitochondrial dysfunction, inflammation, cholesterol hypothesis and amyloid beta pore formation hypothesis) are considered as a secondary hypothesis.

1.8 Cholinergic Hypothesis

As stated earlier, the cholinergic hypothesis is one of the earliest known hypotheses put forward for AD which correlates the function of ACh- a neurotransmitter, in learning and memory.[28] According to this hypothesis, cholinergic neuron degeneration in the forebrain, cerebral cortex and other associated areas of the brain results in loss of cholinergic neurotransmission and thus, significantly contributes to the loss of ACh-dependent cognitive function as observed in AD patients.[28] Thus, in other words, decreased levels of ACh can be found which is related to the

cholinergic neuron degeneration. To make the situation worse, two ACh hydrolyzing enzymes AChE) and BuChE further reduces the level of ACh.[32,33] Under normal conditions, AChE, which is present on the post-synaptic membranes in the neuromuscular junctions, helps in terminating the excess signal transmission by hydrolyzing ACh and thus preventing overexcitement of the postsynaptic neurons. In the case of cholinergic neuronal degeneration, the ACh levels are already marginalized, and further hydrolysis of ACh by AChE significantly reduces the ACh levels which compromise the cognitive functions. To eliminate this situation, various small molecules have been developed which acts as cholinesterase inhibitors which bind to these enzymes and thus prevent the hydrolysis of ACh.[9,28,33,34] These small molecules are known as cholinesterase inhibitors (ChEIs) and form the first and the only line of therapy currently available for AD management.[35] E.g. of cholinesterase inhibitors approved by FDA for AD management are donepezil (Aricept®), (*S*)-rivastigmine (Exelon®) and galantamine (Razadyne®).[9]

1.8.1 Cholinergic neurotransmission

Neurotransmission in cholinergic neurons depends on ACh as a neurotransmitter to initiate and transmit signals between cholinergic neurons. ACh is synthesized in the cholinergic nerve endings from acetyl CoA and choline using choline acetyltransferase (ChAT) as the catalytic enzyme. Upon synthesis, ACh gets stored in vesicles. Vascular ACh transporter (VAChT) is the carrier responsible for entry of ACh into the storage vesicles. Such transportation is facilitated by ATPase and H^+ gets countertransport (outside the vesicles) keeping the iso-osmotic and electroneutrality intact. ACh remains stored within the vesicles till there is no action potential generated by the neurons. Once a neuron gets excited (action potential is generated), neuronal membrane depolarization takes places by the influx of Ca^{2+} ions through calcium channels. The elevated levels of Ca^{2+} inside the cytosol help in the infusion of vesicles with vesicle-associated membrane

proteins (VAMPs). The fusion of vesicles to the VAMP's result in the release of ACh by the process of exocytosis.[36] When ACh enters the synaptic cleft, it can trigger action potential on the postsynaptic neuron by interacting with nAChR (nicotinic Acetylcholine receptors) or mAChR (Muscarinic Acetylcholine receptors). The nAChR's are associated with the Peripheral Nervous system (PNS), Central Nervous system (CNS) and neuromuscular junctions (NMJs). While mAChR's are specifically for PNS but are also present throughout the body (Fig. 1-5).[36]

ACh which was not being able to generate an action potential gets hydrolysed by AChE enzymes to choline and acetate. The choline released by the hydrolysis of ACh gets recycled and enters the neuron using Na^+- choline co-transporter.[36]

Various studies indicated that in AD, substantial deficits in ChAT levels (the enzyme responsible for the synthesis of ACh). The choline reuptake and ACh release get hindered. The combined effects of which results in a presynaptic cholinergic deficit,[28] thus marginalizing the levels of ACh in the nervous system. The decrease in the levels of ACh results in learning and memory impairments which give rise to the first hypothesis of AD: The cholinergic hypothesis.

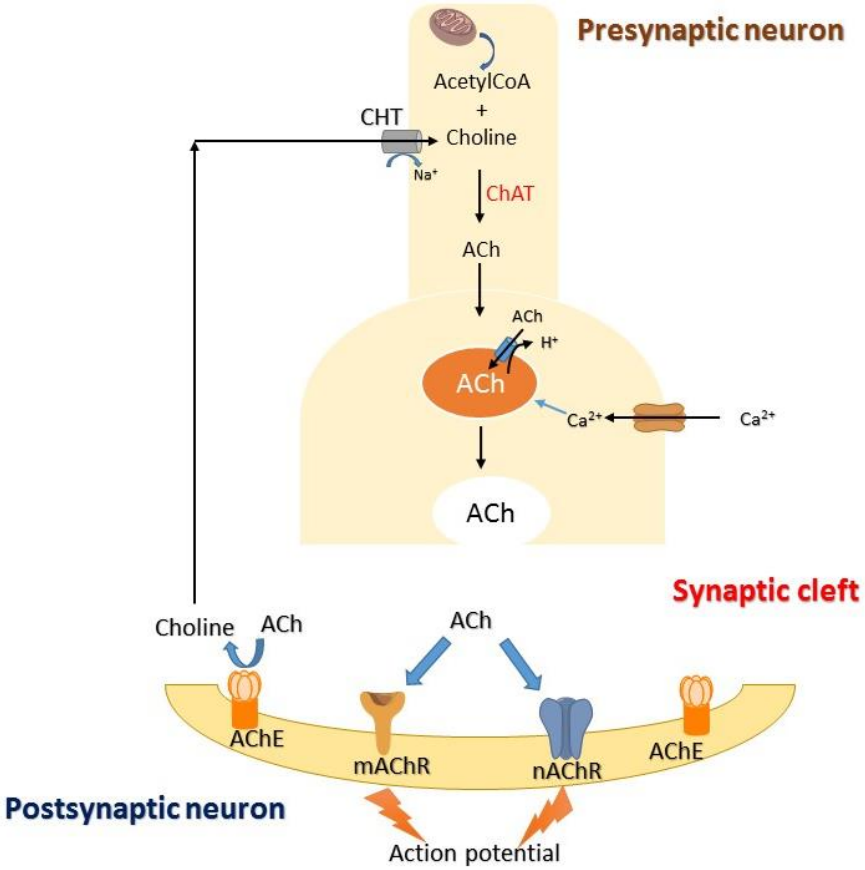

Figure 1-5*:* Synthesis, storage, and release of ACh in a neuron

1.8.2 AChE

The AChE enzyme (Fig.1-6) (EC 3.1.1.7) can be categorized as a serine hydrolase. This enzyme is found both in the CNS and PNS as an ACh hydrolyzing enzyme [34,37] AChE is fully capable of working efficiently as a monomer; other isoforms of the enzyme are also known to be present

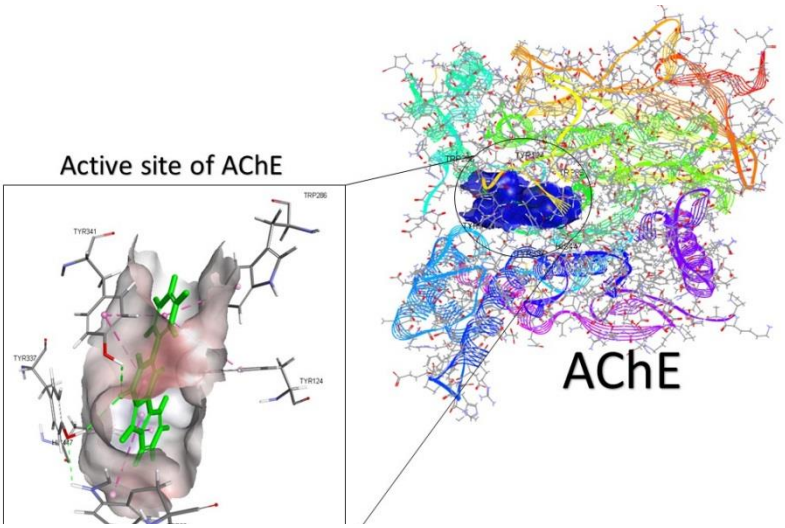

Figure 1-6: AChE enzyme along with its active site (in blue)

in different areas throughout the body. Eg. GPI- anchored dimeric structure of AChE is present on the surface of erythrocytes, while, in CNS, the enzyme is present in tetrameric form.[9]

AChE is the primary target for the anticholinesterase drugs such as donepezil, galantamine, and rivastigmine. The gene responsible for the production of this enzyme is localized to human chromosome 7 (7q22).[38]

1.8.2.1 Molecular structure of AChE

The high catalytic activity of AChE towards various inhibitors can be explained by its unique design of the active site. The X-ray crystallographic studies and site-directed mutagenesis are among the techniques which have been utilized for the characterization of amino acid residues, present in the active gorge of AChE. The shape of the active site gorge is observed to be similar to a bottleneck and as a horseshoe. The active site is present 20 Å below from the entrance (Fig. 1-7).

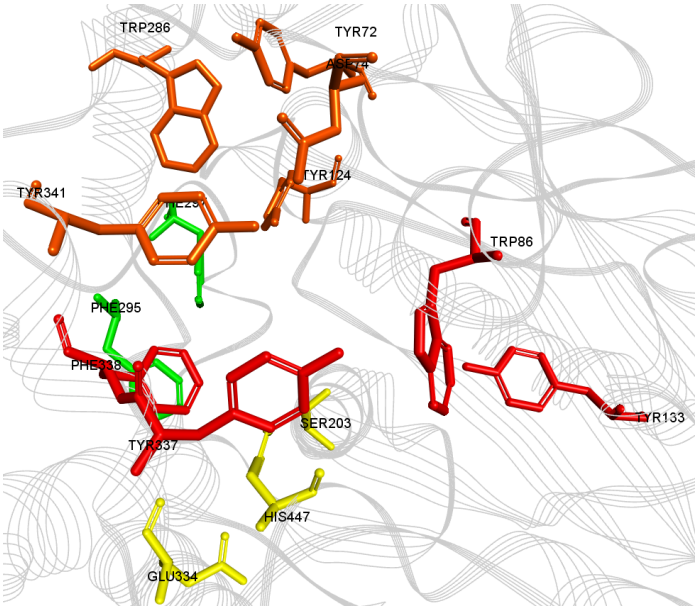

Figure 1-7*:* Subsites for the AChE enzyme. Amino acids in yellow represent the catalytic triad. Amino acids in green represent the acyl pocket. Amino acids in red represent the hydrophobic subsite, while, the amino acids in orange represents the peripheral anionic site.

Various subsites of the active site that play an important role have been reported.[9] The subsites for the human AChE (*h*AChE) can be defined as follows (Fig**.** 1-**7**).

- Catalytic triad [Ser203, His 447, Glu334][38]
- Acyl pocket [Phe295 , Phe297][39]
- Hydrophobic subsite [Trp86, Tyr133, Tyr337, Phe338][38]
- Peripheral anionic site [Tyr72, Asp74, Tyr124, Trp286, Tyr341][32]

Catalytic triad represents the three main amino acid residues which are responsible for the hydrolysis of ACh. Acyl pocket, on the other hand, helps in stabilization of the acetyl group of the ACh. A subset of 14 amino acids at the entrance of AChE enzymes consisting of aromatic amino acids such as Tyr and Trp represent the peripheral anionic site (PAS). Some studies suggest that blocking the activity of PAS will help in preventing AChE-induced aggregation of Aβ.[9]

1.8.2.2 Hydrolysis of ACh by AChE

In the synaptic cleft, as soon as ACh gets released from the presynaptic cleft, it is subjected to hydrolysis by AChE. It has a very high specific catalytic activity.One AChE enzyme molecule is known to hydrolyze about 25,000 molecules of ACh per second.[40] Hydrolysis of ACh by AChE can be considered as a stepwise mechanism which involves the formation of one intermediate and two transition states.[41,42] In the first step, a proton transferred from Ser 203 to His447 takes place which results in the formation of deprotonated Ser203 and protonated His447 species. In the second step, a nucleophilic attack by deprotonated Ser203 to the carbonyl carbon of ACh results in the formation of a zwitterionic form of acyl-enzyme intermediate. In the final step, the acetylated AChE undergoes hydrolysis by releasing acetate molecule as shown in (Fig. 1-8).

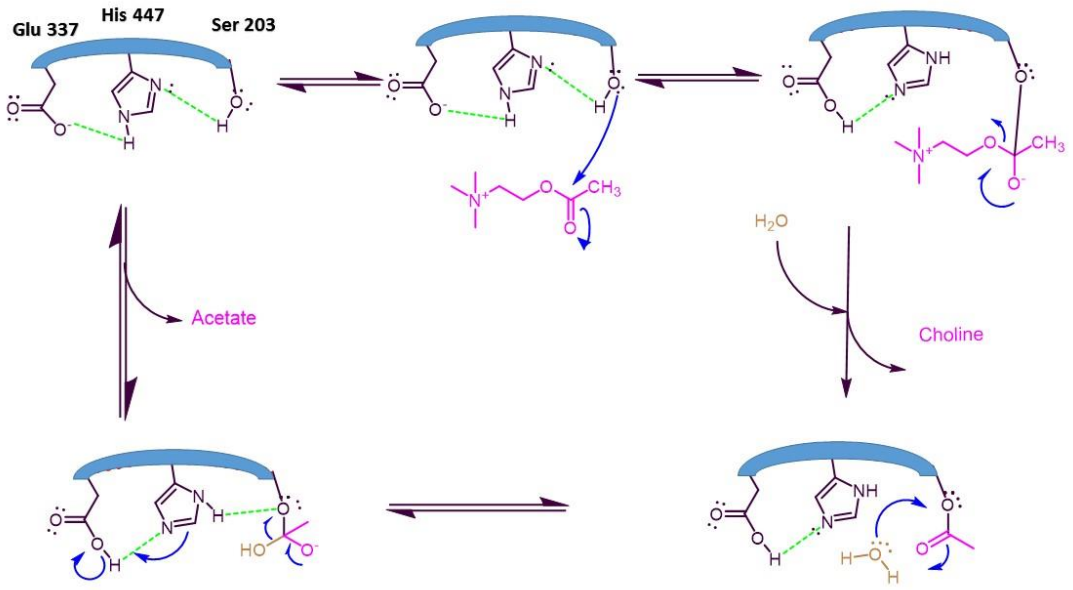

Figure 1-8*:* Hydrolysis of ACh by AChE

1.8.3 BuChE

Butyrylcholinesterase (BuChE) also known as acylcholine aceylhydrolase, or pseudocholinesterase (EC 3.1.1.8) is a homologous analog of enzyme AChE and belongs to the class of α/β fold family, similar to AChE. This means that the structure of BuChE, as well as AChE, contains a central β sheet which is surrounded by α-helix.[43] This enzyme is known to hydrolyze choline substrates such as butyrylcholine (BuCh) specifically and can also hydrolyze ACh, but at a lesser efficiency. Moreover, BuChE is also known to hydrolyze non-choline esters such as cocaine, aspirin, and heroin.[43] BuChE is found primarily in the organs of the body such as heart, liver, kidneys, lungs, intestine, as compared to AChE, which is present predominantly in the synaptic cleft of the neurons.[44] It has been reported that in certain species including humans, horse, and mice, higher activity of BuChE has been observed in plasma than AChE. While, in some animal species like rats, AChE activity is predominant in plasma.[44] This is because, in some

species, the enzyme biosynthesis takes place in the liver which can then diffuses in the plasma and thus, those animal species show the higher activity of BuChE in blood plasma. The primary function of BuChE in plasma is still unclear, but, it has been observed that in the case of ingestion of nerve poisons such as organophosphates (OP's), BuChE is known to scavenge to OP's and thus helps to prevent OP mediated toxicity.[43,44] Apart from the role of BuChE as a safety net for protecting the cholinergic transmission from various nerve poisons, it has also been a target for the activation of some prodrugs into their active forms. Bambuterol is one such example which is hydrolyzed by BuChE to give terbutaline, which has substantial antihistaminic activity. Similarly, heroin is converted to 6-acetylmorphine by the action of BuChE. The metabolized form of heroin is t lipophilic enough to cross the blood-brain barrier (BBB) and gets metabolized further to produce morphine in the brain. It is interesting to note that BuChE is the only enzyme present in the human blood plasma which can hydrolyze heroin.[44] In the brain, BuChE gets synthesized by glial cells and accounts for around 10% of the total cholinesterase activity in a healthy brain.[45] It has been observed that in AD, there is almost 50% reduction in the brain AChE levels at the later stages of the disease, while, the predominance of BuChE elevates to 90% and thus, BuChE inhibition forms an essential target for the disease, particularly in the later stages of the disease. As far as homology is concerned, BuChE and AChE share a structural and functional resemblance. The amino acid sequence homology between BuChE and AChE is around 65%, and the gene responsible for the production of BuChE was found to be localized on human chromosome 3 (3q26).[46]

1.8.3.1 Active sites in BuChE

The monomeric structure of BuChE contains 574 amino acids with a few asparagine-linked carbohydrate chains and three inter-chain disulfide bridges which maintain the three-dimensional

globular structure of BuChE. Unlike the structure of AChE, BuChE contains a much larger active site with 55 amino acid residues. It is almost 60% larger compared to AChE active site volume (~501 $Å^3$ vs. 302 $Å^3$).The amino acid residues from different subsites which can be categorized into:

- Catalytic triad (esteric site) – includes His438, Glu325, and Ser198
- Acyl Pocket or acyl binding site - Contains Leu286 and Val288
- Choline binding site (cation- π site) – contains Trp82, Tyr337

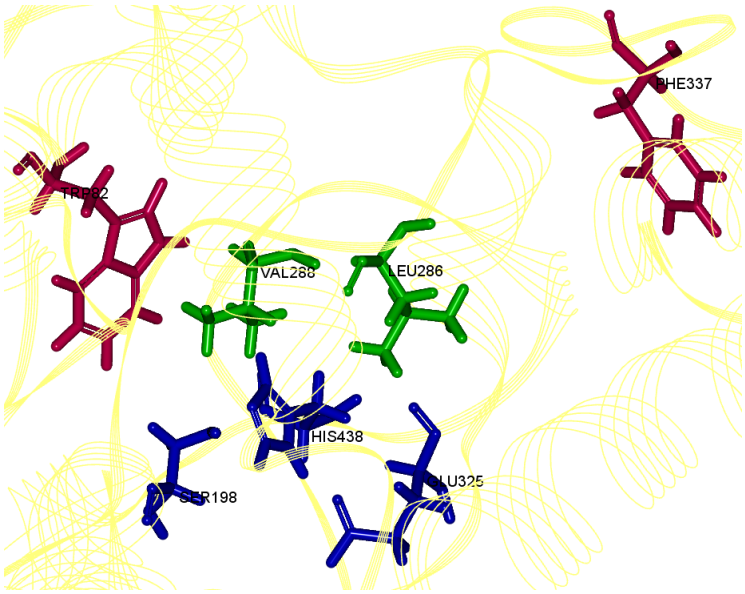

The catalytic triad in BuChE also contains three amino acids namely histidine, serine, and glutamic acid. The function of these amino acids is known to be similar to AChE. (Fig. 1-9)

Figure 1-9*:* Key amino acids in the BuChE binding site.

Acyl pocket in BuChE contains two primary amino acids namely leucine and valine. These aliphatic amino acid residues allow the entry of larger molecules such as butyrylcholine (BuCh) or other large acyl group containing compounds into the active subsite of the BuChE enzyme. This observation is different from AChE as the active subsite of AChE contains larger aromatic phenylalanine ring systems in the acyl pocket and thus, forms a narrower active site of about 302$Å^3$

as compared to 501Å^3 volume of the active gorge in BuChE. This larger size of the active gorge allows the entry of larger molecules in the active site of BuChE.[47]

Comparing the fourteen (14) amino acids present at the entry of the cholinesterase enzymes, AChE's amino acids residues are bulky and aromatic in nature which forms the part of PAS. In BuChE, half of these amino acid residues are aliphatic in nature and thus allows BuChE more flexibility and less steric hindrance so that even large molecules could reach to the active site of the enzyme. When compared to the active site of cholinesterase enzymes, BuChE's active site is around 200Å^3 bigger than active site of AChE[44,47] because of the presence of aliphatic amino acid chains in the active site of the enzyme.

1.8.4 Conclusion derived from cholinergic hypothesis

Acetylcholine (ACh) forms an empirical part of the cholinergic neurotransmission, and appropriate level of this neurotransmitter is required to maintain homeostasis. Reduced level of ACh in the brain due to neuronal loss is linked to the loss of memory and cognition. Two cholinesterase enzymes namely AChE and BuChE are capable of hydrolyzing ACh with AChE playing the primary role. The BuChE's contribution to the hydrolysis of ACh is around 10%. In AD, to maintain an acceptable level of ACh, the only current possible way is to inhibit the activity of these cholinesterase enzymes. As discussed earlier, the activity of BuChE increases as the disease progresses, it is thus essential to target BuChE so as to maintain healthy ACh levels at the later stages of the disease. Therefore dual inhibition of AChE and BuChE is desired. Currently, all available FDA-approved AD treatments prevent the hydrolysis of ACh by inhibiting both AChE and BuChEs. Donepezil, rivastigmine and galantamine are some of the examples of ChEIs. In conclusion, ChE inhibitors provide only symptomatic relief and are effective as a long-term treatment option in the AD pharmacotherapy.

1.9 Amyloid Beta (Aβ) Hypothesis

The occurrence of some unusual metabolic substances in the brain, which according to Alois Alzheimer, stain differently from healthy neurons, and the pathology which he then described does not fit with any of the disease known during that time.[48] Based on a series of research findings initiated by Alois Alzheimer's, the amyloid beta hypothesis was then put forward by Hardy and Allsop in 1991.[31,48] It was based on the fact that a protein like material whose deposits were found in the meningeal vessels of the brain of an AD patient, was found to be identical to the protein found in patients with Down syndrome, and the same was also the part of the senile plaques formed a link between Down syndrome and AD.[31] More details about the correlation between AD and Down syndrome is explained in the next section of this thesis.

The Aβ hypothesis remains the best scientifically supported theory used to describe AD.[31] According to this hypothesis, the progression of AD can be attributed to the progressive accumulation and aggregation of small peptides either extracellularly or intracellularly or both. Such aggregates are made up of a peptide with 40 to 42 amino acid chain length, and these peptides tangle to form insoluble quasi-crystalline deposits of amyloid fibrils. Further aggregation of these fibrils in a circular manner results in the formation of senile plaques or neuritic plaques (Fig.1-10). This type of aggregate can be either self-induced or promoted by AChE, as hypothesized by some researchers.[33,49,50]

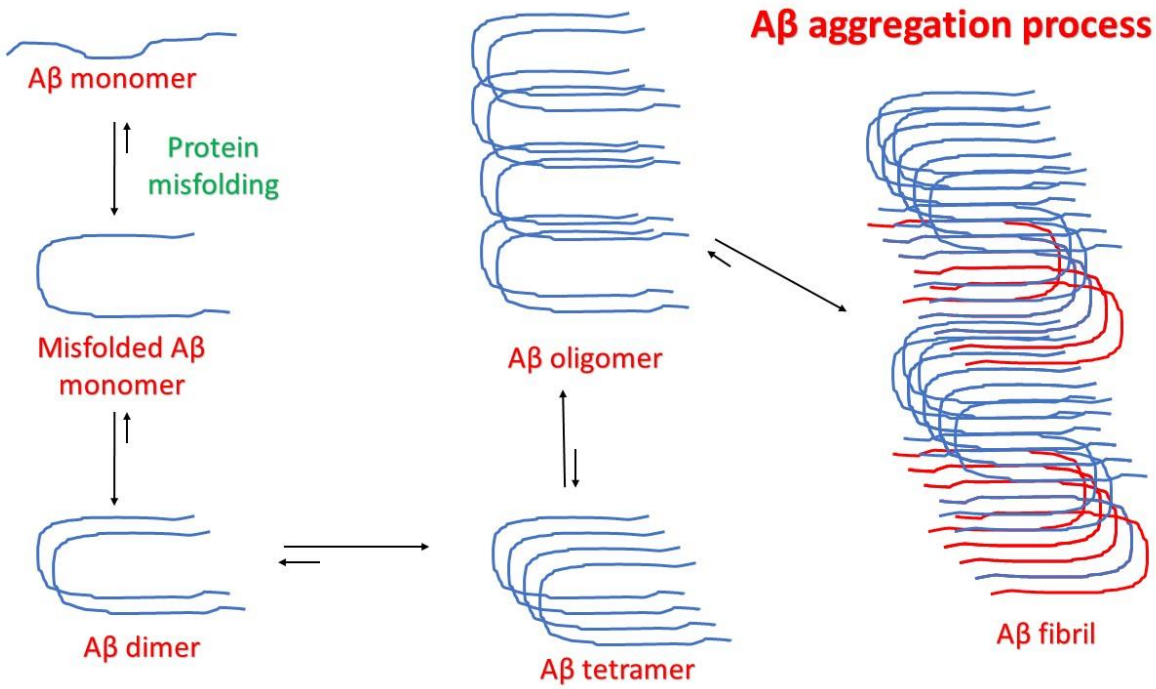

Figure 1-10*:* Steps in the aggregation of Aβ monomer to oligomers and fibrils.

Senile plaques contain aggregates of Aβ as the core while, activated microglia, dystrophic neurites, and reactive astrocytes form the outer covering, and thus senile plaques form extracellular lesions of the brain.[12] In 1984, Glanner and Wong became the first researchers to report the purification and partial structure of Aβ, which they named amyloid β protein[51] and soon after, a complete peptide sequence structure of the Aβ was reported. It was in early 2002 that Nussinov group first published the 3D model of $A\beta_{16-35}$ oligomers. The structure of the oligomers was reported to have a bent structure: U-shape, due to the presence of an intermolecular salt bridge between Asp23 and Lys28.[52] This molecular structure was described using molecular modeling studies and then confirmed by solid-state NMR analysis in 2006 by Tycko and coworkers. In 2015, the complete structure of $A\beta_{42}$ fibril was solved using solid-state NMR technique by Xiao and coworkers.[53]

1.9.1 AD and Down Syndrome: is there a connection between these two distinct diseases?

As mentioned before, the Aβ protein- whose molecular weight was found to be four kDa, was also found in patients suffering from Down Syndrome; along with neurofibrillary tangles, indicating that there are a strong connection and common origin of both the diseases.[12] Genetic studies on patients with AD and Down Syndrome also supported this observation. Beyreuther and coworkers in 1987 cloned a gene responsible for the expression of amyloid precursor protein (APP) and found it to be localized on the long arm of chromosome 21. Interestingly, in Down Syndrome, an extra chromosome 21 (and thus, known as 21 trisomy) is present. Hence, one would expect that due to the presence of an additional set of chromosome 21 in Down syndrome patients, APP expression would elevate and thus cause an early occurrence of AD type symptoms.[12,29]

1.9.2 Production of Aβ

It is noted that both healthy individuals and patients with AD produce Aβ. It is a matter of fact that in healthy individuals, the generated Aβ gets cleared by various hydrolyzing enzymes.[31] In AD patients, the Aβ clearance mechanism is hindered by various unknown mechanisms which cause an imbalance in the generation and removal of this protein.[27] It is interesting to know, how Aβ gets cleared out of the body. More explanation will be discussed in the next section.

Aβ is known to be present in extracellular fluids, including plasma and CSF (cerebrospinal fluid).[54] Production of Aβ is an example of regulated intramembrane proteolysis (RIP) of APP.[15,55,56] RIP is a cascade of events in which the ectodomains of the proteins (present on the surface of the membrane—in the case of AD, this surface protein is APP) is first cleaved by protease enzyme; which are present on the membrane itself, also known as secretases, keeping the trans-membrane and endo-domains intact. Transmembrane domains (TMD's) and endodomains are then cleaved

by another membrane-anchored enzyme to release small hydrophobic peptides into extracellular space and endodomains into cytoplasm respectively. (Fig.1-11).

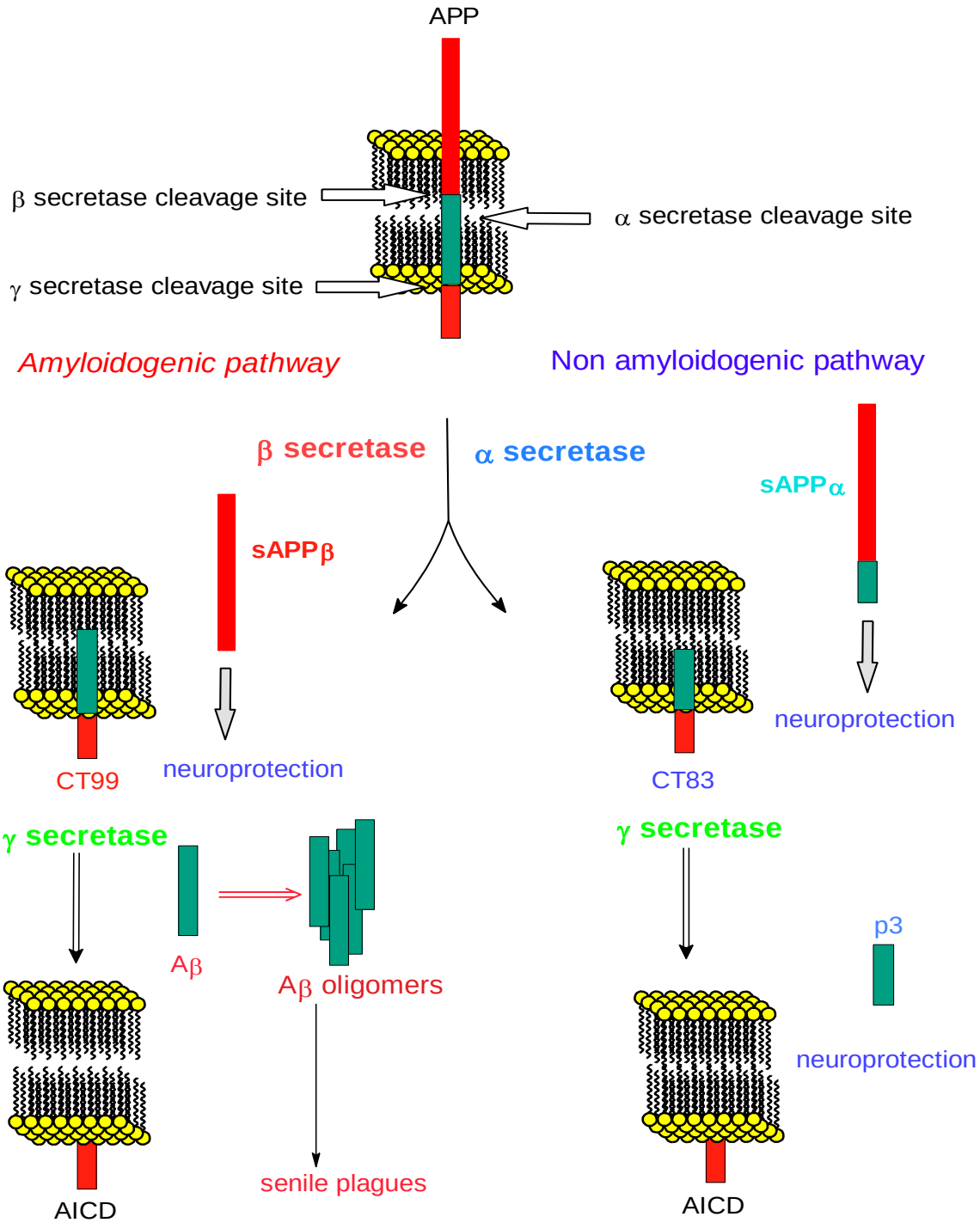

Figure 1-11: Production of Aβ from APP

Similar to the proteolysis explained above, three proteases, namely α- secretase, β- secretase and γ-secretase act on APP (surface protein), resulting in either production of neurotoxic $A\beta_{1\text{-}40/42}$ peptides or soluble and non-toxic peptides of shorter amino acid sequence (Fig.1-12).[57,58] A brief summary about these enzymes is given below:

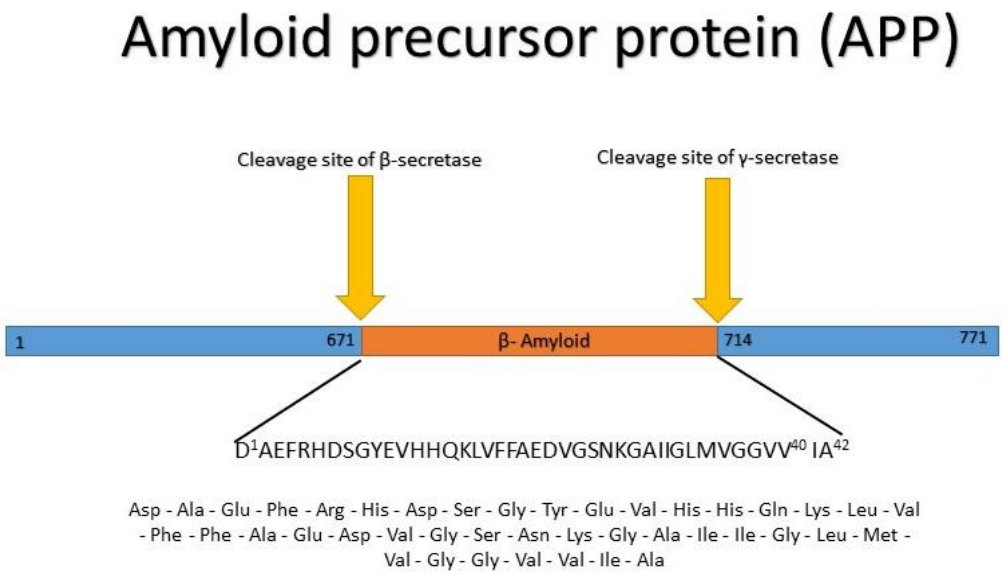

Figure 1-12*:* Structure of APP along with sites of proteolysis by β and γ secretases

1.9.2.1 α- secretase: This enzyme belongs to A disintegrin and metalloprotease (ADAM) family of zinc metalloproteases. There are around 21 different enzymes that belong to the ADAM class. The α- secretase can be categorized into ADAM9, ADAM10 or ADAM17/TACE.[59] ADAM belongs to type-1 transmembrane proteinases. ADAM-9 is known to increase the basal and protein kinase c-dependent APPsα release, while ADAM-17 is involved in the cleavage of pro-TNF-α; which is a type-1 membrane glycoprotein. The cleavage of APP by α-secretase between amino acid 687 and 688 (Fig. 1-13) of APP results in the generation of sAPPα (which is supposed to have neuroprotective and neurotrophic properties) and CT83. The CT83 so formed becomes the

substrate for γ-secretase which results in the formation of non-toxic p3 (3kDa peptide) and AICD (Fig. 1-11). Thus, we can say that the metabolic pathway of α- secretase follows the non-amyloidogenic pathway. It has also been hypothesized that over-expression/ stimulation of α-secretase should prevent the proliferation and aggregation of Aβs to from Aβ oligomers and fibrils.[57]

1.9.2.2 β-secretase: It is an aspartyl protease enzyme, also known as β-site APP cleaving enzyme or BACE.[60] It is responsible for cleaving ectodomain part of APP to release sAPPβ, (soluble APP) into extracellular fluids, similar to α-secretase but, cleaving sites are different from α-secretase. The β secretase cleaves between amino acid 671 and 672 of APP (Fig. 1-13) resulting in the formation of sAPPβ, which does not have any neuroprotective or neurotrophic properties. The CT99 fragment is generated after the initial processing of APP by β secretase, which then becomes a substrate for another cleavage enzyme known as γ-secretase, to produce Aβ fragments and AICD. Fragments of the Aβ produced after the final cleavage of CT99 by γ-secretase tends to aggregate with other Aβ fragments to form oligomers and then Aβ fibrils. Hence, the cleavage process carried out by β secretase is considered as the amyloidogenic pathway.[60,61]

1.9.2.3 γ-secretase: This enzyme also belongs to the class of aspartyl protease, and contains four different domains: Presenilin-1 (PS1) or (PS-2), nicastrin, APH1, and PEN2, and is known to carry out cleavage of its substrates at different sites (γ, ε, and ζ cleavage).[62] After the processing of APP by the BACE-1 enzyme, γ-secretase can cleave CT99 at various cleaving sites and can produce Aβ of different amino acid chains (Fig.1- 13). The γ cleavage can generate Aβ as $A\beta_{1-38,}$ $A\beta_{1-40}$ or $A\beta_{1-42}$. The ζ- cleavage by γ-secretase produces $A\beta_{1-46}$, while ε cleavage produces Aβ as $A\beta_{1-49}$ (Fig. 1-13). [62–64]

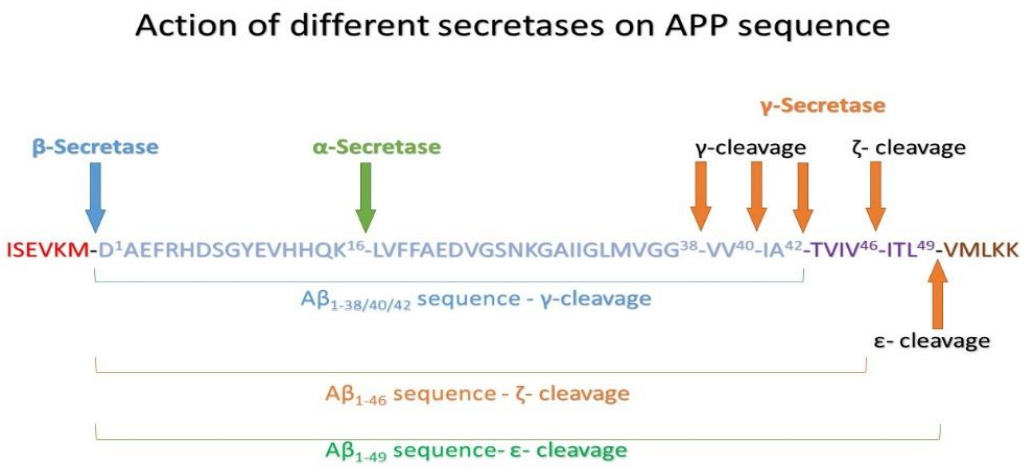

Figure 1-13: Summary of action of α, β and γ secretase on APP sequence

1.9.3 Clearance mechanism of Aβ

It is essential for the body to disintegrate the Aβ so that normal physiological functions of the brain could be preserved. Elevated levels of Aβ in the brain; in synapse mainly, can impact the excitatory transmission and can hinder neuronal hyperactivity.[27] Certain protease enzyme such as neprilysin, insulin degrading enzyme- belonging to the class of thiol metalloendopeptidases, endothelin converting enzyme, angiotensin converting enzyme and matrix metalloprotease (MMP9) are all capable of breaking Aβ into smaller peptides.[65] For example, in the case of MMP9, Aβ can be divided into various C-terminal Aβ fragments such as $Aβ_{1-16}$, $Aβ_{1-20}$, $Aβ_{1-23}$, $Aβ_{1-30}$, $Aβ_{1-33}$, $Aβ_{1-34}$.[65] The smaller Aβ fragments are known to be less toxic than $Aβ_{1-40}$ and $Aβ_{1-42}$ species.

1.9.4 Aβ induced toxicity

As discussed previously, Aβ peptide is produced from the cleavage of APP by various secretase enzymes. APP or amyloid precursor protein is a surface enzyme expected to be responsible for cellular adhesion between neurons and is believed to have neurotrophic as well as neuroprotective properties.[66,67]. After a certain interval of time, this surface protein is subjected to replacement, and this is done by using various secretase enzymes. One of the cleaved products of APP is Aβ. The Aβ peptide produced usually undergoes clearance, but, in the case of AD, this protein tends to aggregate and forms Aβ fibrils, which are the main constituents of senile plaque.[56]. However, before Aβ aggregates to form a stable, non-soluble fibril structure, the soluble forms of Aβ are known to be highly toxic to most of the biological processes.[31,56]. The Aβ monomers, dimers and oligomers come under this category of being soluble and extremely toxic to the normal biological processes. It has been observed that Aβ oligomers are the most toxic species among other forms[49]. The Aβ mediated toxicity can be classified into five main categories as below (Fig. 1-14):[31,68]:

- Aβ mediated mitochondrial dysfunction
- Aβ mediated oxidative stress
- Aβ mediated synaptic dysfunction
- Aβ mediated changes in the membrane permeability
- Aβ mediated telomerase inhibition

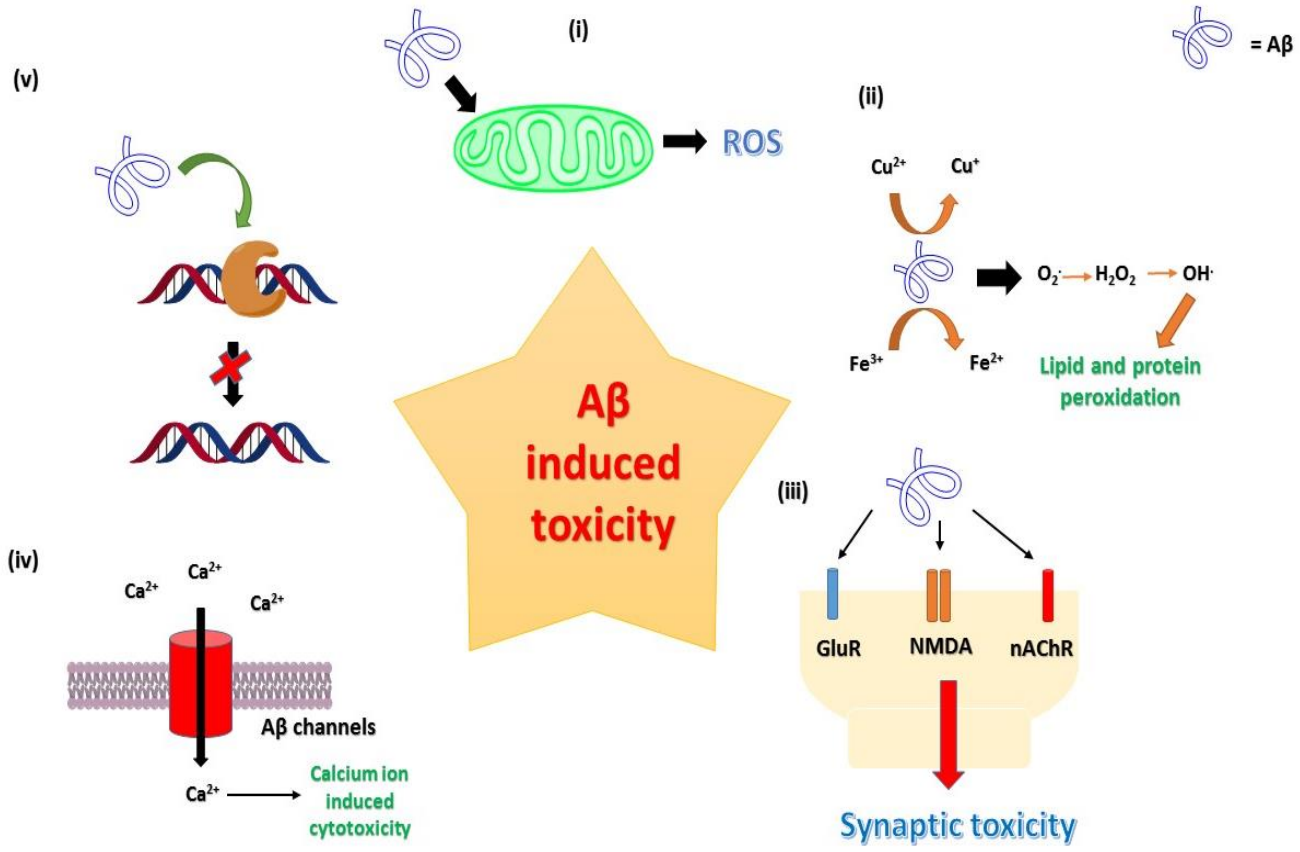

Figure 1-14*:* Aβ induced mitochondrial dysfunction and oxidative stress

1.9.4.1 Aβ mediated Oxidative stress

Aβ is known to have some metal binding properties. Free metal ions such as Cu^{2+} and Fe^{3+} are known to form Aβ-metal chelate complexes.[69,70] The ability of the Aβ to bind to these metal ions can be explained by the presence of histidine (His6, His 13 and His14) and tyrosine (Tyr10) in the molecular structure of Aβ. These amino acid residues are known as the metal binding site, especially for Cu^{2+}. The nitrogen atom of the indole ring in histidine and oxygen of the hydroxyl group in the tyrosine molecule can provide necessary electrons to the metal ions so that metal ion can chelate with Aβ. This metal-Aβ chelate constitutes the base for the reduction of metals by the amino acid methionine (Met35) present in Aβ. The reduced metal ions can then react with

molecular oxygen to generate superoxide anion. These superoxide ions then produce hydrogen peroxide by accepting protons (in AD, the pH of brain fluid is slightly acidic). Hydrogen peroxide further reacts with reduced metal ions to form hydroxyl radical by Fenton reaction. Superoxide ions can also react with hydrogen peroxide to generate hydroxyl ions via Haber-Weiss reaction. It should be noted that all these reactions take place due to the generation of reduced form of metal chelated to Aβ. The overall redox reaction by which the metal reduction occurs can be explained as follows[69–71]:

$$A\beta\ Met(S) + Cu^{2+} \longrightarrow A\beta\ Met(S^{+}) + Cu^{1+}$$

$$Cu^{1+} + O_2 \longrightarrow Cu^{2+} + O_2^{\cdot -}$$

$$O_2^{\cdot -} + O_2^{\cdot -} + 2H^{+} \longrightarrow H_2O_2 + O_2$$

$$Cu^{1+} + H_2O_2 \longrightarrow Cu^{2+} + OH^{\cdot} + OH^{-} \quad \{\text{Fenton Reaction}\}$$

$$O_2^{\cdot -} + H_2O_2 \longrightarrow OH^{\cdot} + OH^{-} + O_2 \quad \{\text{Haber- Weiss reaction}\}$$

The Aβ- metal- radical form is capable of abstracting protons from the neighboring proteins and lipids and thus causing lipid peroxidation. Also, metal chelated Aβ is susceptible for accelerated aggregation as compared to the metal free Aβ.[70]

1.9.4.2 Aβ mediated mitochondrial dysfunction

Aβ mediated mitochondrial dysfunction can be proceeded by two major ways (Fig. 1-14). These two major pathways are;

- **Changes in the membrane permeability of cells-** this phenomenon is caused by the formation of Aβ pores on the surface of the cells. These pores can carry Ca^{2+} ions freely from the extracellular fluid into the cytosol of the cells. This causes an elevation of Ca^{2+} in

the cytosol and thus, mediates the Ca^{2+} induced mitochondrial dysfunction. Ca^{2+} enters the mitochondria and causes disruption of electron transport chain (ETC), oxygen consumption, the membrane potential of mitochondrial membranes. An interruption in the ETC soon causes the release of cytochrome C which will initiate a cascade of reactions and causes apoptosis of the cells via caspase mechanism.[72–76]

- **The presence of interneuronal Aβ:** It is evident from various microscopic studies that Aβ can penetrate the cell wall and can accumulate within different cell organelles of the neurons; mitochondria in particular. Aβ aggregates have been present the mitochondria of the AD patients as well as AD mouse models. It has been hypothesized that Aβ when present in mitochondria can chelate to the metal ions such as copper and iron. These metal ions are required for proper functioning of ETC, and thus, the presence of Aβ can hinder ETC efficiency and thus causes cells to die off because of reduced production of ATP in the neuronal cells.[72–74]

1.9.4.3 Aβ mediated changes in the membrane permeability

As it has already been discussed previously, that Aβ causes the change in the membrane permeability. This occurs due to insertion of Aβ peptides inside the cell wall of the neurons and causes an increase in the permeability of the cell wall by forming Aβ channel pores. A soluble form of Aβ i.e. monomers, dimers and oligomers are known to interact with the cholesterol molecules which are present on the surface of the cell walls. This interaction between Aβ and cholesterol causes Aβ to get inserted into the cell wall without compromising the elasticity of the cell wall. The cell wall with Aβ channel pores is highly permeable to the $Ca^{2+,}$ and this results in elevated Ca^{2+} levels within the neuronal cells and thus results in various Ca^{2+} regulated downstream processes such as mitochondrial dysfunction and Ca^{2+} induced synaptic dysfunction.[77,78].

1.9.4.4 Aβ mediated synaptic dysfunction

AD is considered to be a disorder of synaptic dysfunction. In mild AD, hippocampal synapse begins to collapse, and a decrease in synaptophysin (a presynaptic vesicle protein) is observed. All these events have been linked to the effect of Aβ's presence at the synaptic cleft region. Soluble forms of Aβ: mostly oligomers, is known to impair synaptic plasticity by disturbing the balance between long-term potentiation (LTP) and long-term depression (LTD). Both LTP and LTD are related to the activity of AMPA (2-amino-3-(3-hyrdoxy-5-methylisoxazol-4-yl)-propionic acid) receptors. LTP is caused by the increased activity of AMPA receptors in the postsynaptic membrane, while, AMPARs constant removal and decreased function is related to cause LTD. This observation becomes a hypothesis that AMPARs number and function exhibit a significant role in AD pathology.[12,66,79] It was observed that Aβ oligomers are known to have an endocytotic effect when present near AMPARs which leads to LTD. With NMDA (N-methyl-D-aspartate) receptors, the effect of Aβ is different. The NMDA receptors, similar to AMPA receptors, belong to the category of glutamate receptors, but the mechanism by which Aβ modifies the activity of NMDA receptors is completely different. It is believed that Aβ causes excessive activation of the NMDA receptors and this leads to excessive accumulation of Ca^{2+} within the neurons which leads to neuronal excitotoxicity. This observation was proved when a solution of $A\beta_{40}$ was given to hippocampal cells causing cell death of the hippocampal cell lines. Neuroprotection was observed in the presence of memantine (NMDA receptor antagonist) in the cell cultures. This observation supported the idea that NMDA receptor plays a vital role in Aβ induced neurotoxicity.[22,80–83] The Aβ is also known to impair the activity of acetylcholine receptors (AChRs) by either inhibiting the binding of ACh to the receptors or by permanently blocking them.[75]

A summary of the mechanism of the Aβ hypothesis can be represented in a flow diagram as follows (Fig. 1-15).

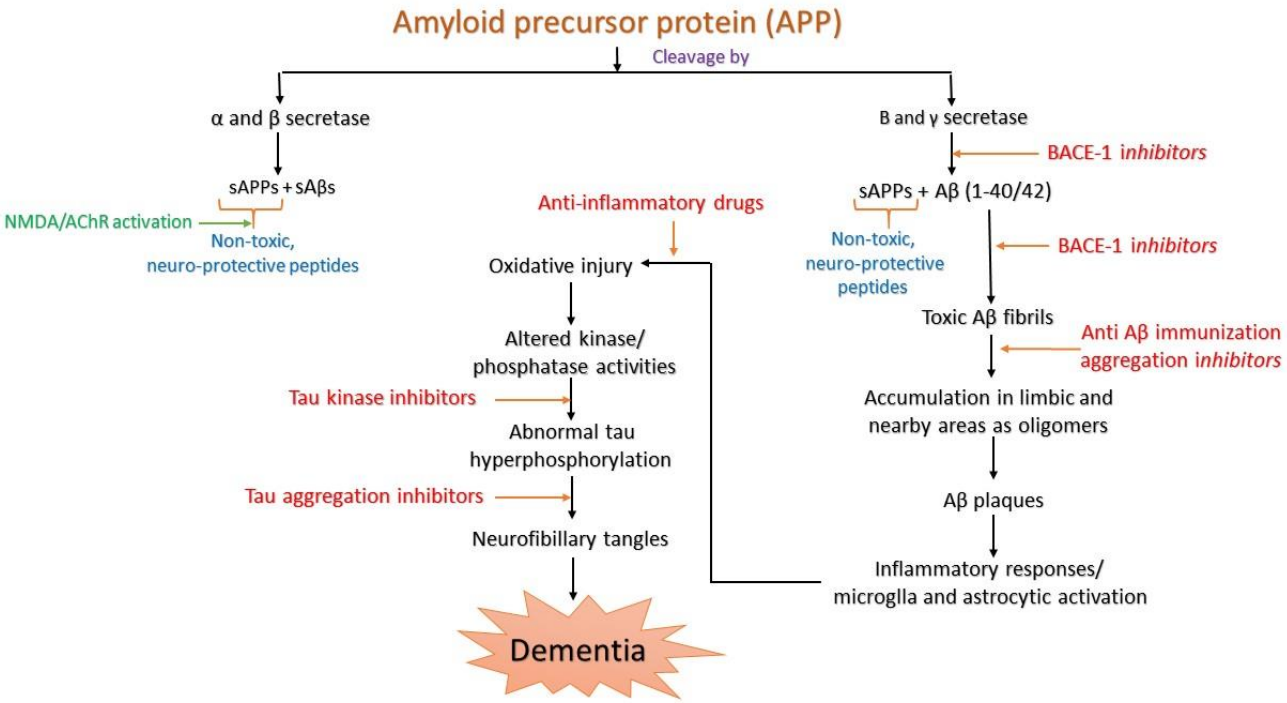

Figure 1-15*:* Summary of the mechanism of Aβ hypothesis

1.9.5 Approaches for Targeting Amyloid- β

There are various methods which can be considered while targeting the Aβ cascade as potential therapeutics for AD management. The primary target is based on using small molecules as Aβ aggregation inhibitors. Though this sounds one of the easiest methods; this might not be entirely application to a wide variety of patients. It has been observed that by the time patients are diagnosed with AD, the Aβ load is high. As a result, this particular type of approach might not apply to patients with advanced AD symptoms. Other targets have been characterized by the Aβ production which can be utilized in either preventing the production of Aβ as a whole or by

reducing the Aβ load in the brain. Ideally, if potential therapeutic could reduce the Aβ load in the brain of the patient and initiate neurogenesis, that drug could be able to reverse the pathophysiology of AD. Despite rigorous efforts, investment in time and s and money, no new anti-AD drug has reached the market yet. Some AD targets are as follows:

1.9.5.1 β-secretase inhibitors: BACE-1 inhibitors work on the principle of inhibiting the production of Aβ production by inhibiting the activity of the enzyme responsible for the production of Aβ from APP. Preventing Aβ production in the brain, though sounds an ideal option, is challenging because of the various reasons such as (1) inability of most of the BACE-1 inhibitors to penetrate the blood-brain barrier (BBB); (2) Therapeutic considerations for its safety, efficacy, and tolerability; (3) Prediction of mechanism-based toxicity/ side effects..[84–89] Some small molecules have made progress in the discovery ladder:

- **Verubecestat**: developed by Merck & Co. is currently in phase-III clinical trials (Fig. 1-16).

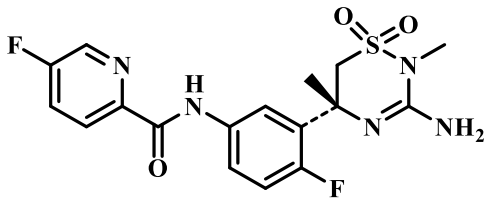

Figure 1-16*:* Molecular structure of Verubecestat

Verubecestat is a potent BACE-1 inhibitor with an IC_{50} of 13nM for BACC-1. This drug is known to bind to the aspartate amino acid residues in the active site of BACE-1 and prevents the activity of the β-secretase enzyme. This drug, in early clinical studies, is known to exhibit excellent safety profile with limited to none immediate side effects. A

single administration of this drug via oral route has been observed to reduce the load of Aβ in CSF by 92%.[89,90]

- AZD3293- developed conjointly by AstraZeneca and Eli Lilly (Fig. 1-17) is currently undergoing Phase-III clinical trials and targets BACE-1 for preventing Aβ production.[89,90] Currently in Phase-III clinical trials.

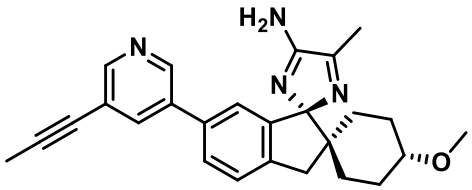

Figure 1-17*:* Molecular structure of AZD3293

- CNP520 developed by Novartis and Amgen pharmaceuticals and JNJ-54861911 developed by Johnson and Johnson are some of the other drugs which are currently under investigation for Phase-II/III trials.[89,90]

1.9.5.2 Aβ aggregation inhibitors: Small molecules are specifically designed to prevent the formation of Aβ oligomeric aggregates, which are insoluble and toxic in nature. Some small molecules have metal chelating properties which can further enhance their efficacy.[91,92]. According to Atwood and coworkers, Cu^{2+} and Zn^{2+} ions are associated with the aggregation of Aβ, and administration of metal chelator molecule which can cross the blood-brain barrier can drastically reduce the aggregation of Aβ.[69,71]

1.9.5.3 Aβ Immunotherapy: Immunotherapy involves the administration of peripheral antibodies, for which aggregated $Aβ_{1-42}$ acts as an antigen and are effective in reducing the deposition of Aβ aggregation. It also helps in suppressing the amyloid-associated pathology which includes synaptic degeneration, neuritic dystrophy and early tau accumulation by which

improvement in synaptic plasticity was observed.[93–96] The table (Table 1) below provides a list of antibody therapies aimed at scavenging various Aβ aggregates [90]:

S. No.	*Antibody*	*Aβ Target*	*status*	*company*
1	Crenezumab	Oligomers	Phase-III	Genentech/ Roche
2	Bapineuzumab	Monomers, oligomers, and plaques	Failed Phase-III	Johnson & Johnson/ Pfizer
3	Solanezumab	Soluble monomers	Failed Phase-III	Eli Lilly
4	Gentenerumab	Plaques	Failed Phase-III	Roche
5	Aducanumab	Plaques and oligomers	Phase-III	Biogen

Table 1-1*:* Various antibodies currently undergoing clinical trials

Chapter 2. Hypothesis and Design Rationale

2.1 Proposal

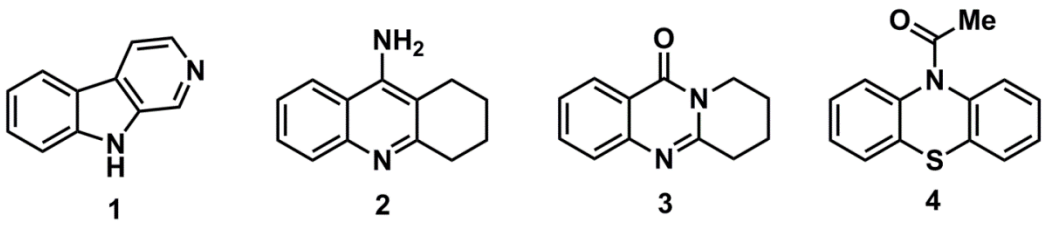

Figure 2-1: Cholinesterase inhibitors (**1**–**4**) with a fused tricyclic ring template

The fused tricyclic ring is a common chemical feature present in a number of cholinesterase inhibitors (Fig 2.1). The β-carboline (compound **1**) is a known cholinesterase inhibitor whereas the 1,2,3,4-tetrahydroacridine containing tacrine (**2**) was the first drug marketed to treat Alzheimer's disease[9]. Another natural product mackinazolinone (compound **3**, Fig 2.1) based derivatives and the phenothiazine (**4**) derivatives are known to exhibit dual cholinesterase inhibition[91]. These compounds have smaller molecular volumes (range ~ 139.9–153.5 $Å^3$) and bind to the catalytic sites of both AChE (monovalent inhibitors) and BuChE enzymes. The complexity of AD is highlighted by the fact that addressing only the cholinergic hypothesis using cholinesterase inhibitors can provide only symptomatic relief and is not a long-term solution[2,12]. These findings led us to design novel fused tricyclics capable of exhibiting multi-targeting potential. The objective was to develop small molecules to inhibit (i) the cholinesterase enzymes; (ii) prevent Aβ aggregation and (iii) exhibit antioxidant properties. A literature search led us to a novel fused tricyclic ring template pyrazino[1,2-*a*]indol-1(2*H*)-one (Fig 2-2). Initial modeling studies indicated that this novel tricyclic ring was able to bind in the catalytic site of AChE enzyme (Figure 2.3, panel A). Our goal was to modify the structure of this template to provide bivalent inhibition. It is known that the PAS of AChE is involved in promoting AChE-mediated Aβ

aggregation[97,98]. Based on this observation, we decided to pursue 3-phenylpyrazino[1,2-*a*]indol-1(2*H*)-one (abbreviated as *PPI* in this thesis) derivatives (Fig 2-2) as the molecular docking experiment of *PPI* in AChE shows that the core fused tricyclic pyrazino[1,2-*a*]indol-1(2*H*)-one ring was interacting with the catalytic site of AChE (Fig 2-3, panel B) whereas the C3 phenyl was oriented in the PAS of AChE suggesting its potential exhibit bivalent inhibition. In addition, we anticipated that the *PPI* could stabilize the dimer assembly and prevent Aβ self-assembly and aggregation into higher order structures. In this regard, the molecular docking study of *PPI* in the Aβ40 dimer model suggests that the molecular structure of *PPI* and its derivatives are capable of preventing the Aβ aggregation by interacting with the hydrophobic regions of the Aβ protein such as *KLVFFA* region. (Fig 2.4) represents the molecular docking studies of *PPI* with the dimer model of $A\beta_{40}$.

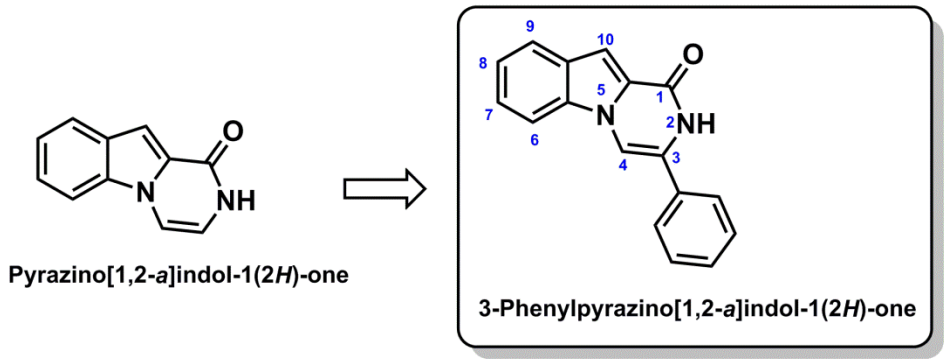

Figure 2-2*:* The chemical structure of proposed novel fused tricyclic ring system 3-phenylpyrazino[1,2-*a*]indol-1(2*H*)-one (*PPI*).

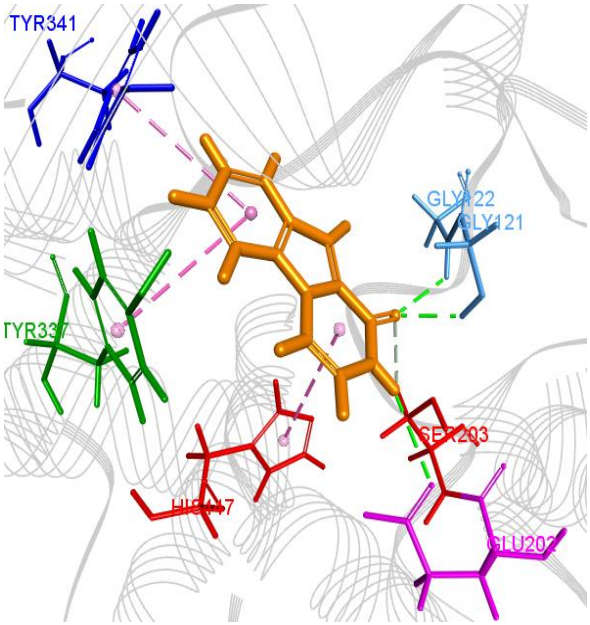

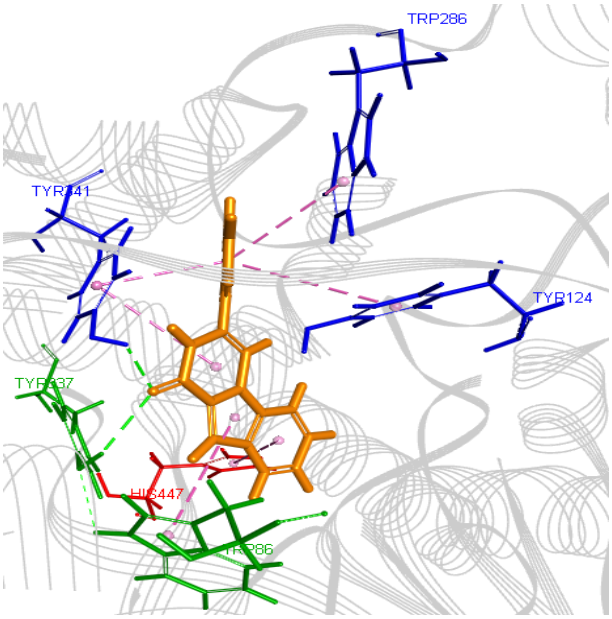

(A) (B)

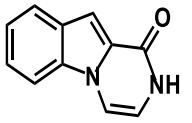

pyrazino[1,2-*a*]indol-1(2*H*)-one

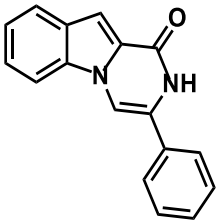

3-phenylpyrazino[1,2-*a*]indol-1(2*H*)-one

(C) (D)

Figure 2-3: Binding modes of pyrazino[1,2-*a]*indol-1(*2H*)-one (panel A) and 3-phenylpyrazino[1,2-*a]*indol-1(*2H*)-one (Panel B) in the active site of human AChE enzyme.

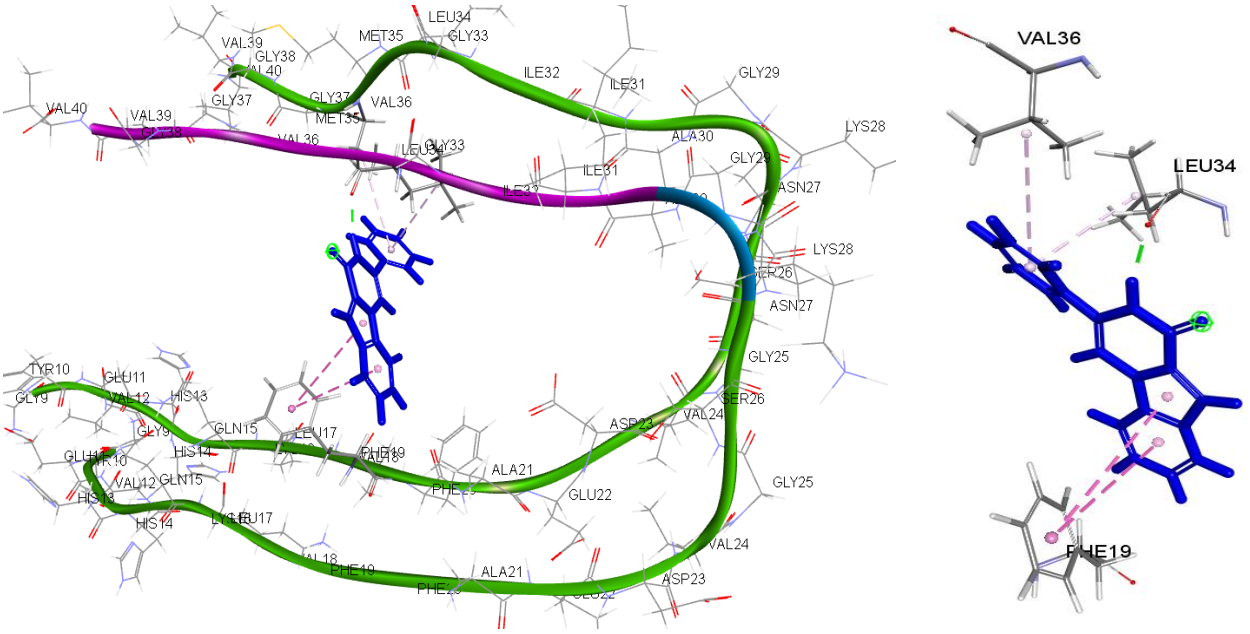

(A) **(B)**

Figure 2-4: Binding mode of 3-phenylpyrazino[1,2-*a]*indol-1(*2H*)-one (Panel A and B) in the Aβ40 dimer assembly.

2.1.1 3-Phenylpyrazino[1,2-*a]*indol-1(*2H*)-one (*PPI*)

The pyrazino[1,2-*a*]indole derivatives are known to exhibit a number of biological activities ranging from serotonin antagonists, thrombolytic, CNS depressants, anxiolytics, antihistamines, anticonvulsants, protein kinase inhibitors, antifungal and as antibacterial agents.[99] Various substituted Pyrazino[1,2-*a]* indoles have known biological activities and have been investigated for its actions ranging from serotonin antagonists, thrombolytic, CNS depressants and, anxiolytics for which the BBB penetration is essential[99].

We aim to incorporate C3 pharmacophores capable of providing anti-Aβ and antioxidant properties (Fig. 2-5). For example, a 3,4-dimethoxyphenyl substituent will be incorporated at the

C3 position. Previous studies from the Nekkar Rao lab has shown that the presence of a 3,4-dimethoxybenzyl substituent in tacrine and quinazoline-based derivatives provided dual cholinesterase inhibition and anti-Aβ aggregation properties.[100] Other proposed C3 substituents include adding phenolic groups that possess antioxidant properties such as 3-methoxy-4-hydroxyphenyl and 4-hydroxy-3-methoxyphenyl substituents at the C3 position. These substituents are known to be in the natural antioxidant curcumin.[101]

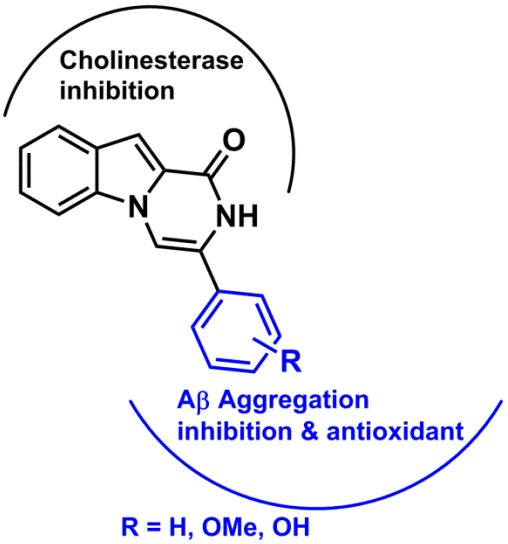

Figure 2-5: Proposed *PPI* derivatives as multi-targeting agents. ClogP value ranges from 2.97 to 3.69

2.2 Conclusion

AD is a complex disease. The current pharmacotherapy options based on cholinesterase inhibition is inadequate. The amyloid cascade hypothesis shows that aggregation of Aβ is a major event known to promote neurotoxicity, mitochondrial dysfunction, oxidative stress, neurodegeneration and cognitive decline. Our proposal has identified a novel fused tricyclic 3-phenylpyrazino[1,2-*a]*indol-1(*2H*)-ones (*PPI*) as a suitable system to incorporate multi-targeting activity such as cholinesterase and Aβ aggregation inhibition, and antioxidant activity. A library of *PPI* derivatives will be synthesized and evaluated by structure-activity relationship (SAR) studies to understand the structural requirements for multi-targeting activity. The planned experiments include compound library synthesis, their characterization, in vitro studies using human AChE and BuChE enzymes, Aβ aggregation kinetics, transmission electron microscopy (TEM) experiments and molecular docking studies. These results would provide evidence on the suitability of *PPI* derivatives as potential anti-AD agents.

Chapter 3. Methodology

3.1 Introduction

This chapter describes (i) the synthetic chemistry methods used to prepare *PPI* derivatives and the reaction mechanisms involved; and (ii) the principles of biological assay methods used including cholinesterase inhibition, $A\beta_{40}/A\beta_{42}$ aggregation kinetics studies, transmission electron microscopy, molecular docking and antioxidant assays.

3.2 Preparation of *PPI* derivatives

The synthetic summary to prepare the *PPI*s library is shown in Scheme 3.1. It was commenced by using commercially available substituted or unsubstituted indole-2-carboxylic acids (**1a-c**, Scheme 3.1). Esterification of these indole carboxylic acids under mild conditions provided ethyl indole-2-carboxylates (**2a-c**) in excellent yields (yield 75-80%). Coupling of these indole carboxylates with substituted or unsubstituted 2-bromoacetophenones (**3a-m**) provided ethyl 1-(2-oxo-2-phenylethyl)-1*H*-indole-2-carboxylates(**4a-n**) with yields ranging from 14-45%. Cyclization of **4a-n** coupled product gave us the targeted compounds (**5a-n**) in excellent yields 65-75% as shown in Scheme 3-1. The reaction conditions used and the mechanisms are discussed in the following sections.

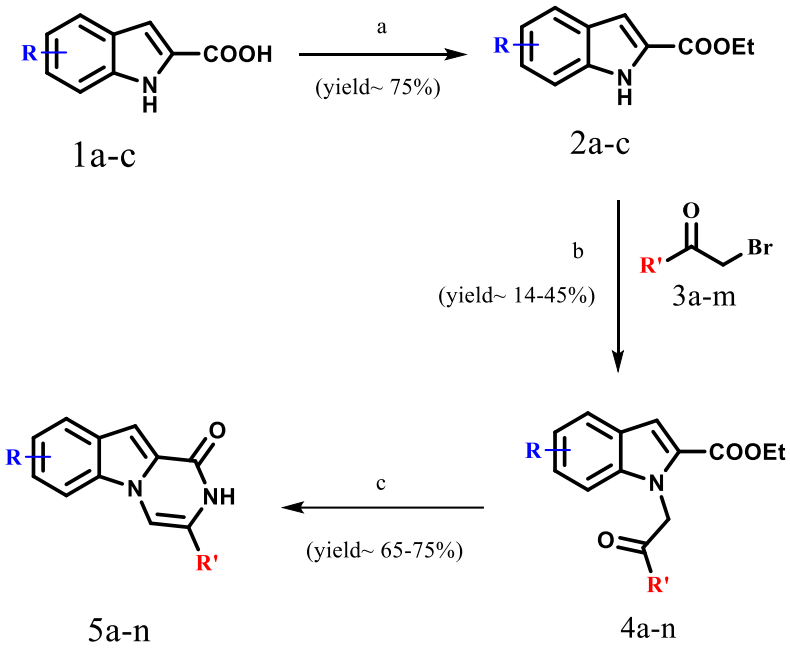
R
COOH
N
H
a
(yield~ 75%)
COOEt
1a-c
2a-c
b
(yield~ 14-45%)
O
Br
R'
3a-m
NH
c
(yield~ 65-75%)
5a-n
4a-n

R=

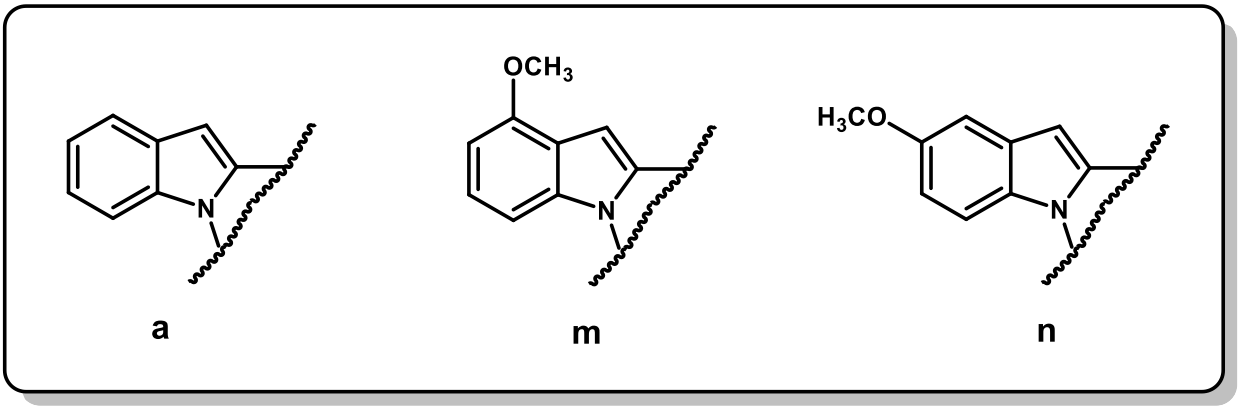
OCH3
H3CO
N
a
m
n

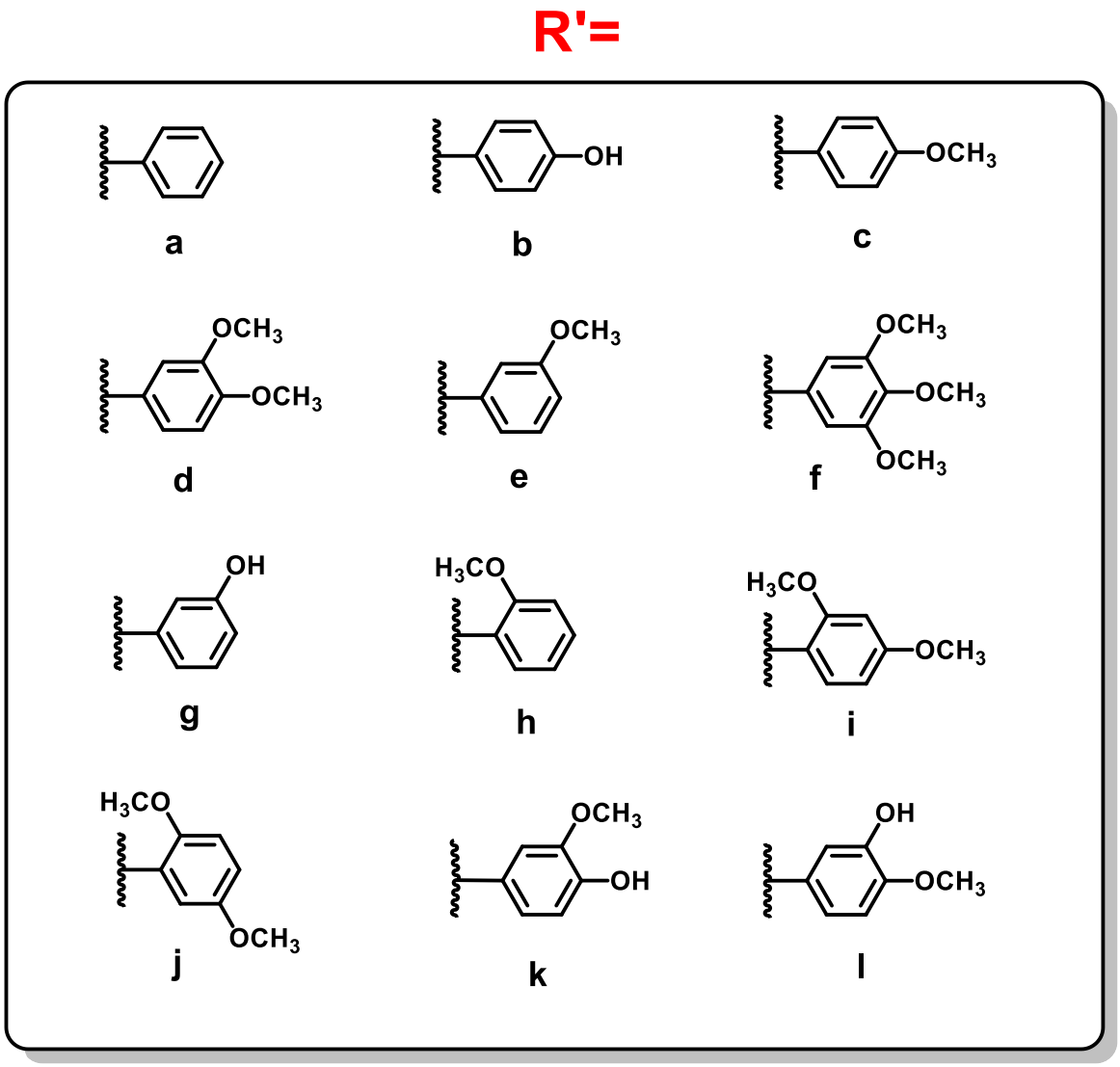

Scheme 3-1*:* General scheme to synthesize *PPI* derivatives 5a-o. Reagents and conditions– (a) EtOH, Conc. H_2SO_4, Reflux, 78°C, 24h; (b) Substituted 2-bromoacetophenone (1.2 eq), Cs_2CO_3 (2 eq), KI (catalytic qty.), ACN, reflux at 70°C for 24h ; (c) CH_3COONH_4 (10 eq.), BuOH: CH_3COOH (4:1), PV, 150°C for 8h.

3.2.1 Preparation of ethyl indole-2-carboxylates 2a-c

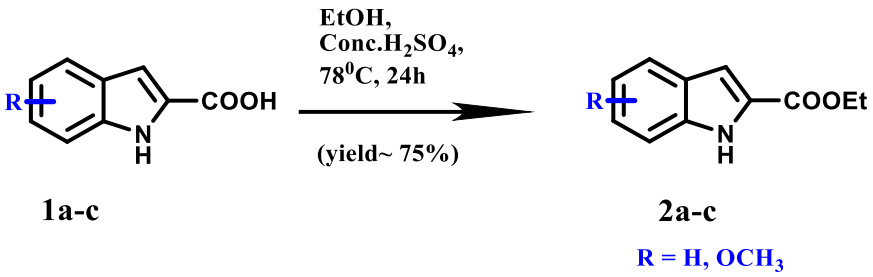

1a-c **2a-c**

R = H, OCH_3

Scheme 3-2: Synthesis of ethyl indole-2-carboxylates (**2a-c)**

Indole-2-carboxylic acids **1a-c** were subjected to an esterification using ethanol in the presence of catalytic amounts of conc. H_2SO_4 under reflux. The product was obtained in excellent yields (~75%). The reaction mechanism is shown in Figure 3-1. :

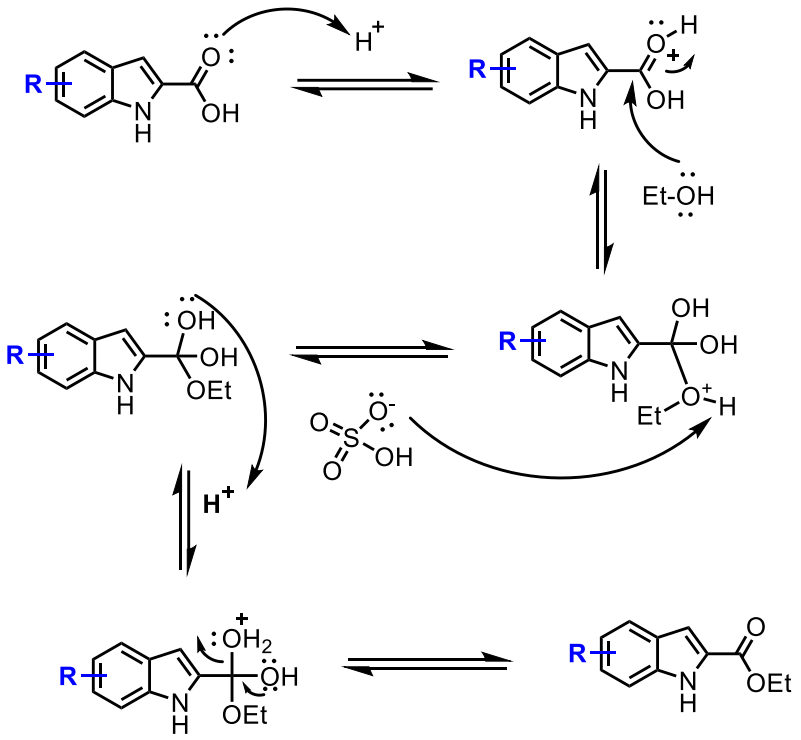

Figure 3-1: Fisher esterification of indole-2-carboxylic acids.

3.2.2. Preparation of ethyl 1-(2-oxo-2-phenylethyl)-1H-indole-2-carboxylates (4a-n)

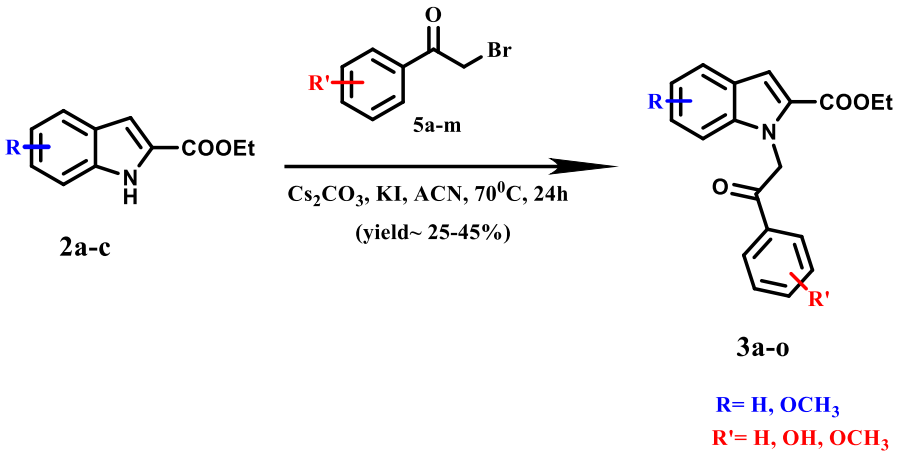

Scheme 3-3*:* Synthesis of ethyl 1-(2-oxo-2-phenylethyl)-1H-indole-2-carboxylates 4a-n

Ethyl-1-(2-oxo-2phenylehyl)-1H-indole-2-carboxylates (**4a-n**) were synthesized by coupling ethyl indole-2-carboxylates (**2a-c**) with 2-bromoacetophenones (**3a-m**) in the presence of CS_2CO_3 and KI as a catalyst under reflux as shown in Scheme 3-3. This reaction provided moderate to good yields (14-45%).

This coupling reaction follows S_N2 type mechanism and can be written as follows:

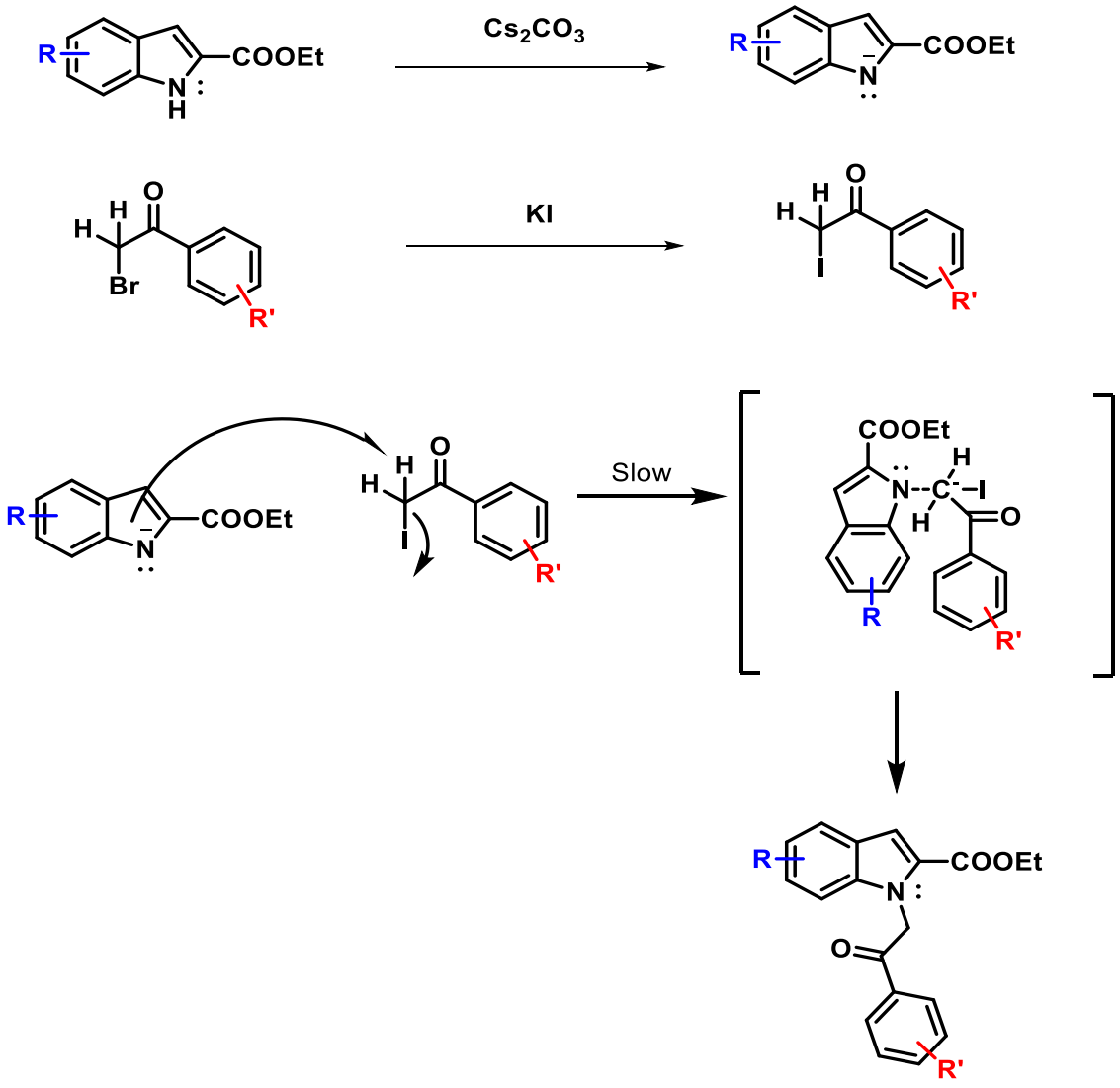

Figure 3-2*:* The reaction mechanism of ethyl indole-2-carboxylate and Bromo acetophenone coupling

3.2.3. Preparation of 3-phenylpyrazino[1,2-*a*]indo-1-(*2H*)-ones (*PPI*s) 5a-n

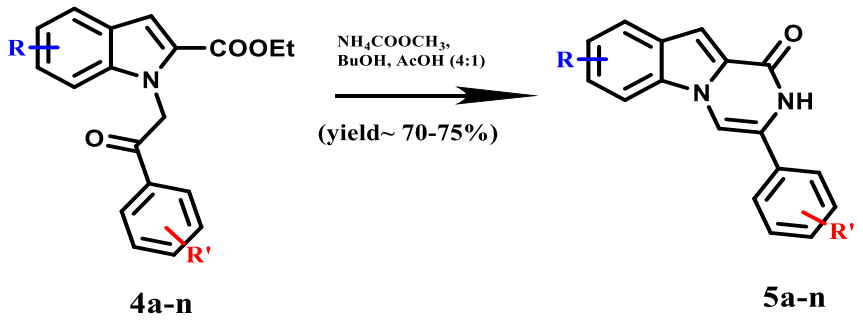

4a-n **5a-n**

R=H, OCH_3

R'=H, OH, OCH_3

Scheme 3-4*:* Synthesis of 3-phenylpyrazino[1,2-*a*]indo-1-(*2H*)-ones

This is the last step in the preparation of target *PPI* compounds. We started by adding CH_3COONH_4 to ethyl 1-(2-oxo-2-phenylehyl)-1H-indole-2-carboxylates (**4a-n**) in *n*-BuOH and AcOH (4:1 ratio) in a pressure vial. The reaction mixture was then subjected to react under high temperature (150 ^{0}C using an oil bath) to afford the target compounds **5a-n** in good yields (65-75%). The proposed mechanism is given in Figure 3-3.

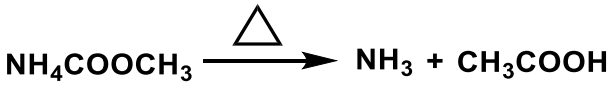

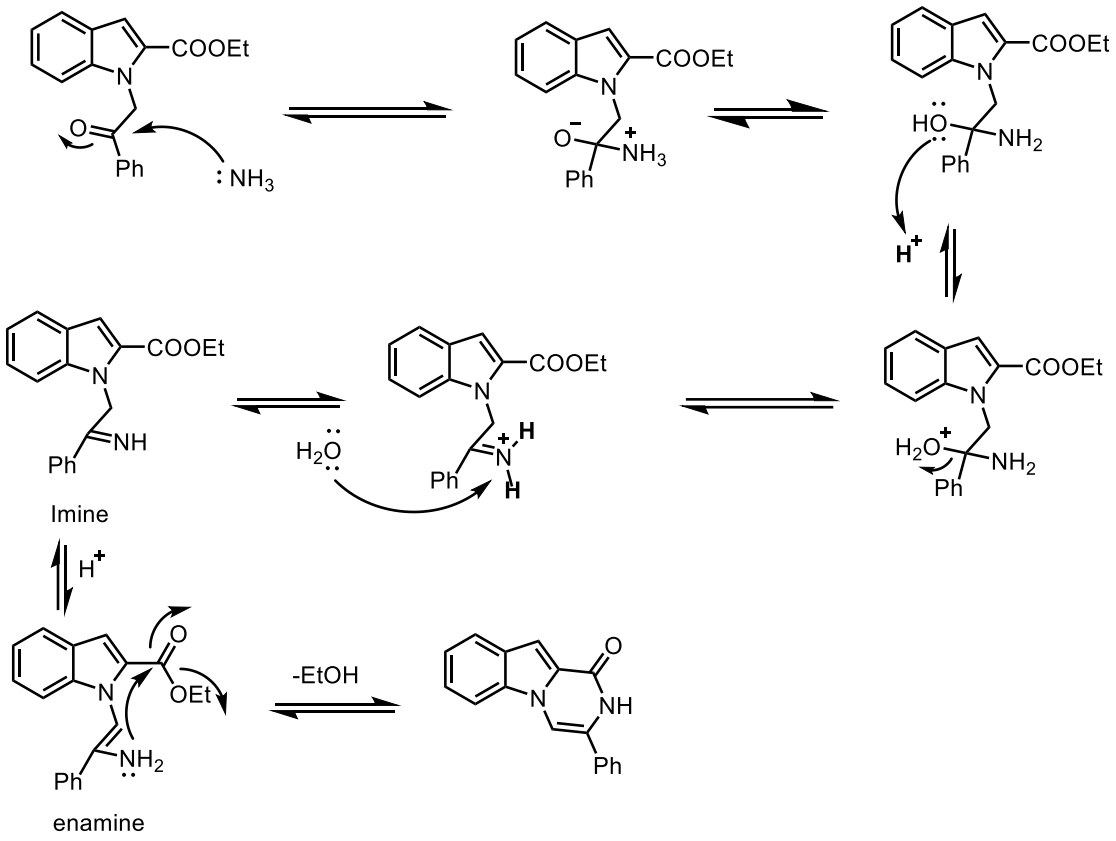

Figure 3-3*:* The proposed intramolecular cyclization of ethyl-1-(2-oxo-2-phenylehyl)-1H-indole-2-carboxylate to afford 3-phenylpyrazino[1,2-*a]*indo-1-(*2H*)-one

3.2.3.1 Preparation of substituted 2-bromo acetophenones (3a-m)

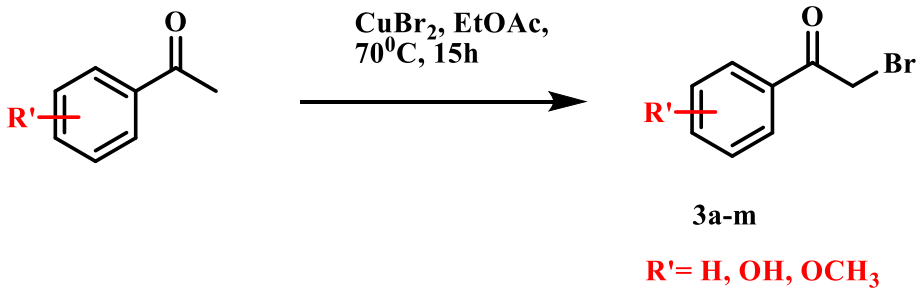

Scheme 0-5*:* Synthesis of 2-bromoacetophenones

All the 2-bromoacetophenones (**3a-m**) utilized in the synthesis were prepared in-house by brominating substituted acetophenones with $CuBr_2$ as the source of bromine (Scheme 3-5). The reaction was initiating by activating $CuBr_2$ in EtOAc under heating after which substituted acetophenones was added to the reaction mixture, and the reaction mixture was stirred under reflux conditions to afford 2-bromoacetophenones (yield range 70-90%). $CuBr_2$ mediated bromination can be explained by the following mechanism[102]:

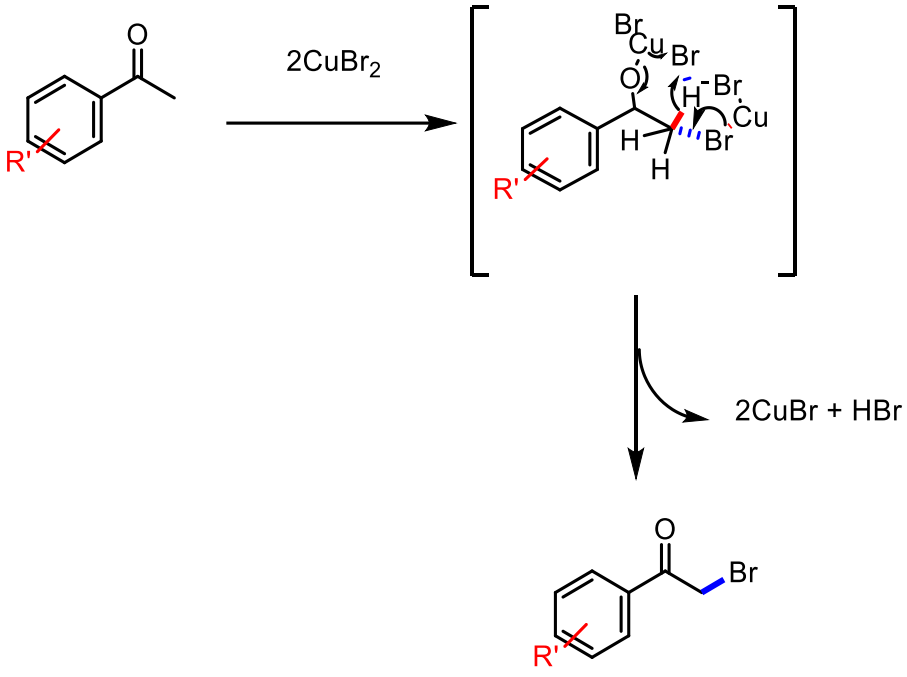

Figure 3-4*:* Reaction mechanism of acetophenone bromination

O-Tert-butyldimethylsilyl (O-TBDMS) protection of 2-bromo-hydroxyacetophenones

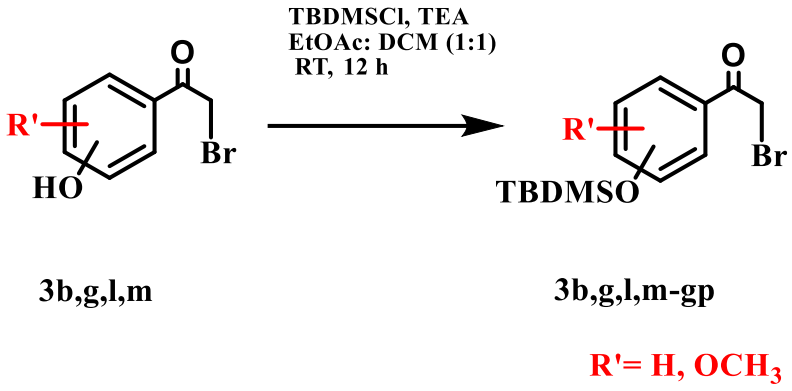

Scheme 3-6*:* OTBDMS protection of hydroxy acetophenone

To prevent the reactivity of hydroxy acetophenone during their coupling with the indole esters (**2a-c**, Scheme 3-3), the phenolic groups were protected using the TBDMSCl reagent as shown in Scheme 3-1. The reaction of hydroxy acetophenone with TBDMSCl in the presence of base triethylamine at r.t. Provided OTBDMS-protected Bromo acetophenones in good yields (~50%). The mechanism of which is as given in Fig 3.5.

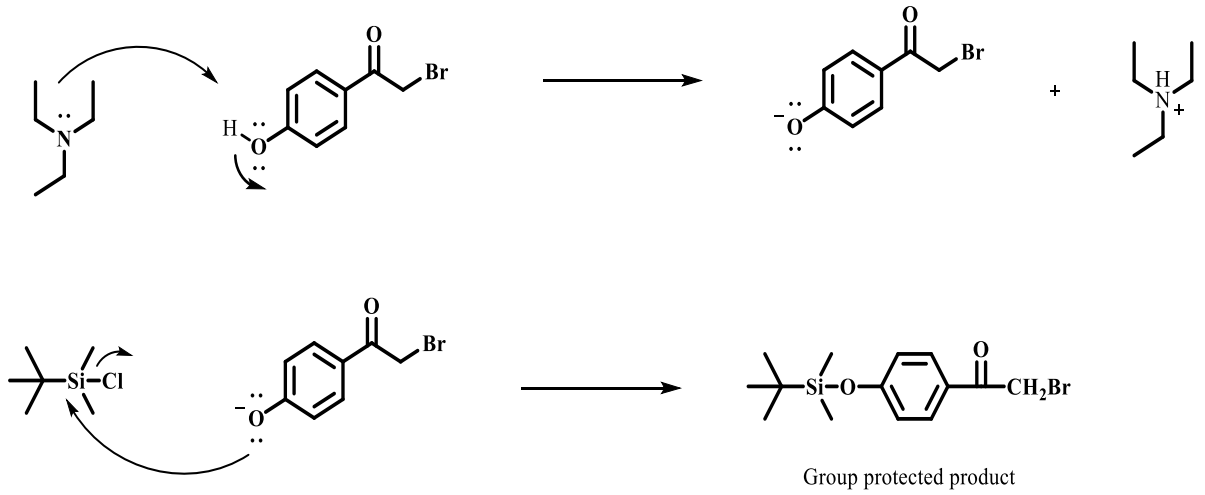

Figure 3-5*:* Reaction mechanism of OTBDMS protection

Deprotection of the OH group was done in the second step itself when the reaction mixture was washed with 1M HCl solution before washing it with conc brine solution. Additional washing with the HCl solution helped to remove the protecting group, giving the free –OH.

3.3. Biological assay methods

3.3.1 Cholinesterase (ChE) enzyme inhibition assays

In 1961, Ellman described an easy and rapid colorimetric method for defining the anticholinesterase activity of small organic molecules[103,104]. In this approach, sulfur analogs of ACh (ATCh- thioacetylcholine) and BuCh (BuTCh- thiol butyrylcholine) were used as substrates. In the absence of ChE inhibitors, these sulfur analogs were hydrolyzed by ChE to form thiocholine and respective acids (i.e. acetic acid and butyric acid). The thio-choline generated reacts with on dithiobis-(2-nitrobenzoic acid) (DTNB), to produce 2-nitro-5-thiobenzoic acid (NTB). The NTB is a yellow chromophore (Fig.3-6), which can be detected at a wavelength ranging from 405 nm to 412 nm. In the presence of an inhibitor, the generation of thiocholine by the hydrolysis of ATCh/ BuTCh gets reduced which can be quantified to determine ChE inhibition (IC_{50} values). Reference agents such as donapezil and rivastigmine were included for comparison of inhibitory potency of *PPI* derivatives.

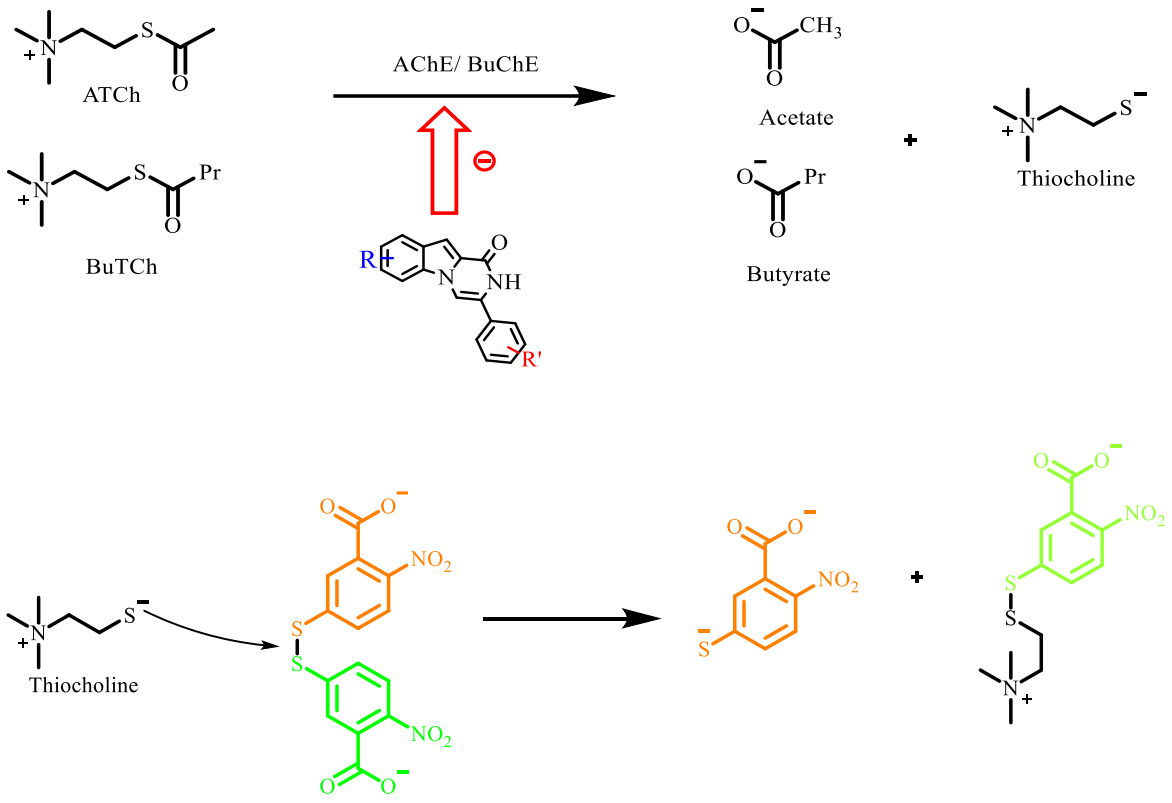

Figure 3-6: Principle of Ellman assay to determine ChE inhibition

3.3.2. Aβ aggregation inhibition assay

This method is based on the principle that a change in the intensity of the fluorescence is observed when fluorescent dyes such as thioflavin T (ThT) bind to the β-sheet structure of Aβ which can be monitored at 450 nm (Excitation wavelength) and 490 nm (emission wavelength)respectively[105,106]. A linear correlation between the relative fluorescence unit (RFU) and the aggregation process can be made[106]. Molecules which can inhibit the aggregation of Aβ in solution when ThT is present will result in lower relative fluorescence units (RFU's) and molecules which cannot inhibit the aggregation of Aβ or, which can induce the aggregation of Aβ will have a higher RFU. Hence, a linear relationship can be observed by monitoring fluorescence — Higher RFU value indicates the inability of the molecule to slow or inhibit the Aβ aggregation. The assay

was conducted using Aβ40/42. The known Aβ aggregation inhibitor orange G was used as a reference compound.

3.3.3. Molecular modeling

Molecular docking studies of *PPI* derivatives were performed using Discovery Studio (DS) Structure-Based-Design, version 4.0 (BIOVIA, San Diego, U.S.A). For performing the docking studies, X-ray crystal structure of AChE (PDB:4EY7), BuChE (PDB: 2XQJ), $A\beta_{40}$ (PDB:2LMN) and $A\beta_{42}$ (2NAO) were obtained from RCSB protein data bank. To the enzyme structure, hydrogens were added. Test compounds were built in 3D using Build Fragment tool, and energy minimization were performed for 1000 iterations using steepest descent and conjugate gradient minimizations respectively. The CDOCKER algorithm in the receptor-ligand interactions was used to dock the molecules with appropriate enzymes after defining a 15 Å sphere radius within the enzyme which covers all the active site amino acids. CHARMm force field was used for the docking studies. The quality of ligand-enzyme complex was evaluated based on CDOCKER Interaction energy and CDOCKER energy in kcal/mol. Also, polar and nonpolar interactions were visualized to assess the critical interactions involved in compound binding with the respective enzyme/ protein.

3.3.4. Anti-oxidant activity

The ability of *PPI* derivatives to scavenge and neutralize free radicals was determined by using a stable free radical 2,2-diphenyl-1-picrylhydrazyl (DPPH)[107,108]. DPPH radical in solution appears to be purple in color with strong absorbance at 517nm. The neutralization of this radical by an antioxidant source results in the formation of a stable DPPH species which have a very weak absorbance at 517 nm (Fig. 3-7).[109] Trolox and resveratrol were used as reference agents.

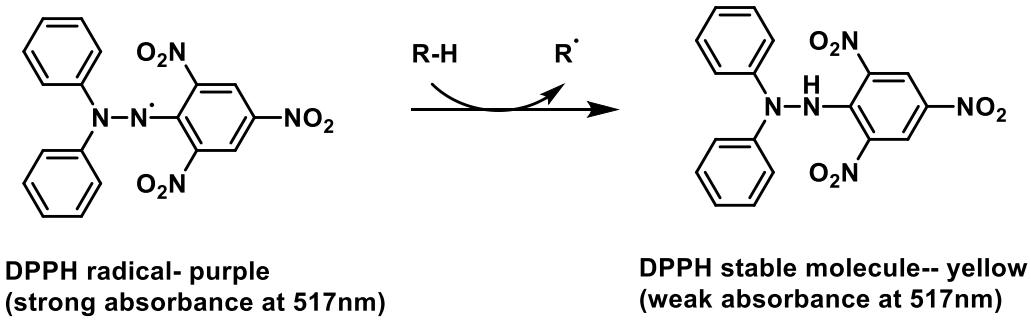

Figure 3-7*:* Scavenging of DPPH radical to form stable DPPH molecule.

3.3.5: Transmission electron microscopy (TEM)

To assess the morphology of amyloid beta protein after the incubation of the protein with or without the presence of synthesized compounds, transmission electron microscopy (TEM) is used. TEM imaging assay results were used to support the results obtained from the Aβ aggregation kinetics assay. Images obtained from TEM can be used to explain the mechanism of Aβ aggregation by comparing the images of Aβ alone as well as the morphology of the Aβ observed when an aggregation inhibitor is present.[110,111]

Chapter 4. Results and Discussion

4.1 Introduction

As discussed in Chapter 2, the primary aim of this research project was to synthesize a compound library based on *PPI* template, acquire SAR data and assess its anti-AD potential.

In this segment, we will discuss the observed biological activities of the compound library toward ChE enzymes, amyloid protein $A\beta_{40/42}$ aggregation properties and their antioxidant properties. We will also support our results with TEM experiments (for supporting anti-$A\beta_{40/42}$ aggregation properties) as well as in silico molecular docking studies to understand the binding interactions (for ChE inhibition properties and anti- $A\beta_{40/42}$ aggregation properties). Best molecular candidates will be those compounds which can exhibit ChE inhibition properties, inhibit aggregation of Aβ and exhibit antioxidant properties.

4.1.1: Cholinesterase (ChE) enzyme inhibition assays: The ability of the synthesized *PPI* compound library (**5a-q**) to exhibit cholinesterase inhibition activity was the first and foremost biological evaluation performed. Known ChE inhibitors donepezil and rivastigmine were used as reference agents. We expect the compounds based on *PPI* template to show dual AChE/ BuChE inhibition properties. Our modeling studies suggest that *PPI* derivatives would be more specific to inhibit AChE than BuChE due to the difference in the active size of these enzymes. This difference has been explained previously in Section: **1.8.3.1** (Chapter 1).

The anti-AChE/ BuChE data is shown in Table 4-1. The results have been presented as IC_{50} values which define the amount of compound required to inhibit the activity of the compound by 50%[112]. Other parameters such as partition coefficient (clogP), selectivity index, and molecular volume have also been included.

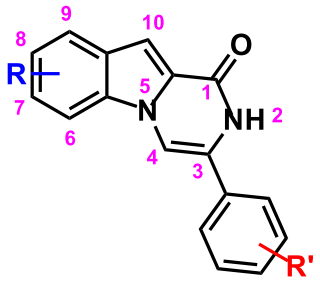

S.No.	Cmpd. Name	R	R'	IC_{50} AChE (μM)	IC_{50} BuChE (μM)	ClogP	MV(Å^3)
1.	**5a**	H	H	8.73 ± 0.17	19.81 ± 0.99	3.69	189.67
2.	**5b**	H	4-OH	7.7 ± 0.74	19.82 ± 1.7	3.14	207.17
3.	**5c**	H	4-OMe	7.53 ± 0.32	18.40 ± 0.46	3.67	216.08
4.	**5d**	H	3,4-diOMe	7.47 ± 0.54	15.18 ± 0.62	3.39	243.52
5.	**5e**	H	3-OMe	7.56 ± 0.79	> 50	3.67	218.49
6.	**5f**	H	3,4,5-triOMe	7.21 ± 0.53	17.98 ± 0.70	3.01	294.97
7.	**5g**	H	3-OH	7.01±0.31	19.59± 0.2	3.14	199.28
8.	**5h**	H	2-OMe	7.30 ± 0.41	1.9 ± 0.03	3.11	220.2
9.	**5i**	H	2,4-diOMe	7.67 ±0.72	21.42 ± 1.1	3.18	244.21
10.	**5j**	H	2.5-diOMe	7.91 ± 0.72	17.07 ± 0.07	3.18	243.52
11.	**5k**	H	4-OH, 3-OMe	8.7 ± 0.42	>50	2.97	231.18
12.	**5l**	H	3-OH, 4-OMe	7.60 ± 0.97	>50	2.97	232.89
13.	**5m**	9-OMe	H	7.18±0.61	>50	3.65	216.43
14.	**5n**	8-OMe	H	6.34±0.27	>50	3.67	218.14
15.	**Donepezil**			0.003 ± 0.001	3.6 ± 0.7	4.59	321.7
16.	**Rivastigmine**			8.57 ± 0.014	12.29 ± 0.65	2.62	226.3

Table 4-1: Compiled data for compounds **5a-n** (a) IC_{50} data for against AChE/ BuChE, (b) CLogP values (c) Selectivity index of **5a-n** towards AChE against BuChE (d) Molecular volume of the compounds **5a-n.**

IC_{50} values of the compounds presented in the table are the mean of three separate experiments (n = 3), and the standard deviation is represented as (± values) from its average value. ClogP values were calculated using ChemDraw Professional software from CambridgeSoft company. Molecular volume (MV) was calculated using Discovery Studio program from BIOVIA Inc (San Diego, CA).

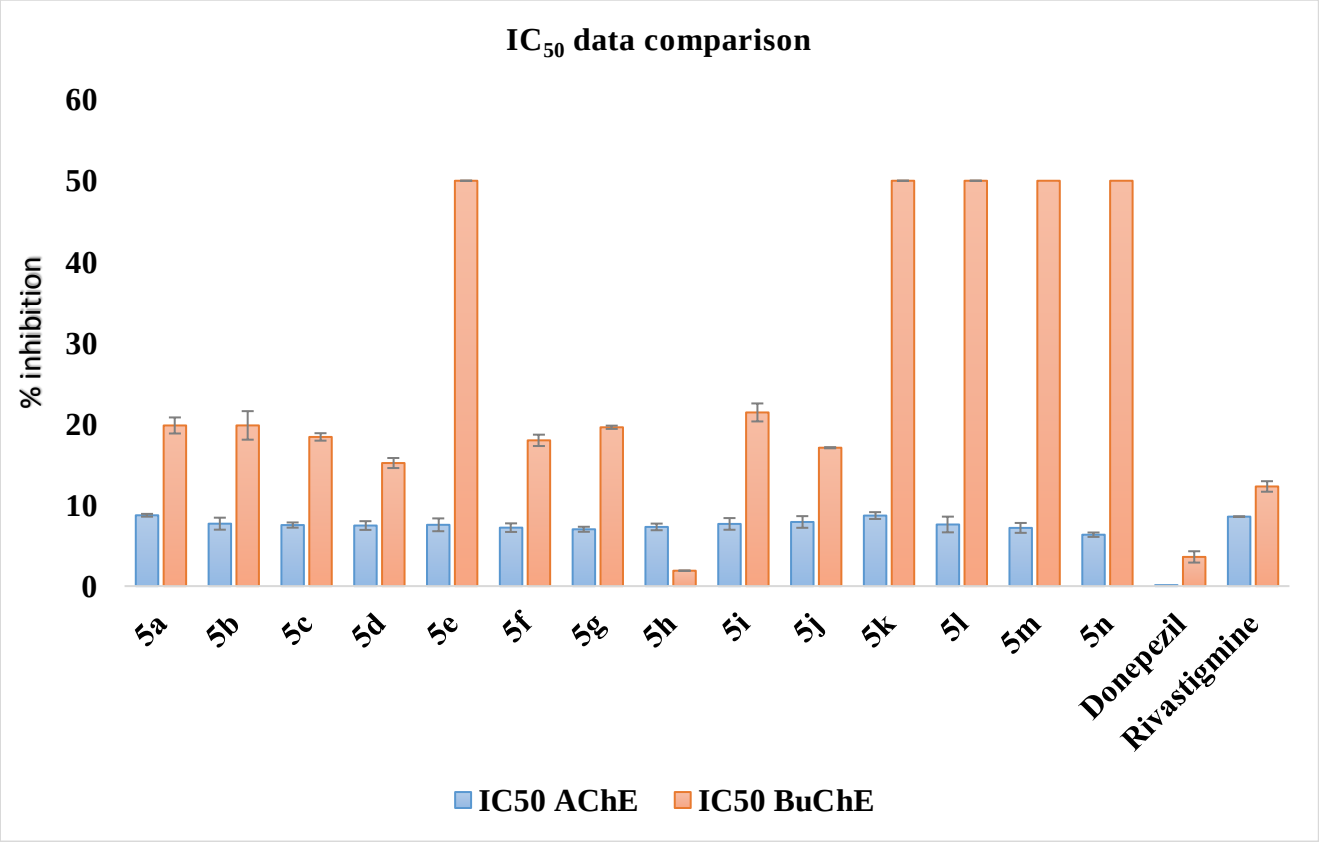

Figure 4-1: Bar graph of AChE and BuChE inhibition profile of PPI derivatives 5a-n. Results are expressed as average of three independent experiments (n=3)

The OMe substituted compounds became the largest subset of the substitutions made at the C3 phenyl moiety as well as at position C8 and C9 of the indole moiety in the *PPI* ring system. Under this subset, seven compounds were synthesized, and their activity was compared. In the C3 phenyl substituted series of compounds, it was interesting to note that almost all of them showed similar activity (by comparing the IC_{50} values) toward AChE. The IC_{50} range was between 7 to 8 μM (Table 4-1, Figure 4-1) which were similar to that of rivastigmine (IC_{50} ~8.5 μM). This similarity in the activities of these compounds towards AChE can be explained by the fact that, the volume of AChE active site is narrow and small (~302 $Å^3$), while the molecular volume of the compounds lies in the range of (189.69$Å^3$ to 294.97$Å^3$). Thus, C3 methoxy-substituted compounds **5c, 5d, 5e, 5f, 5h, 5i, 5j** exhibited a similar range of activity and were not potent inhibitors of AChE compared to donepezil (AChE IC_{50} = 3nM, Table 1). In contrast, much weaker inhibitory activity was observed when the compounds were tested against BuChE (Table 4-1, Figure 4-1) and most of the compounds were less potent compared to their AChE inhibition profile. In general, the inhibition activity ranged from 15-21 μM with few compounds not exhibiting any inhibition at the maximum concentration tested (IC_{50} < 50 μM, Table 1, Fig. 4-1). In the BuChE SAR, it appears that the C3 phenyl substituents contributed in enhancing BuChE inhibitory potency with the unsubstituted C3 phenyl containing compound **5a** (Table 1) exhibiting weak BuChE inhibition (IC_{50}~ 20 μM) whereas increasing the size this ring led to gradual improvements in BuChE inhibitory potency with compound **5c** (R^1 = 4-methoxyphenyl; BuChE IC_{50} = 18.4 μM) and **5d** (R^1 = 3,4-dimethoxyphenyl; BuChE IC_{50} = 15.1 μM) exhibiting better inhibition (Table 1).

The addition of a C3 3,4,5-trimethoxyphenyl ring (compound **5f**) did not further improve the activity toward BuChE (IC_{50}~ 18 μM). Interestingly, compound **5h** (3-(2-methoxyphenyl)pyrazino[1,2-*a*]indol-1(*2H*)-one) was the most potent BuChE inhibitor in this

series (BuChE IC_{50} = 1.90 μM, Table 4.1) and was almost 1.8-fold more potent compared to the reference agent donepezil (BuChE IC_{50} = 3.60 μM). At this point, we are not able to explain the reason for this observation. It is plausible that the intramolecular interaction with the OMe and NH of pyrazinone (Fig. 4-2) can potentially lock compound **5h** in a favorable conformation within the BuChE active site. Molecular docking of **5h** in BuChE is discussed later in this chapter.

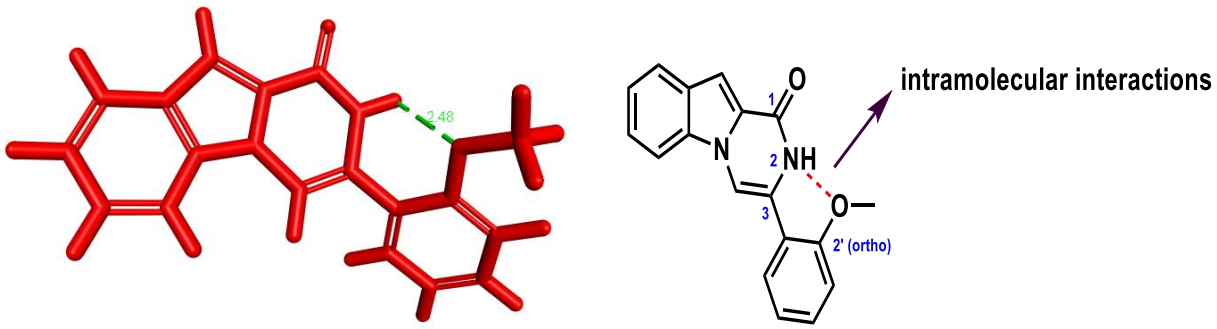

Figure 4-2: Proposed intramolecular interaction of ortho-OMe substituent with pyrazinone

The corresponding regioisomers **5n** and **5m** which had substituents at either C8 or C9 position (on the indole ring) that exhibited similar AChE inhibition properties as C3 phenyl substituted compounds with IC_{50} values of 7.18 μM and 6.34 μM respectively for compounds **5n** and **5m**. Interestingly, both of these compounds were found to be inactive against BuChE (IC_{50} > 50 μM, Table 4.1).

To incorporate antioxidant properties, we included phenolic groups at the C3 position (compounds **5b** and **5g**, Table 4.1). These compounds were able to exhibit dual ChE exhibition and did not show any significant difference compared to the unsubstituted compound **5a** (**5b**: IC_{50} AChE= 7.7 μM, IC_{50} BuChE= 19.82 μM; **5g**: IC_{50} AChE=7.01 μM, IC_{50} BuChE= 19.59 μM, Table 4.1). In

contrast, incorporation of another antioxidant pharmacophore viz: 4-hydroxy-3-methoxyphenyl or 4-methoxy-3-hydroxyphenyl substituents at the C3 position provided selective inhibition of AChE in compounds **5k** and **5l** (AChE IC_{50} ~ 7.7 μM; BuChE IC_{50} < 50 μM).

4.1.2: Molecular docking of 5m and 5d using AChE enzyme

The binding interactions of best candidates with ChE inhibition was investigated by molecular docking experiments. The most potent AChE inhibitor **5m** (IC_{50} ~ 6.3 μM) was investigated using the known x-ray crystal structure of human AChE enzyme (Figure 4-3). It was observed that the compound **5m** was mostly interacting with the amino acids present in the PAS- Trp286, Tyr124, Asp74, andTyr341. Strong hydrogen bonding was found between the C1 carbonyl oxygen and the –OH of Tyrosine341 amino acid (distance~ 2Å), as well as between NH at 2^{nd} position and carbonyl carbon of the Asp74 (distance ~2.9Å). Even though it was present very close (distance~ 3.6Å) from to the His447 (part of the catalytic triad), no interactions were observed between the **5m** and the amino acids of the catalytic triad in AChE.

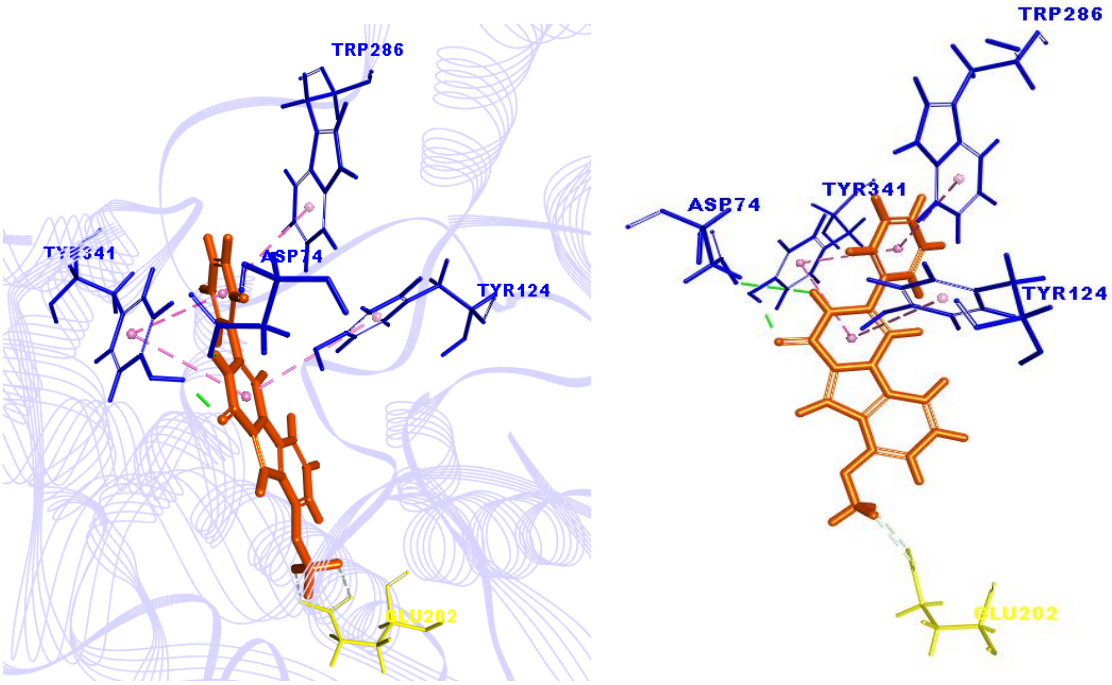

Figure 4-3: The binding mode of compound **5m** in the active site of human AChE enzyme.

Next, we investigated the binding interactions of the dual ChE inhibitor **5d** in the active site of AChE (Figure 4-4). It was interesting to note the orientation of compound **5d** in the active pocket of the hAChE enzyme. The tricyclic ring system was found to be away from the catalytic triad (distance from His447~ 3.9Å), and no interactions were found between the tricyclic ring and the catalytic triad. Rather, the tricyclic ring system was found closer to the acyl pocket (~ 3Å from Phe295), PAS (~ 5.5 Å from Tyr124) and the hydrophobic subsite (~4.8Å and 5.2 Å from Trp86 and Tyr337 respectively). While the C3 diOMe-phenyl ring was found to interact with the Tyr124 via pi-pi T-shaped interactions (distance ~ 5.2 Å) in the PAS. This study shows that the 3,4-dimethoxyphenyl ring orients are closer to the PAS region and exhibit bivalent inhibition of AChE enzyme.

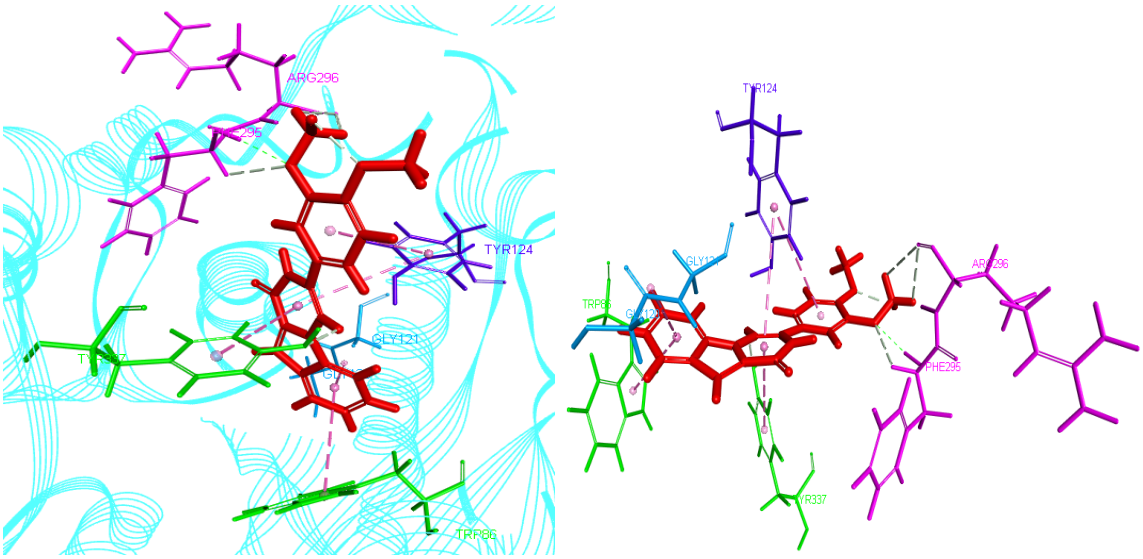

Figure 4-4: The binding mode of compound **5d** in the active site of human AChE enzyme.

Molecular docking of 5h in the active site of BuChE enzyme

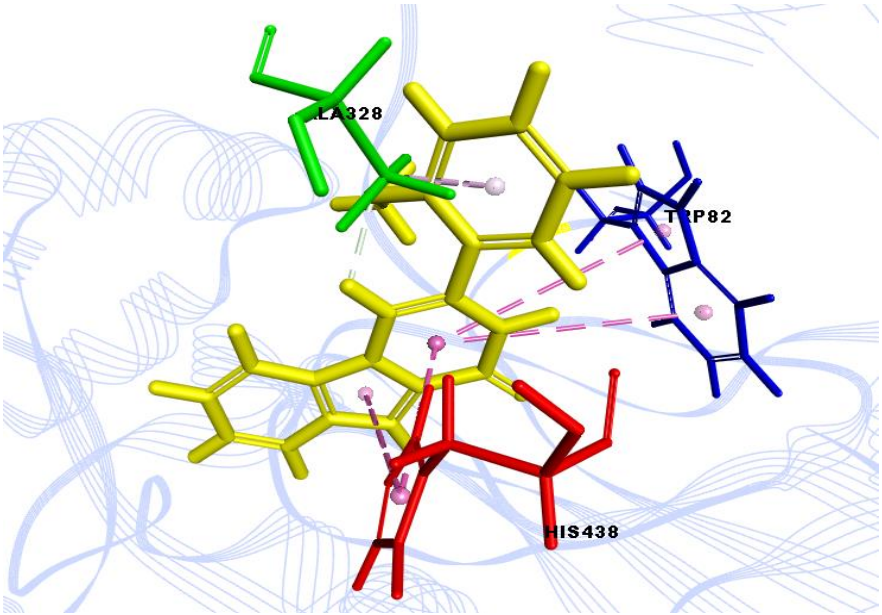

Figure 4-5: The binding mode of compound **5h** in the active site of human BuChE enzyme.

Mode of interaction of compound **5h** with *h*BuChE (PDB: 1POI) has been depicted in fig. 4-5. It was observed that the tricyclic moiety was in proximity (distance ~ 4.4 Å) to the catalytic triad of

the BuChE enzyme and was interacting with the His438 (part of the catalytic triad) via pi-pi-T stacking interactions. Compound **5h** also targeted the choline binding site (Trp82) via pi-pi-T stacking interactions (distance ~ 5.6 Å). Due to the ability of 5h to target both catalytic triads as well as choline binding site resulted in its capacity to block the activity of BuChE.

4.1.3: Conclusions: Our results indicate that majority of the *PPI* derivatives evaluated exhibit dual cholinesterase inhibition with some compounds exhibiting selective AChE inhibition. Among, the compounds synthesized, compounds **5e**, **5k,** and **5l** were identified as selective AChE inhibitors with IC_{50} values ranging from ~7-9 μM. Compound **5h** was recognized as the most potent BuChE inhibitor (IC_{50} = 1.9 μM) and was 1.8-fold more potent compared to the reference agent donepezil. In this *PPI* library compound **5h** (Fig. 4-6) was identified as the best compound with dual AChE/ BuChE inhibition profile (AChE IC_{50} =7.3 μM; BuChE IC_{50} =1.9 μM). Some of the best compounds from the series are highlighted in Fig.4-6. These studies show that *PPI* derivatives do have ChE inhibition properties. However, they exhibit weak inhibition profile compared to marketed ChE inhibitors (e.g., donepezil). Nevertheless, the study suggests that *PPI* template is amenable to further SAR optimization.

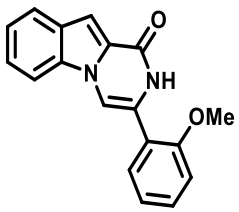

5h

IC_{50} AChE = 7.3 μM

IC_{50} BuChE = 1.9 μM

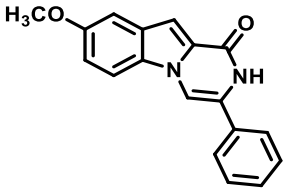

5n

IC_{50} AChE = 6.3 μM

IC_{50} BuChE = >50 μM

Figure 4-6: Chemical structures of best *PPI* derivatives with ChE inhibition

4.2: Amyloid-beta aggregation inhibition studies

After estimating the anti-ChE activity of synthesized compounds, *PPI* derivatives **5a-n** were further evaluated for their ability to inhibit aggregation of $A\beta_{1\text{-}40/42}$ by using ThT based fluorescence. The test compounds were tested at three different concentrations of 1, 5 and 25 μM. The results are presented as average % inhibition ± s.d. n = 3 for three independent experiments and were compared with the known inhibitor orange G.

4.2.1: Activity of *PPI* derivatives toward $A\beta_{1\text{-}40}$ aggregation

The % inhibition of compounds **5a-n** at 1, 5 and 25 μM have been summarized in Table 4.2.

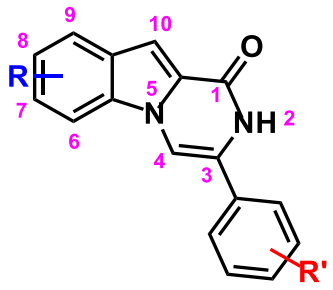

Compound	R	R'	% inhibition at 1 μM	% inhibition at 5 μM	% inhibition at 25 μM
5a	H	H	60.7	62.8	67.4
5b	H	4-OH	41.6	59.3	63.0
5c	H	4-OMe	32.4	42.9	50.9
5d	H	3,4-diOMe	49.9	56.2	83.3
5e	H	3-OMe	41.6	37.5	17.6
5f	H	3,4,5-triOMe	23.2	43.2	52.9
5g	H	3-OH	7.8	29.8	74.4
5h	H	2-OMe	33.0	40.1	67.7
5i	H	2,4-diOMe	48.7	55.5	71.9
5j	H	2.5-diOMe	42.6	29.2	19.2
5k	H	4-OH, 3-OMe	61.7	53.9	58.4
5l	H	3-OH, 4-OMe	41.1	40.0	42.5
5m	9-OMe	H	P.A.	14.5	32.7
5n	8-OMe	H	1.6	13.0	43.4
Orange-G			51.8	57.2	59.0

Table 4-2: $A\beta_{1-40}$ aggregation inhibition activity of *PPI* derivatives **5a-n**.

The results are expressed as average ± SD (n = 3) for three independent experiments. The aggregation kinetics assays were carried out using a ThT-based fluorescence assay (excitation = 440 nm and emission = 490 nm) in the presence of 5 μM of $A\beta_{1-40}$ in phosphate buffer pH 7.4 at 37 ºC with shaking over a period of 24 h.

Compounds with OMe substituents at either C3 phenyl or indole ring (**5m-o**) exhibited good $A\beta_{40}$ aggregation inhibition properties (compounds **5c-f**, **5h-j**, **5m** and **5n**). Compound **5d** with a C3 3,4-dimethoxyphenyl substituent exhibited superior anti-$A\beta_{40}$ aggregation property at all the tested

concentrations (~ 50%, 56% and 83% inhibition of aggregation at 1, 5 and 25 μM respectively, Table 2). The C3 phenyl unsubstituted compound **5a** exhibited good aggregation properties at all the concentrations. However, there were no significant changes observed in the concentration range tested with 60-67% inhibition seen (Table 4-2). Both compounds **5a** and **5d** exhibited superior inhibition at 25 μM (67% and 83% inhibition respectively, Table 4.2) compared to the reference agent Orange G (59% inhibition, Table 4-2). Replacing the C3 3,4-di-OMe-phenyl substituent in **5d** with a 2,4-di-OMe-phenyl substituent in **5i** reduced the anti-Aβ aggregation activity compared to **5d**, although the compound **5i** did exhibit better activity compared orange G at 25 μM (71.9% inhibition). Interestingly, the presence of a 2,5-di-OMe-phenyl substituent in compound **5j** led to a gradual decline in its anti-aggregation activity as the compound concentration was increased from 1 to 25 μM (19.2% at 25 μM; Table 4.2). Addition of a C3 3,4,5-trimethoxyphenyl substituent (compound **5f**) provided anti-Aβ aggregation activity (23-53% inhibition, Table 4.2). However, it was not as potent as the di-OMe substituted derivatives **5d** and **5i**. Mono OMe substitution at the C3 phenyl (compounds **5c** and **5e**) showed weaker inhibition of Aβ aggregation compared to the 2,4-/3,4-di-OMe and 3,4,5-tri-OMe-phenyl substituted derivatives. The presence of phenolic groups in compounds **5b** (63% inhibition) and **5g** (74% inhibition) provided better inhibition compared to the corresponding OMe derivatives **5c** and **5e** (Table 4.2). The presence of OMe substituent at either the C8 or C9 position (indole ring) in compounds **5n** and **5m** exhibited weaker inhibition of Aβ aggregation (33% and 43% inhibition at 25 μM) about the OMe substituted derivatives at the C3 phenyl ring (Table 4.2). Incorporation of both OH and OMe substituents at the C3 phenyl rings (compounds **5k** and **5l**) led to retention of Aβ aggregation inhibition properties with compound **5k** exhibiting similar activity (58% inhibition at 25 μM) as the reference agent orange G (Table 4.2). The aggregation kinetics profile of the

best *PPI* inhibitor **5d** is shown in Figure 4.4(b) and is compared with orange G kinetics (Figure 4.4(a)). In the absence of test compounds, the $A\beta_{40}$ aggregation kinetic curve follows a sigmoidal pattern (represented as 100% control- yellow line, Figure 4.4). This pattern can be divided into various phases representing (a) a lag phase (flat line till ~ 10 h mark), (b) growth phase- exponential growth in the aggregation of the peptide, and (c) saturation phase- corresponding to stabilization of Aβ fibril formation. A compound which can decrease the intensity of the fluorescence at these phases can be considered as an inhibitor of $A\beta_{1\text{-}40}$ aggregation.

Orange G exhibits a concentration-dependent decline in the fluorescence intensity which indicates its ability to reduce $A\beta_{1\text{-}40}$ fibril load. At 25 μM, it was able to reduce the growth and saturation phase significantly suggesting its ability to interact with various $A\beta_{1\text{-}40}$ aggregates and prevent fibril formation (Figure 4.7 (a)). The aggregation kinetics profile of **5d** exhibited a similar trend with a concentration-dependent decline in the fluorescence intensity (Figure 4.7 (b)). Compound **5d** was able to prevent the growth phase and reduce $A\beta_{1\text{-}40}$ aggregation similar to orange G. The kinetic aggregation curves suggest that compound **5d** is capable of interacting with lower order $A\beta_{1\text{-}40}$ aggregates and prevent their self-assembly into higher order structures.

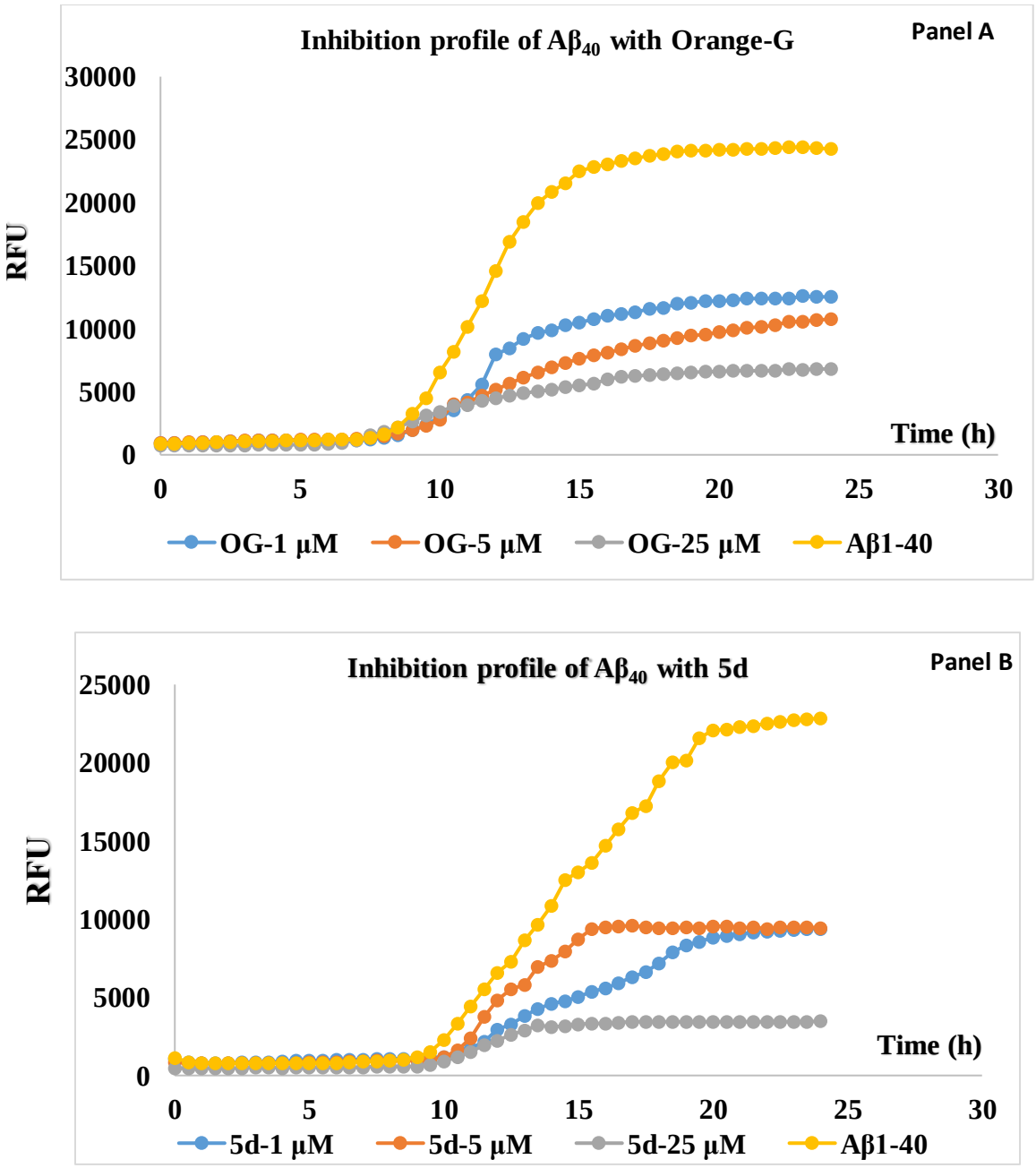

Figure 4-7: (a) Aggregation kinetics of orange G at 1, 5 and 25 µM in the presence of $A\beta_{1-40}$ (5 µM) over a period of 24 h in phosphate buffer pH 7.4, at 37 ºC; (b) Aggregation kinetics of compound **5d** at 1, 5 and 25 µM in the presence of $A\beta_{1-40}$ (5 µM) over a period of 24 h in phosphate buffer pH 7.4, at 37 ºC

4.2.2: Molecular docking studies of *PPI* derivatives with $A\beta_{1-40}$

Compound **5d** was found to be the most potent compound in the series with ~85% inhibition at 25 μM for $A\beta_{40}$ aggregation. Compound **5d** was studied for its interaction with dimer and fibril models of the $A\beta_{40}$ peptide (PDB:2LMN). Molecular docking of **5d** with dimer model of the $A\beta_{40}$ is given in Fig.4-8 and 4-9. It was observed that 5d was interacting with both the C- and N-terminal amino acids of the dimer assembly. $A\beta_{40}$ forms a "U" shaped conformation which consists of a long arm, a short arm and the bend which connects the long and the short arm. The long arm spans the region made up of amino acids Asp1 to Val24 followed by amino acids Gly25 to Lys28 which forms the turn region of the peptide. The short arm of the dimer model consists of amino acids Gly29 to Val40. [53,113]

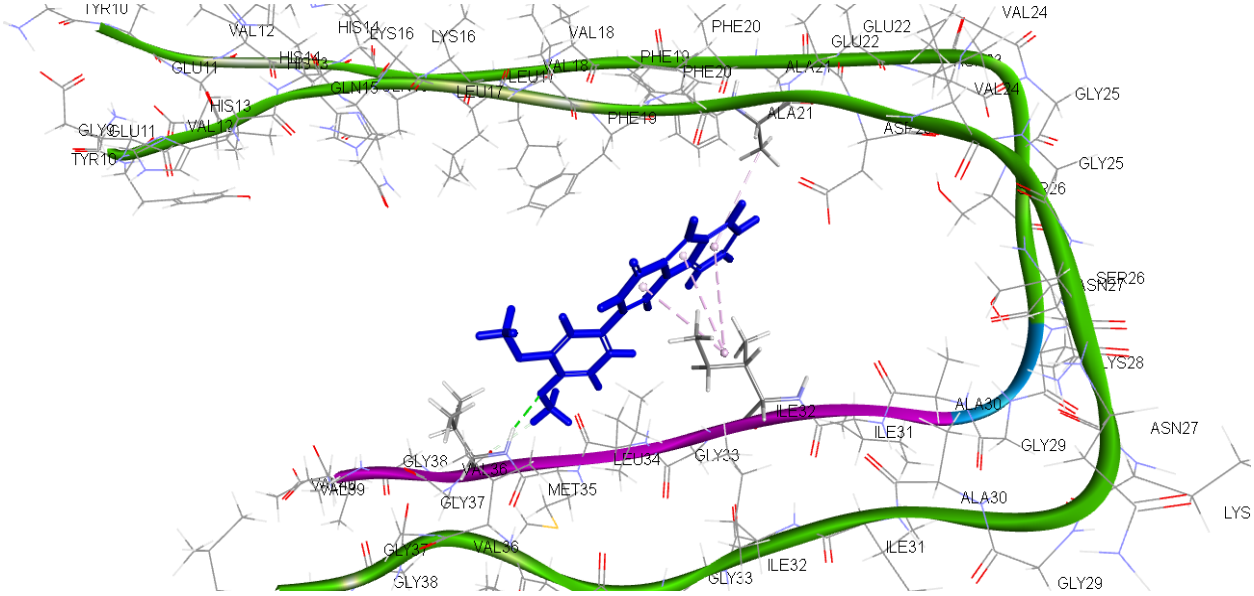

Figure 4-8: Molecular docking studies of compound 5d with the dimer model of $A\beta_{1-40}$

5d was observed to interact with Ala21 (part of the long arm) via pi-alkyl interactions (distance ~4.8Å). Ala21 also forms the part of the KLVFFA region in Aβ which is known to be the seeding point of the Aβ aggregation. The interaction of **5d** with Ala21 could be crucial in its ability to prevent $A\beta_{40}$ aggregation. At the C-terminal end, pi-alkyl interactions were observed with Ile32 (distance ~4.4Å), and strong hydrogen bonding was seen between OMe group of **5d** and the NH and the carbonyl (C=O) groups of Val36 (distance~ 2.4Å). These interactions might stabilize the dimer assembly and prevent further aggregation.

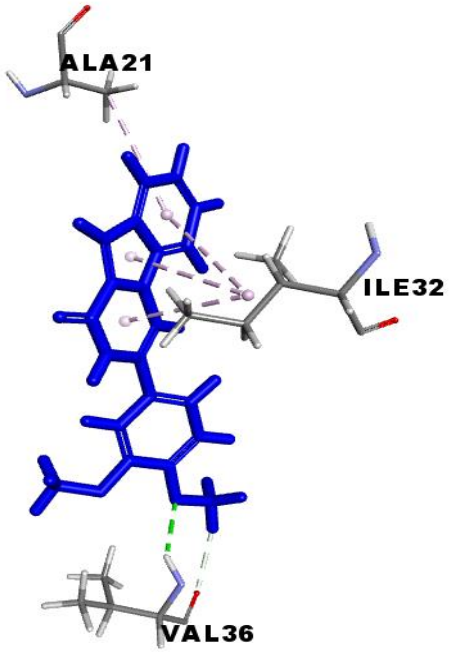

Figure 4-9: A Closer look at the interactions of 5d with amino acids present in $A\beta_{1-40}$ dimer model.

Docking studies of compound **5d** with the fibril model of $A\beta_{9-40}$ (PDB:2LMN) (Fig. 4-10) show that the compound can interact at the steric-zipper interface between individual oligomer assembly.

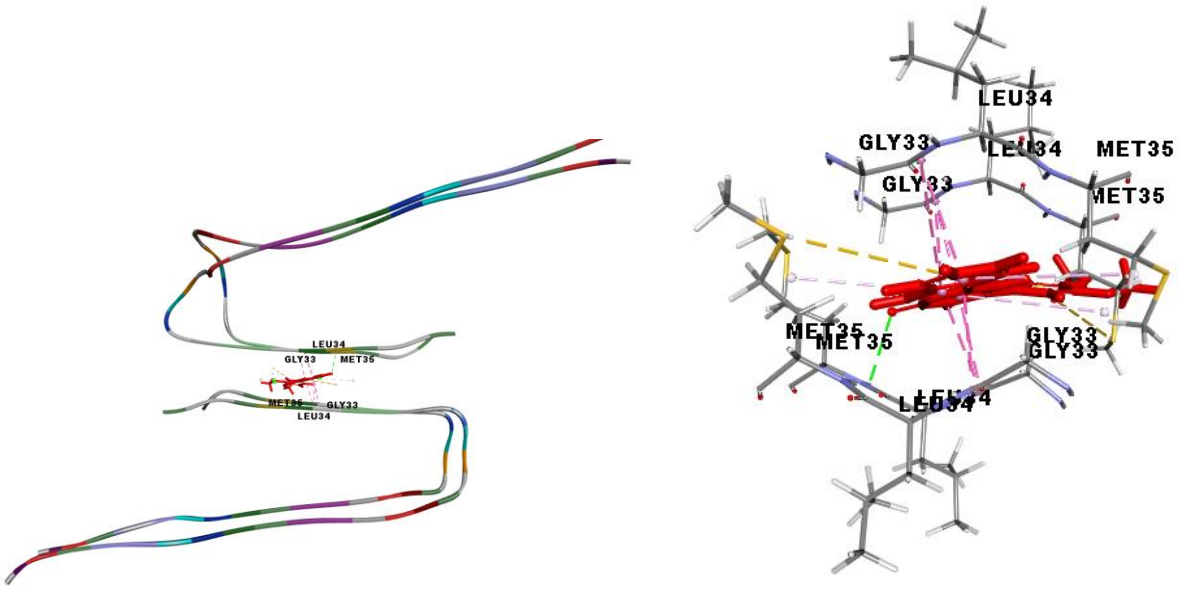

Figure 4-10: Molecular docking studies of compound 5d with (a) Fibril model of $A\beta_{9-40}$ (b) Closer look at the interactions of 5d with amino acids present in $A\beta_{9-40}$ fibril model.

Compound **5d** was found to be primarily interacting with the C-terminal amino acids of the $A\beta_{40}$ peptide sequence i.e. Gly33 to Met35. Amide-Pi stacking between the Gly33, and Leu34 with compound **5d** was found to be the most favorable type of interactions with an average distance of ~3.8Å. Strong hydrogen bonding (distance~2.9Å) between the carbonyl oxygen at the C1 position with the free NH group of the Leu34 made the molecular assembly between **5d**- $A\beta_{9-40}$ fibril structure stable. Compound **5d** also formed pi-sulfur interactions with Met35 (distance~ 5.6Å), which is known to play an important role in the reduction of metal ions such as Cu^{2+} and Fe^{3+}. This reduction of metal ions is known to initiate Aβ induced oxidative stress cascade.[31,67,70] These observations suggest that the *PPI* derivative **5d** can interact with the $A\beta_{40}$ fibril assembly potentially preventing its conversion to higher order fibrils and plaques

4.2.3: Activity of *PPI* derivatives toward $A\beta_{1-42}$ aggregation

The $A\beta_{42}$ aggregation studies for *PPI* derivatives **5a-n** were conducted at four different concentrations (1, 5, 10 and 25 μM) and compared with orange G and resveratrol. In general *PPI* derivatives exhibited better inhibition of $A\beta_{42}$ at all concentrations tested compared to their inhibition profile toward $A\beta_{40}$. The results are summarized in Table 4-3.

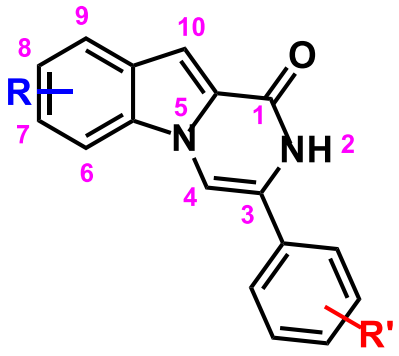

Compound	R	R'	% inhibition at 1 μM	% inhibition at 5 μM	% inhibition at 10 μM	% inhibition at 25 μM
5a	H	H	34.7	40.0	64.3	75.8
5b	H	4-OH	36.5	56.7	70.1	76.3
5c	H	4-OMe	40.0	51.9	63.1	70.5
5d	H	3,4-diOMe	41.7	48.9	67.8	90.0
5e	H	3-OMe	*P.A.*	1.5	***N.D***	10.7
5f	H	3,4,5-triOMe	57.4	45.1	56.6	72.9
5g	H	3-OH	*P.A.*	8.4	32.4	54.2
5h	H	2-OMe	52.1	43.9	66.1	93.8
5i	H	2,4-diOMe	61.2	59.9	80.7	***N.D***
5j	H	2.5-diOMe	55.8	44.2	52.5	71.1
5k	H	4-OH, 3-OMe	41.5	48.6	64.4	62.7
5l	H	3-OH, 4-OMe	34.3	61.1	73.3	74.5
5m	9-OMe	H	*P.A.*	*P.A.*	*P.A.*	*P.A.*
5n	8-OMe	H	*P.A.*	35.6	N.D.	54.2
Orange-G			59.0	69.4	79.4	90.0
Resveratrol			72.3	82.5	87.8	91.3

Table 4-3: $A\beta_{1-42}$ aggregation inhibition activity of *PPI* derivatives **5a-n**

The results are expressed as average ± SD (n = 3) for three independent experiments. The aggregation kinetics assays were carried out using a ThT-based fluorescence assay (excitation = 440 nm and emission = 490 nm) in the presence of 5 μM of $A\beta_{1-42}$ in phosphate buffer pH 7.4 at 37 ºC with shaking over a period of 24 h. ***N.D*** – Not determined, *P.A.*- promotes aggregation.

The C3 phenyl substituted compound **5a** exhibited a gradual increase in $A\beta_{42}$ inhibition with the maximum inhibition seen at 25 μM (75.8% inhibition, Table 4-3). Incorporating OMe groups at either ortho, meta or para-position of the C3 phenyl ring provided contrasting results with compound **5c** exhibiting a concentration-dependent inhibition whereas **5e** exhibited either none or weak inhibition at 25 μM (Table 4.3). Compound **5h** showed excellent inhibition (93.8% inhibition at 25 μM) and exhibited better inhibition compared to the reference agents orange G and resveratrol (Table 4.3). The presence of di-OMe substituents in compounds **5d** (Fig. 4-11(b)), **5i** and **5j** provided good to excellent inhibition ranging from 40-90% (Table 4-3). The presence of 3,4,5-tri-OMe phenyl substituent in **5f** provide consistent and good inhibition of $A\beta_{42}$ aggregation at all the compound concentrations tested (45-73% inhibition range, Table 4.3). The presence of phenolic groups at the C3 position provided mixed results with the compound **5b** (R^1 = 4-hydroxyphenyl) exhibiting similar inhibition profile as the unsubstituted compound **5a** (R^1 = phenyl, Table 4-3), whereas compound **5g** (R^1 = 3-hydroxyphenyl) was less potent compared to **5b**. The C7 and C8 OMe substituted compounds (indole ring) **5m** and **5n** showed either no or weak inhibition (Table 3). In other SAR modification, the presence of either a C3 4-hydroxy-3-methoxyphenyl or a 4-methoxy-3-hydroxyphenyl substituent provided good inhibition (compounds **5k** and **5l**, Table 4.3) at 25 μM with ~63% and ~75% inhibition respectively.

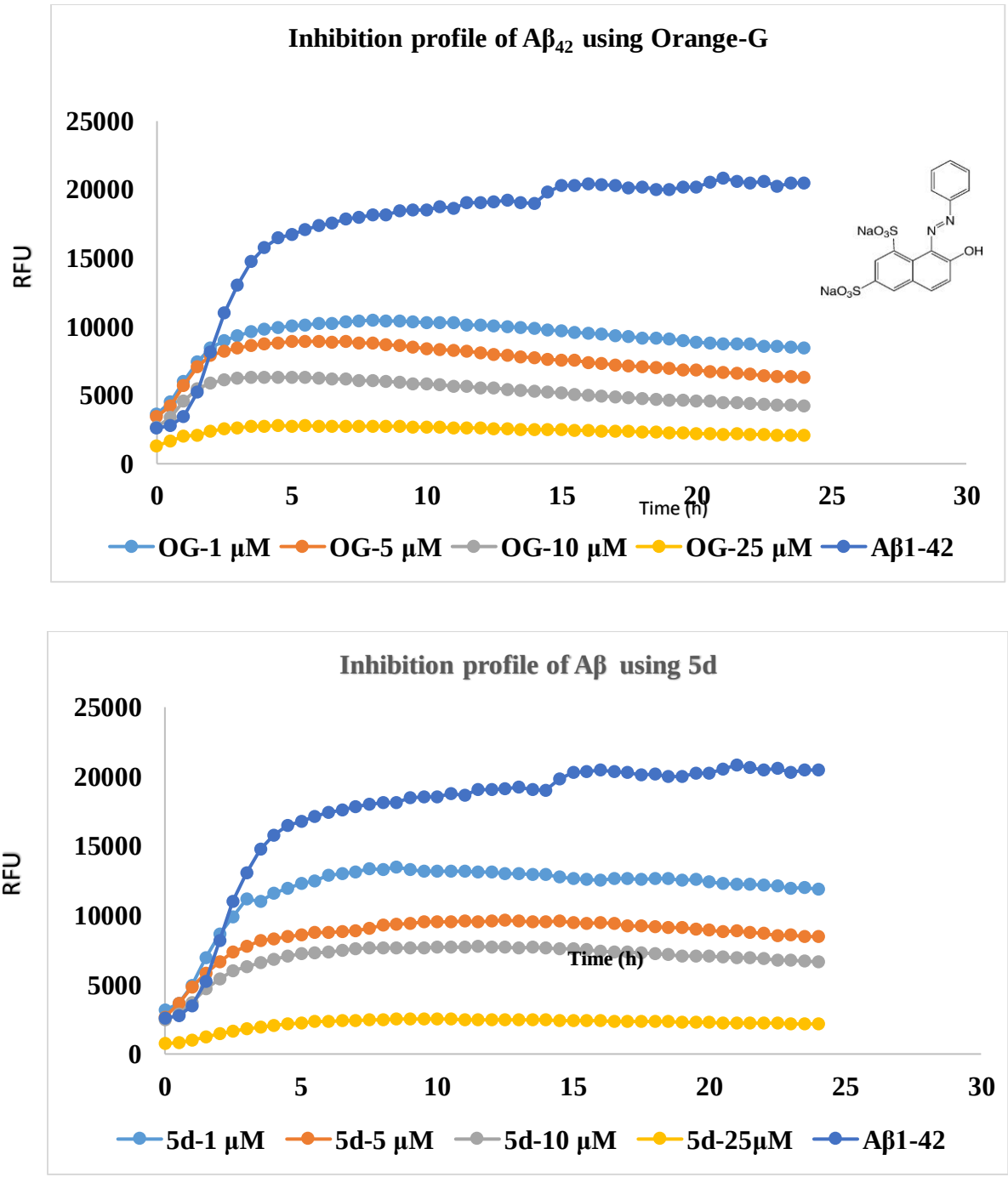

Figure 4-11: (a) Aggregation kinetics of orange G at 1, 5 and 25 µM in the presence of $A\beta_{42}$ (5 µM) over a period of 24 h in phosphate buffer pH 7.4, at 37 ºC; (b) Aggregation kinetics of compound **5d** at 1, 5 and 25 µM in the presence of $A\beta_{1\text{-}42}$ (5 µM) over a period of 24 h in phosphate buffer pH 7.4, at 37 ºC

4.2.4: Molecular docking studies of *PPI* derivatives with $A\beta_{1-42}$

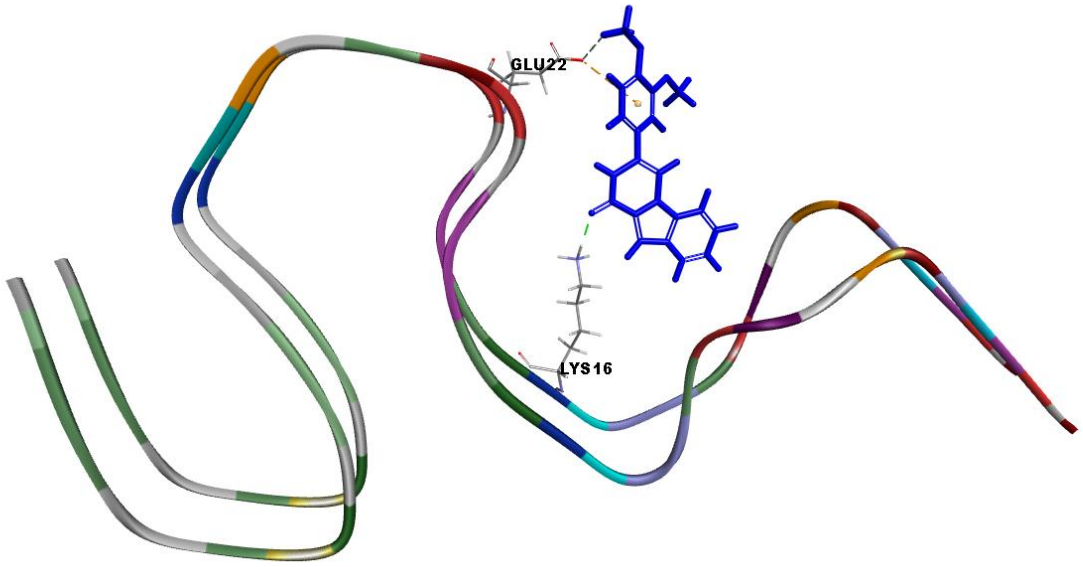

Figure 4-12: Molecular docking studies of compound 5d with dimer model of $A\beta_{42}$ (PDB:2NAO)

Compound **5d** was found to be the most potent compound in the series with ~90% inhibition at 25 μM for $A\beta_{42}$ aggregation. Compound **5d** was studied for its interaction with dimer models of the $A\beta_{42}$ peptide (PDB:2NAO). Molecular docking of **5d** with dimer model of the $A\beta_{42}$ is given in Fig. 4-12. It was observed that 5d was interacting with the KLVFFA region of the dimer assembly. **5d** was found to interact with Lys16 via hydrogen bonding interactions (distance ~1.85Å). Lys16 forms the part of the KLVFFA region in Aβ which is known to be the seeding point of the Aβ aggregation. The interaction of **5d** with Lys16 could be crucial in its ability to prevent $A\beta_{42}$ aggregation and might stabilize the dimer assembly.

4.2.5: Conclusions

Our studies show that *PPI* derivatives exhibit anti-Aβ aggregation properties. More significantly, they had activity toward both Aβ40 and Aβ42 peptides which is highly desirable as Aβ42 aggregates are known to be relative more toxic compared to Aβ40 aggregates (Reference). To our satisfaction, the core *PPI* template with a C3 phenyl ring (compound **5a**), itself exhibited dual inhibition of Aβ40/Aβ42 aggregation ranging from 67-76% inhibition at 25 μM. Furthermore, the presence of a C3 3,4-dimethoxyphenyl substituent in **5d** (3-(3,4-dimethoxyphenyl)pyrazino[1,2-*a]*indol-1(*2H*)-one, Fig. 4-13) provided excellent inhibition of both $A\beta_{40}$ and $A\beta_{42}$ aggregation with 83% and 90% respectively at 25 μM.

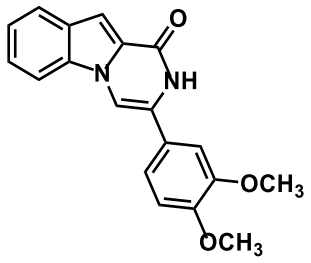

5d (3-(3,4-dimethoxyphenyl)pyrazino[1,2-*a]*indol-1(*2H*)-one)

% inhibition $A\beta_{40}$ (at 25 μM) = 83%

% inhibition $A\beta_{42}$ (at 25 μM) = 90%

Figure 4-13: Chemical structure of best *PPI* derivatives (**5d)** with best overall $A\beta_{40/42}$ inhibition profile.

4.3: Antioxidant activity

The antioxidant activity of some of the selected compounds was evaluated using DPPH assay method, and the results were compared with standard compounds with known antioxidant activity such as Trolox, resveratrol, and curcumin.[91,92] It was observed that compounds based on *PPI* template exhibit antioxidant activity as shown in Table 4.4. The C3 phenyl substituted compound **5a** itself exhibited antioxidant activity (33-34% DPPH scavenging, Table 4.4, Fig. 4-14) which suggests that the core *PPI* template itself has antioxidant activity. The phenolic compound **5b** exhibited better antioxidant activity (46% and 55% DPPH scavenging at 25 μM and 50 μM, Table 4.4) compared to **5a**. Compound **5d** which exhibited excellent $A\beta_{40/42}$ inhibition also exhibited good antioxidant activity (~48% DPPH scavenging at 50 μM). The best compound in the series was compound **5k** which possess an antioxidant pharmacophore at the C3 position (R^1 = 4-hydroxy-3-methoxyphenyl) and exhibited ~56% and 83% scavenging at 25 and 50 μM concentrations respectively. It was able to exhibit superior antioxidant activity compared to the known antioxidant resveratrol (49% and 64% DPPH scavenging at 25 μM and 50 μM, Table 4.4). These studies show that *PPI* templates possess inherent antioxidant activity and are a suitable system to design and develop multi-targeting agents to treat AD.

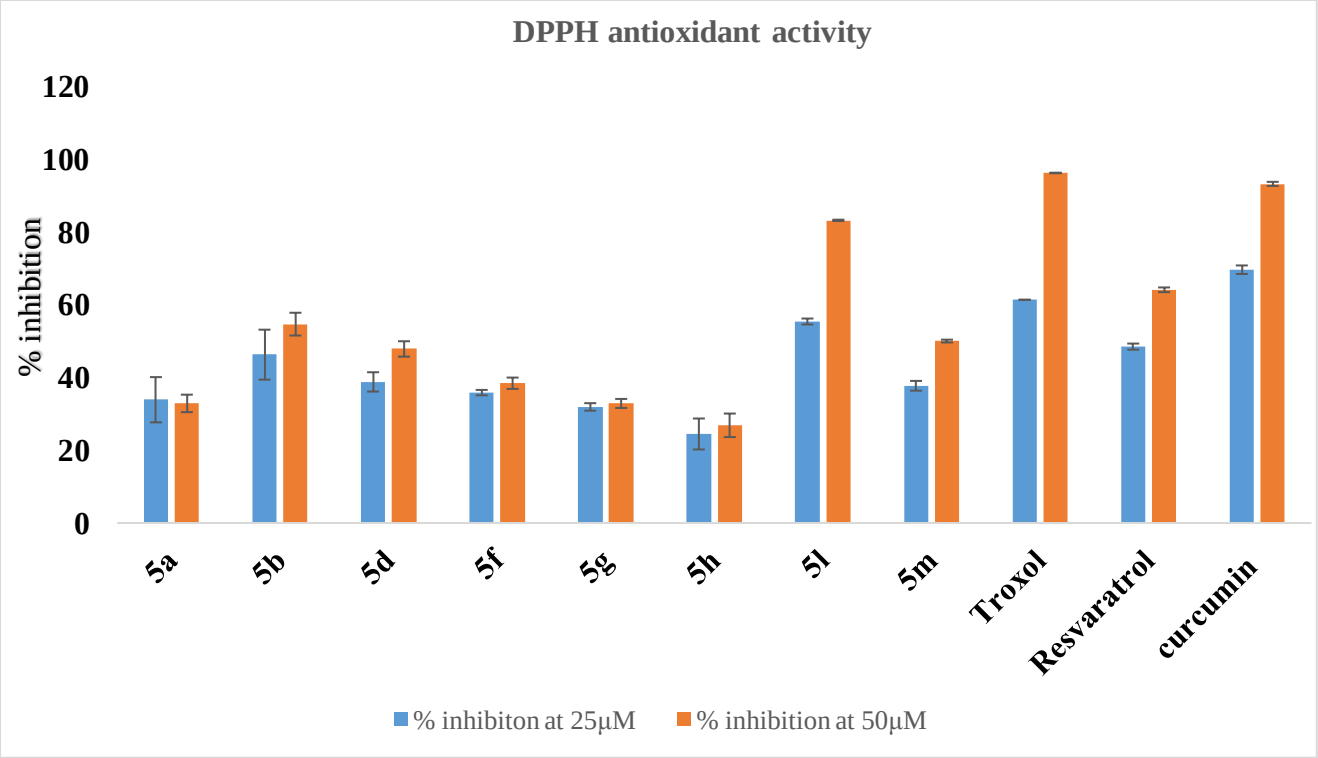

Figure 4-14: The antioxidant activity of *PPI* derivatives **5a**, **5b**, **5d**, **5f**, **5h**, **5k** and **5l** as % DPPH scavenging.

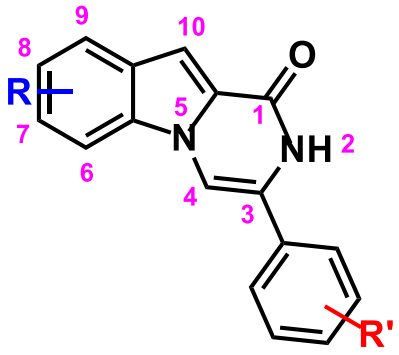

Compound	R	R'	% DPPH Scavenging at 25 μM	% DPPH Scavenging at 50 μM
5a	H	H	33.9	32.8
5b	H	4-OH	46.3	54.7
5d	H	3,4-diOMe	38.8	47.8
5f	H	3,4,5-triOMe	35.8	38.4
5g	H	3-OH	31.9	32.8
5h	H	2-OMe	24.4	26.8
5k	H	4-OH, 3-OMe	55.4	83.2
5l	H	3-OH, 4-OMe	37.7	50.0
TROLOX			61.4	96.2
Resveratrol			48.5	64.1
curcumin			69.6	93.2

Table 4-4: DPPH radical scavenging activity of *PPI* derivatives

Results are obtained as average ± s.d. (n = 3) for two independent experiments. The test compounds (25 and 50 μM) were incubated with DPPH (56 μM) at r.t for one h, and the absorbance was measured at 517 nm.

4.4: Transmission electron microscopy (TEM)

TEM imaging on Aβ peptides was carried out in the presence of best *PPI* derivatives based on the aggregation kinetics assay results to study Aβ aggregate morphology after 24 h of incubation at 37^0C.[110] A 1:1 ratio of Aβ (25 μM) to test compound (25 μM) was used to prepare copper mesh grids. The grids were analyzed and compared with a control group which did not include any test

compound. The images are shown in Figure 4-15. In the absence of test compounds $A\beta_{40}$ and $A\beta_{42}$ aggregates and forms fibrils when incubated at 37 ºC for 24 h (Figure4-15 (a) and (c)). In the presence of orange G (25 μM) a significant reduction is fibril content in seen (Figure4-15 (d)). Strikingly, in the presence of our best *PPI* compound **5d** and **5h**, we observed a drastic reduction in $A\beta_{40}$ $A\beta_{42}$ aggregation and fibril load (Figure4-15 (b) (e) and (f)) indicating its potent anti-aggregation effect. These studies show the anti-Aβ potential of *PPI* derivatives.

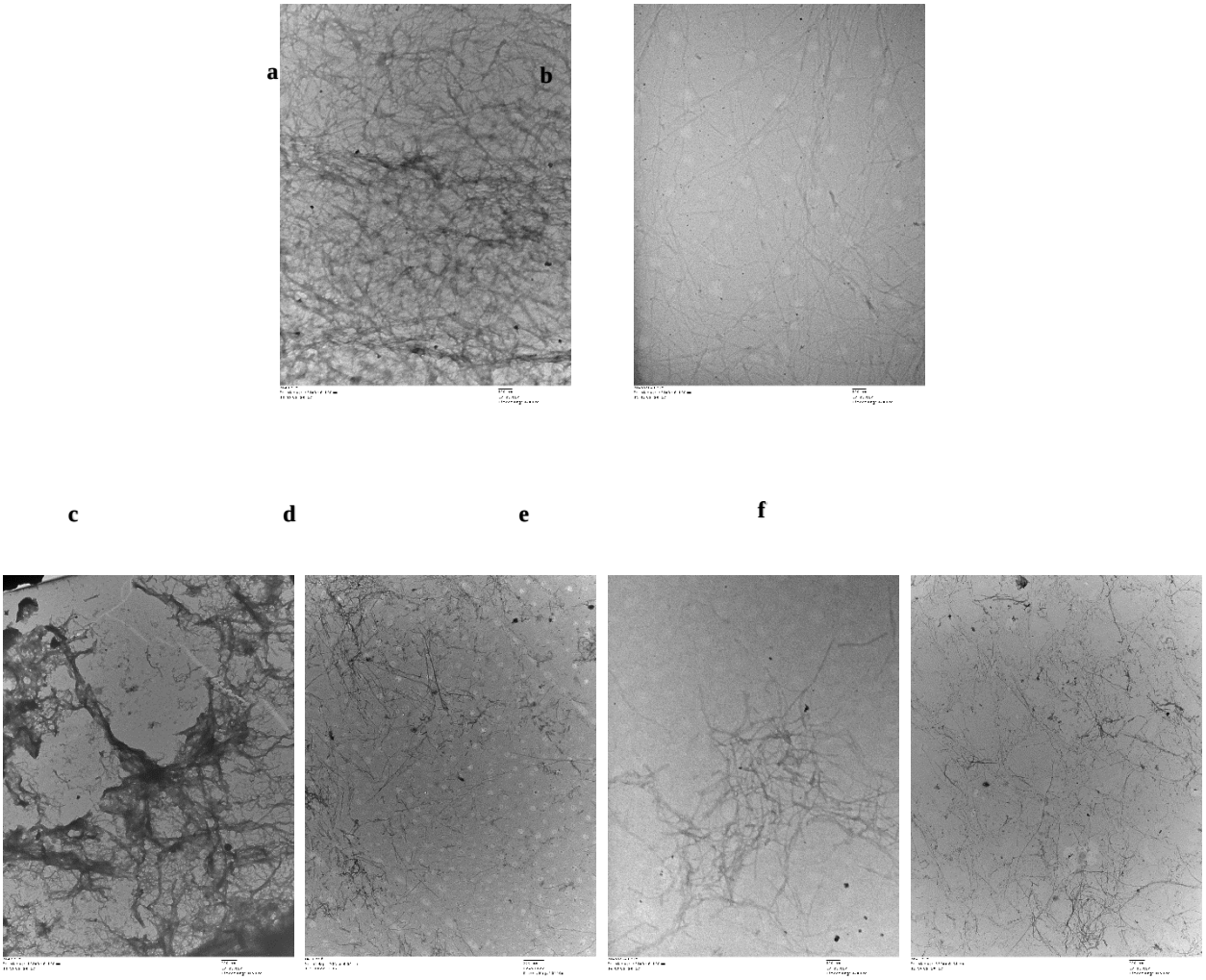

Figure 4-15: TEM images of $A\beta_{40}$ alone (a); $A\beta_{40}$ in the presence of 25 μM compound **5d**; (c) $A\beta_{42}$ alone; $A\beta_{42}$ in the presence of 25 μM orange G and (d); $A\beta_{42}$ in the presence of 25 μM of compound **5d** (e)**;** $A\beta_{42}$ in the presence of 25 μM of compound **5h** (f)

Chapter 5. Conclusions and Future Directions

5.1 Conclusions

This MSc thesis project embarked on the design and synthesis of small molecule library based on a 3-phenylpyrazino[1,2-*a]*indol-*1*(*2H*)-one (*PPI*) ring template as novel anti-AD agents. *PPI* compounds **5a-n** were synthesized using straightforward and efficient chemistry. The biological evaluation included the following in vitro assays: Cholinesterase enzyme (AChE/BuChE) inhibition assay, amyloid-beta ($A\beta_{40}$ and $A\beta_{42}$) aggregation inhibition assay and assessing their antioxidant properties.

The *PPI* template was considered based on the previous literature which has shown that fused tricyclic ring systems exhibit cholinesterase inhibition and preliminary modeling studies. Furthermore, research from Dr. Nekkar's lab and other groups has demonstrated that fused tricyclics rings can be modified by SAR studies to incorporate multi-targeting potential including dual cholinesterase inhibition, Aβ aggregation inhibition and antioxidant properties which are involved in AD pathophysiology. To assess the potency of the *PPI* ring system as a multi-target template for the modulation of different aspects of AD, compounds **5a-n** were synthesized with good yields (65-75%). In vitro biological evaluations for the synthesized compound library was carried out using previously developed and optimized protocols. The biological profiles for the synthesized compounds (**5a-n**) wase obtained using human AChE and BuChE enzymes, $A\beta_{40}$ and $A\beta_{42}$ aggregation inhibition, as well as antioxidant properties for selected compounds. Molecular modeling studies were also conducted to better understand the binding patterns of the compounds with ChE enzymes and Aβ. The $A\beta_{40}$/$A\beta_{42}$ aggregate morphology was evaluated in the presence

of *PPI* derivatives by TEM experiments. A brief summary of the physicochemical properties and biological activity data for the synthesized *PPI* compound library (**5a-n**) is given below:

Molecular Weights (MW): 189.69- 294.97 Å^3

Partition coefficient (ClogP): 2.97- 3.69

AChE Inhibition (IC_{50}): 6.3- 8.7 μM

BuChE Inhibition (IC_{50}): 1.9- 50 μM

$A\beta_{40}$ aggregation inhibition (%inhibition at 25 μM): 17.4- 83.3%

$A\beta_{42}$ aggregation inhibition (%inhibition at 25 μM): 10.2- 93%

Antioxidant capacity (% inhibition at 25 μM): 24- 55.4%

Antioxidant capacity (% inhibition at 50 μM): 26-83.2%

All the final compounds synthesized based on the novel *PPI* ring system (**5a-n**) showed moderate activity toward the AChE (IC_{50} = 6-9 μM). While only ~65% of the compounds (nine out of fourteen compounds synthesized) exhibited weak inhibitory properties towards BuChE (IC_{50} = ~15-20 μM). It was also observed that thirteen out of fourteen compounds showed some selectivity toward AChE inhibition, except for compound **5h** [3-(2-methoxyphenyl)pyrazino[1,2-*a*]indol-1(*2H*)-one] - which showed a strong BuChE selectivity with an IC_{50} value of 1.9 μM and it was the most potent BuChE inhibitor identified. Compound **5h** exhibited better BuChE inhibition that the reference drugs donepezil and rivastigmine. Compounds **5m** [9-methoxy-3-phenylpyrazino[1,2-*a*]indol-1(*2H*)-one] with -OMe substitution at C9 of the indole ring was the

most potent AChE inhibitor (AChE IC_{50} ~ 6.3 μM) and had no observed activity towards BuChE activity (IC_{50} > 50 μM). The best compound in the series which exhibited dual AChE/ BuChE inhibitory properties was compound **5h** (AChE IC_{50} = 7.3 μM; BuChE IC_{50} = 1.9 μM).

The *PPI* derivatives 5-o were also screened for their potential inhibitory properties toward the aggregation of $A\beta_{40}$ and $A\beta_{42}$. In the case of $A\beta_{40}$ aggregation inhibition, most of the compounds exhibited very good inhibitory properties (17-84% inhibition). About ~65% of the compounds (nine out of fourteen compounds synthesized) exhibited more than 50% inhibition in $A\beta_{40}$ aggregation at 25 μM. Compound **5d** [3-(3,4-dimethoxyphenyl)pyrazino[1,2-*a*]indol-1(2*H*)-one] was identified as the best compound in the series with ~84% inhibition of the $A\beta_{40}$ aggregation at 25 μM and was better than the reference agent orange G (~59% inhibition at 25 μM). All the synthesized compounds were also tested for inhibition of the $A\beta_{42}$ aggregation. Interestingly, more than 85% of the compounds (twelve out of fourteen compounds) exhibited more than 50% inhibition at 25 μM concentration. The average range of inhibition for $A\beta_{42}$ aggregation was observed to lie in the range of ~10 to 94%. Compounds **5d** [3-(3,4-dimethoxyphenyl)pyrazino[1,2-*a*]indol-1(2*H*)-one]and **5h** [3-(2-methoxyphenyl)pyrazino[1,2-*a*]indol-1(2*H*)-one] became the best compounds in the series with ~90% and 94% inhibition at 25 μM respectively. These results were found to be at par with the reference compounds orange G and resveratrol (~90% and 92% respectively, at 25 μM).

Eight out of fourteen synthesized compounds were also evaluated for their antioxidant properties using DPPH method. The *PPI* derivatives exhibit moderate to very good antioxidant properties at 25 μM (% DPPH scavenging: 24.5 to 55.4%) and 50 μM (% DPPH scavenging: 26.8 to 83%). The unsubstituted compound **5a** also exhibited ~34% antioxidant property. This can be attributed to the presence of the conjugated pyrazinone ring present which can form a stable radical after

reacting with the DPPH radical. The presence of a 4-hydroxy-3-methoxyphenyl pharmacophore in curcumin gives rise to its excellent antioxidant properties (% DPPH scavenging = 93.2% at 50 μM). Adding the same pharmacophore to **5a** at the C3 phenyl ring in compound **5k** [3-(4-hydroxy-3-methoxyphenyl)pyrazino[1,2-*a*]indol-1(*2H*)-one]), drastically improved the antioxidant properties (%DPPH scavenging = 83.2% at 50 μM). In conclusion, compounds based on a novel 3-phenylpyrazino*[*1,2-*a*]indol-*1*(*2H*)-one ring can be used to design small molecules to target the various AD pathologies. Although their cholinesterase inhibition activity is weak, they represent a promising class of compounds. Among them, two compounds, namely **5d** and **5h** exhibit multi-targeting potential in AD.

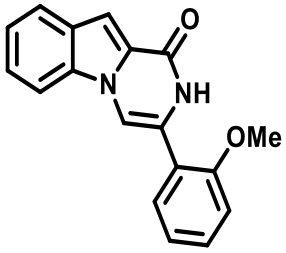

5h

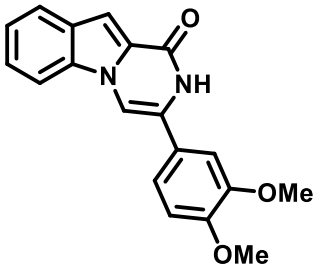

5d

IC_{50} AChE = 7.3 μM	IC_{50} AChE = 7.47 μM
IC_{50} BuChE= 1.9 μM	IC_{50} BuChE= 15.18 μM
% $A\beta_{40}$ inhibition ~ 65% (at 25 μM)	% $A\beta_{40}$ inhibition ~ 84.7% (at 25 μM)
% $A\beta_{42}$ inhibition ~ 94% (at 25 μM)	% $A\beta_{42}$ inhibition ~ 90% (at 25 μM)
Antioxidant capacity (% inhibition at 50 μM) ~47.8%	Antioxidant capacity (% inhibition at 50 μM) ~47.8%

5.2 Future Directions

- Establish toxicity profile of the best compounds identified such as **5d** and **5h** by conducting in vitro cell death assays.
- Structural modifications of compound **5h** by replacing the *ortho*-OMe-phenyl with 2,6-di-*ortho*-OMe-phenyl, *ortho*-OH-phenyl and 2,6-di-*ortho*-OH-phenyl substituents to understand the contribution of *ortho*-OMe toward BuChE selectivity.

Expansion of the compound library by structural modification of the *PPI* template. The addition of various groups at the C3 position such as substituted pyridine ring system or a five and seven-membered heterocyclic ring system (Figure 5.1) will provide SAR data on structure requirements for multi-targeting activity. Other proposed modifications include changing the steric and electronic properties at C4, C6, C7, C8, C9 and C10 positions.

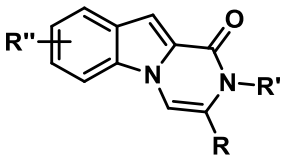

R = H

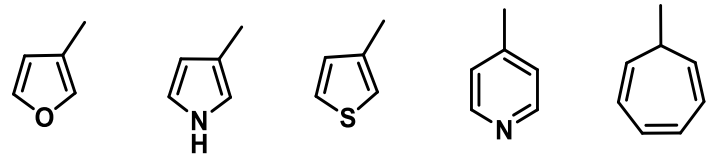

R' =H, -Me, -Et, *n*-alkyl

R'' = H, OH, Cl, NH_2, NHMe

Figure 5-16: Proposed SAR modification of *PPI* template (ClogP: 1.60- 3.41)

Chapter 6. Experimental

6.1 Chemistry

All the chemicals were purchased from Sigma-Aldrich® or Acros Organics® and were more than 95% pure and were used without further purification. Thin layer chromatography (TLC) was performed using silica gel 60 F_{254} (Merck), and spot visualization was done by short (254 nm) or long (365 nm) wavelength. Column chromatography was carried out using Merck 230-400 mesh silica gel. Melting points were determined using the digital melting point apparatus from REACH Devices, USA. ^{1}H and ^{13}C NMR were performed on a Bruker Avance spectrometer (Department of Chemistry, University of Waterloo) using $CDCl_3$ or DMSO-d_6 as the solvent. Coupling constants (*J*-values) were recorded in Hertz (Hz). Abbreviation used to represent NMR signals were s – singlet, d – doublet, t – triplet, m – multiplet, br – broad. Low-resolution mass spectrometry (LRMS) data was obtained using Single Quad LC-MS (1260 infinity model), Agilent Technologies. The purity of the compound was determined using Agilent 6100 series single quad LCMS equipped with an Agilent 1.8 µm Zorbax Eclipse Plus C18 (2.1 x 50 mm) running 30:70 Water: ACN with 0.1% FA with a flow rate of 0.2mL/min. All the final compounds (**5a-n**) were more than 95% pure.

General procedure for the synthesis of substituted ethylindole-2-carboxylates (2a-c)

100 mL round bottom flask was charged with 6.2 mmol of indole-2-carboxylic acids (**1a-c**). To the reaction flask, 40 mL of anhydrous ethanol was added along with 1ml of conc. H_2SO_4. The reaction mixture was refluxed for 24 h at 78 ^{0}C. After the reflux, the solvent was removed in vacuo to give the crude product which was then re-dissolved in 25 mL of ethyl acetate and then transferred into a separatory funnel. The organic layer was firstly neutralized with a saturated

$NaHCO_3$ solution, and then the organic layer was washed three times with 25 mL of saturated brine solution. The organic layer was then dried over anhydrous $MgSO_4$, and the solvent was removed in vacuo to yield the crude product which was then further purified using silica gel flash column chromatography using 100% DCM as an eluent.

Ethyl 1*H*-indole-2-carboxylate (2a): This compound was synthesized by esterification of **1a** as per the method given above to give white solid product. (83.8%), mp: 120-122°C. ^{1}H NMR ($CDCl_3$, 300 MHz): δ = 1.39 (t, 3H, *J* = 7.1 Hz), 4.37 (q, 2H, *J* = 7.1 Hz), 7.12 (t, 1H, *J* = 7.2 Hz), 7.24-7.22 (m, 1H), 7.29 (t, 1H, *J* = 7.0 Hz), 7.40 (d, 1H, *J* = 8.2 Hz), 7.69 (d, 1H, *J* = 8.0 Hz), 8.92 (br, 1H). LRMS (ESI) m/z calc for $C_{11}H_{11}NO_2$ ($[M + H]^+$);189.1 Found 190.2.

Ethyl 4-methoxy-1*H*-indole-2-carboxylate (2b): This product was purchased from Alfa Aesar and was used without further purification (purity ~96%).

Ethyl 5-methoxy-1*H*-indole-2-carboxylate (2c): This product was purchased from Alfa Aesar and was used without further purification (purity ~96%).

General procedure for the synthesis of substituted 2-bromoacetophenones (3a-m)

To a 250 ml RB flask, 100 mL of dry EtOAc was added followed by the addition of 2 eq. (2.0 mmol) of $CuBr_2$ and the mixture was stirred for 15 min. at 70 ^{0}C. Then 1 eq. (1.0 mmol) of the acetophenone dissolved in 10 mL of dry EtOAc was poured into the reaction flask. The reaction mixture was refluxed for 12 h at 70 ^{0}C, cooled to room temperature and was poured on top of a celite bed to filter off the $CuBr_2$ precipitate. The filtered organic layer was collected, washed with brine solution (25 mL x 3). The aqueous layer was discarded and the organic layer was collected and dried over $MgSO_4$. Solvent was evaporated in vacuo and the crude product was further purified by column chromatography using EtOAc: MeOH (5:1) as the eluent.

2-Bromo-1-(4-hydroxyphenyl)ethan-1-one (3b): The product was obtained by brominating 1-(4-hydroxyphenyl)ethan-1-one using $CuBr_2$ to afford a yellowish product. Mp 116-118 ^oC (82%). ^{1} H NMR (300 MHz, DMSO-d_6): δ = 4.47 (s, 2H), 6.82 (d, 2H, *J* = 9.0 Hz), 7.84 (d, 2H, *J* = 9.0 Hz), 10.48 (s, 1H).

2-Bromo-1-(4-methoxyphenyl)ethan-1-one (3c): The product was obtained by brominating 1-(4-methoxyphenyl)ethan-1-one using $CuBr_2$ to afford a yellowish product. Mp 64-66 ^oC (92.1%). ^{1} H NMR (300 MHz, DMSO-d_6): δ = 3.83 (s, 3H), 4.80 (s, 2H), 7.02 (d, 2H, *J* = 9.0 Hz), 7.94 (d, 2H, *J* = 7.0 Hz).

2-Bromo-1-(3,4-dimethoxyphenyl)ethan-1-one (3d): The product was obtained by brominating 1-(3,4-dimethoxyphenyl)ethan-1-one using $CuBr_2$ to afford a yellowish product. (81.9%). ^{1} H NMR (DMSO-d_6, 300 MHz): δ = 3.79 (s, 3H), 3.83 (s, 3H), 4.82 (s, 3H), 7.05 (d, 1H, *J* = 8.4 Hz), 7.45 (s, 1H), 7.64 (d, *J* = 8.4 Hz, 1H).

2-Bromo-1-(3-methoxyphenyl)ethan-1-one (3e): The product was obtained by brominating 1-(3-methoxyphenyl)ethan-1-one using $CuBr_2$ to afford a yellowish product. Yield: 77.9%. ^{1}H NMR (DMSO-d_6, 300 MHz): δ = 3.79 (s, 3H) 4.90 (s, 2H), 7.20 (d, 1H, *J* = 8.3Hz), 7.41 (m, 2H, *J* = 7.9 Hz), 7.54 (d, 1H, *J* = 7.6 Hz).

2-Bromo-1-(3,4,5-trimethoxyphenyl)ethan-1-one (3f): The product was obtained by brominating 1-(3,4,5-trimethoxyxyphenyl)ethan-1-one using $CuBr_2$ to afford a yellowish product. (69.5%). ^{1}H NMR (DMSO-d_6, 300 MHz): δ = 3.72 (s, 3H), 3.82 (s, 6H), 4.92 (s, 2H), 7.21 (s 2H).

2-Bromo-1-(3-hydroxyphenyl)ethan-1-one (3g): The product was obtained by brominating 1-(3-hydroxyxyphenyl)ethan-1-one using $CuBr_2$ to afford a yellowish product. (79.9%). ^{1}H NMR (DMSO-d_6, 300 MHz): δ = 4.83 (s, 2H), 7.02 (d, *J* = 6.8 Hz, 1H), 7.30-7.40 (m , 3H), 9.74 (s, 1H).

2-Bromo-1-(2-methoxyphenyl)ethan-1-one (3h): The product was obtained by brominating 1-(2-methoxyphenyl)ethan-1-one using $CuBr_2$ to afford a yellowish product. (75.7%). ^{1}H NMR (DMSO-d_6, 300 MHz): δ = 3.87 (s, 3H), 4.74 (s, 2H), 7.00 (t, *J* = 7.3 Hz, 1H), 7.14 (d, 1H, *J* = 8.3 Hz), 7.53 (t, 1H, *J* = 6.9 Hz), 7.63 (d, *J* = 7.7 Hz, 1H).

2-Bromo-1-(2,4-dimethoxyphenyl)ethan-1-one (3i): The product was obtained by brominating 1-(2, 4-dimethoxyphenyl)ethan-1-one using $CuBr_2$ to afford a yellowish product. (68%). ^{1}H NMR (DMSO-d_6, 300 MHz): δ = 3.78 (s, 3H), 3.84 (s, 3H), 4.67 (s, 2H), 6.60-6.64 (m, 2H), 7.68 (d, 1H, *J* = 7.9 Hz).

2-Bromo-1-(2,5-dimethoxyphenyl)ethan-1-one (3j): The product was obtained by brominating 1-(2, 5-dimethoxyphenyl)ethan-1-one using $CuBr_2$ to afford a yellowish product. mp?? (76.8%). ^{1}H NMR (DMSO-d_6, 300 MHz): δ = 3.70 (s, 3H), 3.82(s, 3H), 4.75 (s, 2H), 7.06- 7.18 (m, 3H).

2-Bromo-1-(4-hydroxy-3-methoxyphenyl)ethan-1-one (3k): The product was obtained by brominating (4-hydroxy-3-methoxyphenyl)ethan-1-one using $CuBr_2$ to afford a yellowish product. (78.2%). ^{1}H NMR (DMSO-d_6, 300 MHz): δ = 3.79 (s, 3H), 4.77 (s, 2H), 6.80 (d, 1H, *J* = 7.2 Hz), 7.44 (d, *J* = 7.2 Hz, 1H), 7.61 (d, 1H, *J* = 7.2 Hz), 10.47 (s, 1H).

General procedure for the synthesis of OTBDMS protected 2-bromoacetophenones (3b', g', l', and m')

Hydroxy group containing substituted bromo acetophenones (3.9 mmol; 1eq.) were dissolved in 20 mL of DCM/ EtOAc (1:1) solution in a 100mL round bottom flask. To this mixture, 7.8 mmol (2 eq) of TEA was added dropwise, and the mixture was stirred for five min. at room temperature. Then, six mmol (1.5 eq) of TBDMSCl was added directly to the reaction mixture and was stirred for 18 h at room temperature. Afterward, the reaction mixture was transferred to a separatory

funnel, and the organic layer was washed with ten mL of 1M HCl solution. The aqueous layer was discarded, and the organic layer was collected in an EM flask, and the contents were dried over $MgSO_4$. The solvent was removed in vacuo to obtain the crude product which was further purified by silica gel chromatography using *n*-hexanes/ EtOAc (5:1) as eluent.

2-Bromo-1-(4-((*tert*-butyldimethylsilyl)oxy)phenyl)ethan-1-one (3b'): The product was obtained by coupling **3b** with TBDMSCl to obtain a yellowish liquid (58.3%). ^{1}H NMR (DMSO-d_6, 300 MHz): δ = 0.21 (s, 6H), 0.97 (s, 9H), 4.61 (s, 2H), 6.86 (d, 2H, *J* = 9.0 Hz), 7.88 (d, 2H, *J* = 9.0 Hz).

2-Bromo-1-(3-((*tert*-butyldimethylsilyl)oxy)phenyl)ethan-1-one (3g'): The product was obtained by coupling **3g** with TBDMSCl to afford a yellowish liquid(79.9%). ^{1}H NMR (300 MHz, DMSO-d_6): δ= 0.21 (s, 6H), 0.97 (s, 9H), 4.83 (s, 2H), 7.02 (d, 1H, *J* = 6.8 Hz), 7.26 (m, 3H).

2-Bromo-1-(4-((*tert*-butyldimethylsilyl)oxy)-3-methoxyphenyl)ethan-1-one (3k'): The product was obtained by coupling **3k** with TBDMSCl to afford a yellowish liquid (51%), ^{1}H NMR (300 MHz, DMSO-d_6): δ = 0.17 (s, 6H), 0.98 (s, 9H), 3.84 (s, 3H), 4.63 (s, 2H), 6.85 (d, 1H, *J* = 7.2 Hz), 7.41 (d, 1H, *J* = 7.2 Hz), 7.50 (s, 1H).

2-Bromo-1-(3-((*tert*-butyldimethylsilyl)oxy)-4-methoxyphenyl)ethan-1-one (3l'): The product was obtained by coupling **3l** with TBDMSCl to afford a yellowish liquid and was used without purification.

General procedure for the synthesis of substituted ethyl-1-(2-oxo-2-phenylethyl)-1*H*-indole-2-carboxylates (4a-n)

One eq. (4.8 mmol) of ethylindole-2-carboxylates (**2a-c**) was charged in a 250 mL RB flask to which 40 mL acetonitrile was added. The reaction mixture was stirred at 70 ^{0}C till all the starting

material dissolves. To the above reaction mixture, two equivalents (9.6 mmol) of cesium carbonate (CS_2CO_3) was added, and the reaction mixture was kept under stirring at 70 ^{0}C for fifteen minutes. To the above mixture, KI was added in catalytic quantities (~10-15mg) after which the 1.2 eq. of (5.79 mmol) of substituted 2-bromoacetophenones (**3a-m**) was added, and the reaction mixture was refluxed for 24 h at 70 ℃, cooled to r.t., the contents were transferred to a separatory funnel, and the reaction mixture was diluted with 25 mL of EtOAc. The organic layer was washed with brine solution (20 mL x 3), and the organic layer was dried over $MgSO_4$. The solvent was removed in vacuo and the crude product obtained was further purified by silica gel column chromatography using *n*-hexanes/ EtOAc (5:1) to afford yellowish products. The analytical data is given below;

Ethyl 1-(2-oxo-2-phenylethyl)-1*H*-indole-2-carboxylate (4a)

The product was obtained by coupling **2a** with **3a** by the method mentioned above to afford a yellowish solid product (460 mg, yield: 31.2%). mp: 118-120 ^{0}C. ^{1}H NMR ($CDCl_3$, 300 MHz): δ = 1.29 (t, 3H, *J* = 7.2 Hz), 4.23 (q, 2H, *J* = 7.2 Hz), 6.03 (s, 2H), 7.12- 7.32 (m, 4H), 7.41 (s, 1H), 7.49 (t, 1H, *J* = 7.2 Hz), 7.60 (t, 1H, *J* = 7.2 Hz), 7.69 (d, 1H, *J* = 7.8 Hz), 8.04 (d, 2H, *J* = 7.2 Hz,); ^{13}C NMR ($CDCl_3$, 75 MHz): δ = 14.24, 50.93, 60.59, 109.63, 111.14, 120.92, 122.90, 125.33, 126.24, 127.77, 128.88, 133.71, 135.04, 139.73, 162.29, 193.39.

Ethyl 1-(2-(4-hydroxyphenyl)-2-oxoethyl)-1*H*-indole-2-carboxylate (4b):

The product was obtained by coupling **2a** with **3b'** by the method mentioned above to afford a yellowish brown solid product (yield: 48.8%). mp: 109-110 ^{0}C. ^{1}H NMR (DMSO-d_6, 300 MHz): δ = 1.12 (t, 3H, *J* = 7.1 Hz,), 4.15 (q, 2H, *J* = 7.1 Hz,), 6.06 (s, 2H), 6.88 (d, 2H, *J* = 7.4 Hz), 7.26 (d, 2H, *J* = 8.1 Hz), 7.31 (d, 1H, *J* = 8.8 Hz), 7.57 (s, 1H), 7.67 (d, 1H, *J* = 7.0 Hz), 7.93 (d, 2H, *J* = 8.0 Hz), 8.03 (s, 1H).

Ethyl 1-(2-(4-methoxyphenyl)-2-oxoethyl)-1*H*-indole-2-carboxylate (4c):

The product was obtained by coupling **2a** with **3c** by the method mentioned above to afford a yellowish solid product (yield: 39.9%).mp: 108-109 literature value is different ^{0}C. ^{1}H NMR ($CDCl_3$, 300 MHz): δ = 1.29 (t, 3H, *J* = 7.1 Hz,), 3.88 (s, 3H), 4.23 (q, 2H, *J* = 7.1 Hz,), 5.98 (s, 2H), 6.96 (d, 2H, *J* = 6.9 Hz), 7.14- 7.29 (m, 3H, *J* = 8.3 Hz), 7.40 (s, 1H), 7.68 (d, 1H, *J* = 7.9 Hz), 8.01 (d, 2H, *J* = 6.9 Hz).

Ethyl 1-(2-(3,4-dimethoxyphenyl)-2-oxoethyl)-1*H*-indole-2-carboxylate (4d):

The product was obtained by coupling **2a** with **3d** by the method mentioned above to afford a yellowish solid product. mp: 180-182 ^{0}C (25.7%). ^{1}H NMR (300 MHz, $CDCl_3$): δ = 1.23 (t, 3H, *J* = 7.1 Hz,), 3.89 (s, 3H), 3.96 (s, 3H), 4.23 (q, 2H, *J* = 7.1 Hz), 6.00 (s, 2H), 6.92 (d, 1H, *J* = 8.3 Hz), 7.14- 7.32 (m, 3H), 7.40 (s, 1H), 7.52 (s, 1H), 7.68 (t, 2H, *J* = 8.5 Hz).

Ethyl 1-(2-(3-methoxyphenyl)-2-oxoethyl)-1*H*-indole-2-carboxylate (4e)

The product was obtained by coupling **2a** with **3e** by the method mentioned above to afford a yellowish solid product (yield:14%). This compound was taken to the next step without further purification.

Ethyl 1-(2-(3,4,5-trimethoxyphenyl)-2-oxoethyl)-1H-indole-2-carboxylate (4f):

The product was obtained by coupling **2a** with **3f** by the method mentioned above to afford a yellowish solid product (yield:15.9%). mp: 115-116 ^{0}C. ^{1}H NMR (300 MHz, $CDCl_3$): δ = 1.31 (t, 3H, *J* = 7.1 Hz,), 3.83 (s, 3H), 3.89 (s, 6H), 4.24 (q, 2H, *J* = 7.1 Hz,), 5.99 (s, 2H), 7.13-7.33 (m, 5H), 7.40 (s, 1H), 7.69 (d, 1H, *J* = 7.8 Hz).

Ethyl 1-(2-(3-hydroxyphenyl)-2-oxoethyl)-1*H*-indole-2-carboxylate (4g)

The product was obtained by coupling **2a** with **3g** by the method mentioned above to afford a yellowish solid product (yield: 31.2%). This compound was taken to the next step without further purification.

Ethyl 1-(2-(2-methoxyphenyl)-2-oxoethyl)-1*H*-indole-2-carboxylate (4h)

The product was obtained by coupling **2a** with **3h** by the method mentioned above to afford a yellowish solid product (yield: 14%). This compound was taken to the next step without further purification.

Ethyl 1-(2-(2,4-dimethoxyphenyl)-2-oxoethyl)-1*H*-indole-2-carboxylate (4i):

The product was obtained by coupling **2a** with **3i** by the method mentioned above to afford a yellowish solid product (yield: 37.5%). mp: 109-110 ^{0}C. ^{1}H NMR (300 MHz, $CDCl_3$): δ = 1.28 (t, 3H, *J* = 7.1 Hz,), 3.86 (s, 3H), 4.00 (s, 3H), 4.22 (q, 2H, *J* = 7.1 Hz,), 5.90 (s, 2H), 6.54-6.52 (m, 2H), 7.09 (t, 1H, *J* = 7.1 Hz), 7.20-7.33 (m, 2H), 7.38 (s, 1H), 7.67 (d, 1H, *J* = 7.9 Hz), 7.92 (d, 1H, *J* = 8.7 Hz).

Ethyl 1-(2-(2,5-dimethoxyphenyl)-2-oxoethyl)-1*H*-indole-2-carboxylate (4j):

The product was obtained by coupling **2a** with **3j** by the method mentioned above to afford a yellowish solid product (yield: 22.0%). mp: 118-120 ^{o}C. ^{1}H NMR (300 MHz, $CDCl_3$): δ = 1.29 (t, 3H, *J* = 7.1 Hz,), 3.75 (s, 3H), 3.98 (s, 3H), 4.23 (q, 2H, *J* = 7.1 Hz), 5.95 (s, 2H), 6.96 (d, 1H, *J* = 9.0 Hz), 7.07- 7.16 (m, 2H), 7.22- 7.40 (m, 3H), 7.38 (s, 1H), 7.68 (d, 1H, *J* = 7.9 Hz).

Ethyl 1-(2-(4-hydroxy-3-methoxyphenyl)-2-oxoethyl)-1*H*-indole-2-carboxylate (4k):

The product was obtained by coupling **2a** with **3k** by the method mentioned above to afford a yellowish solid product (yield: 75.2%). This compound was taken to the next step without further purification.

Ethyl 1-(2-(3-hydroxy-4-methoxyphenyl)-2-oxoethyl)-1*H*-indole-2-carboxylate (4l)

The product was obtained by coupling **2a** with **3l** by the method mentioned above to afford a yellowish product (yield: 42%). mp: 174-175 ^{0}C. ^{1}H NMR (300 MHz, DMSO-d_6): δ = 1.11 (t, 3H, *J* = 7.1 Hz,), 3.86 (s, 3H), 4.15 (q, 2H, *J* = 7.1 Hz,), 6.04 (s, 2H), 7.07- 7.11 (m, 2H), 7.31-7.40 (m, 2H), 7.40 (s, 1H), 7.55 (d, 1H, *J* = 7.9 Hz), 7.67- 7.70 (m, 2H), 9.43 (s, 1H).

Ethyl 4-methoxy-1-(2-oxo-2-phenylethyl)-1*H*-indole-2-carboxylate (4m)

The product was obtained by coupling **2b** with **3a** by the method mentioned above to afford a yellowish solid product (yield: 45.5%). This compound was taken to the next step without further purification.

Ethyl 5-methoxy-1-(2-oxo-2-phenylethyl)-1*H*-indole-2-carboxylate (4n)

The product was obtained by coupling **2c** with **3a** by the method mentioned above to afford a yellowish solid product (yield: 42.3%). This compound was taken to the next step without further purification.

General procedure for the synthesis of substituted 3-phenylpyrazino[1,2-*a*]indo-1(2*H*)-ones (5a-n)

1 eq. (0.64 mmol) of ethyl 1-(2-oxo-2-phenylethyl)-1*H*-indole-2-carboxylate (**4a**-**o**) was loaded in a pressure vial (PV) and to it 10 eq. (6.4 mmol) of $CH_3COONH_4$was added. Then, *n*-BuOH (4 ml) and glacial acetic acid (1 ml) was added. The sealed PV was heated by placing in an oil bath for 8

h at 150 °C. After which the reaction mixture was cooled and diluted with 15 mL of EtOAc. The contents were transferred in a sepratory funnel, treated ith 10 mL of saturated $NaHCO_3$ solution. The organic layer was washed successively with brine solution, organic layer was collected, dried over $MgSO_4$ and filtered. The solvent was removed in vacuo to give yellow to dark orange product which was further purified by either crystallization using *n*-hexanes- ethyl acetate solution (5:1) or by using silica column chromatography (EtOAc: MeOH -9:1)) . The analytical data is given below:

3-Phenylpyrazino[1,2-*a*]indol-1(2*H*)-one (5a)

This compound was prepared by the cyclization of **4a** using CH_3COONH_4 (10 eq); *n*-BuOH and AcOH (4:1; 5 mL) as the solvent using conditions as mentioned above to yield light yellow solid (110 mg, 76%). mp: 208-210 ^{0}C. ^{1}H NMR (300 MHz, $CDCl_3$) δ = 7.30 (t, 1H, *J* = 7.2 Hz), 7.41-7.58 (m, 8H), 7.70 (d, 1H, *J* = 8.4 Hz), 7.83 (d, 1H, *J* = 8.1 Hz), 8.13 (br, 1H). LRMS (ESI) m/z calc for $C_{17}H_{12}N_2O$ ($[M + H]^+$); 260.1 Found 261.0

3-(4-Hydroxyphenyl)pyrazino[1,2-*a*]indol-1(2*H*)-one (5b)

This compound was prepared by the cyclization of **4b** using CH_3COONH_4 (10 eq); *n*-BuOH and AcOH (4:1; 5 mL) as the solvent using conditions as mentioned above to yield light yellowish orange solid (90 mg, 66.1%). mp: 190-192 ^{0}C. ^{1}H NMR (300 MHz, DMSO-d_6) δ 6.83 (d, 2H, *J* = 5.5 Hz), 7.21- 7.28 (m, 2H), 7.37 (d, 1H, *J* = 7.0 Hz), 7.56 (d, 2H, *J* = 7.0 Hz), 7.80 (s, 1H) 8.06 (s, 1H), 8.16 (d, 1H, *J* = 5.0 Hz), 9.70 (s, 1H), 10.92 (s, 1H). LRMS (ESI) m/z calc for $C_{17}H_{12}N_2O_2$ ($[M + H]^+$); 276.1. Found 277.1..

3-(4-Methoxyphenyl)pyrazino[1,2-*a*]indol-1(2*H*)-one (5c)

This compound was prepared by the cyclization of **4c** using CH_3COONH_4 (10 eq); *n*-BuOH and AcOH (4:1; 5 mL) as the solvent using conditions as mentioned above to yield light yellowish orange solid (110 mg, 71.1%). mp > 250^0C. ^{1}H NMR (300 MHz, DMSO-d_6) δ 3.78 (s, 3H), 7.00 (d, 2H, *J* = 8.7 Hz), 7.23 (s, 1H), 7.26 (d, 1H, *J* = 7.6 Hz), 7.35 (t, 1H, *J* = 7.5 Hz), 7.69 (d, 2H, *J* = 8.7 Hz), 7.78 (d, 1H, *J* = 7.9 Hz) 8.11 (s, 1H), 8.15 (d, 1H, *J* = 8.3 Hz), 10.97 (s, 1H). LRMS (ESI) m/z calc for $C_{18}H_{14}N_2O_2$ ([M + H]$^+$); 290.1. Found 291.0.

3-(3,4-Dimethoxyphenyl)pyrazino[1,2-*a*]indol-1(2*H*)-one (5d)

This compound was prepared by the cyclization of **4d** using CH_3COONH_4 (10 eq); *n*-BuOH and AcOH (4:1; 5 mL) as the solvent using conditions as mentioned above yield light yellowish orange solid (110 mg, 69.1%). mp: > 250^0 C. ^{1} H NMR (300 MHz, $CDCl_3$): δ = 3.94 (s, 3H), 4.00 (s, 3H), 6.96 (d, 1H, *J* = 8.2 Hz), 7.11- 7.17 (m, 2H), 7.29 (t, 1H, *J* = 7.0 Hz), 7.40 (t, 3H, *J* = 7.0 Hz,), 7.71 (d, 1H, *J* = 8.4 Hz), 7.82 (d, 1H, *J* = 8.0 Hz), 8.82 (br, 1H). LRMS (ESI) m/z calc for $C_{19}H_{16}N_2O_3$ ([M + H]$^+$); 320.1. Found 321.0.

3-(3-Methoxyphenyl)pyrazino[1,2-*a*]indol-1(2*H*)-one (5e)

This compound was prepared by the cyclization of **4e** using CH_3COONH_4 (10 eq); *n*-BuOH and AcOH (4:1; 5 mL) as the solvent using conditions as mentioned above to yield light yellowish orange solid (100 mg, 70.4%). mp: >250^0C. ^{1}H NMR (300 MHz – $CDCl_3$) δ 3.89 (s, 3H), 6.89 (d, 2H, *J* = Hz), 7.09 (s, 1H), 7.14 (d, 1H, *J* = 7.1 Hz), 7.30- 7.35 (m, 2H), 7.38- 7.45 (m, 3H), 7.53 (s, 1H), 7.70 (d, 2H, *J* = 8.2 Hz), 7.83 (d, 1H, *J* = 7.7 Hz) 8.26 (s, br,1H). LRMS (ESI) m/z calc for $C_{18}H_{14}N_2O_2$ ([M + H]$^+$); 290.1. Found 291.0.

3-(3,4,5-Trimethoxyphenyl)pyrazino[1,2-*a*]indol-1(2*H*)-one (5f)

This compound was prepared by the cyclization of **4f** using CH_3COONH_4 (10 eq); *n*-BuOH and AcOH (4:1; 5 mL) as the solvent using conditions as mentioned above yield yellow solid (120 mg, 68.8%). mp: >250^{0}C. ^{1} H NMR (300 MHz, $CDCl_3$): δ = 3.91 (s, 3H), 3.98 (s, 6H), 6.83 (s, 2H), 7.31 (t, 1H, *J* = 7.0 Hz), 7.41-7.49 (m, 3H), 7.73 (d, 1H, *J* = 8.4 Hz), 7.83 (d, 1H, *J* = 8.0 Hz), 9.21 (br, 1H). LRMS (ESI) m/z calc for $C_{20}H_{18}N_2O_4$ ($[M + H]^+$); 350.1 Found 351.0.

3-(3-Hydroxyphenyl)pyrazino[1,2-*a*]indol-1(2*H*)-one (5g)

This compound was prepared by the cyclization of **4g** using CH_3COONH_4 (10 eq); *n*-BuOH and AcOH (4:1; 5 mL) as the solvent using conditions as mentioned above yield light yellowish solid (100 mg, 80.1%) mp: 235-237^{0}C, ^{1}H NMR (300 MHz, DMSO-d_6) δ 6.83 (d, 1H, *J* = 7.1 Hz), 7.12- 7.28 (m, 5H), 7.36 (d, 1H, *J* = 7.6Hz), 7.78 (s, 1H), 8.14 (s, 1H), 8.18 (d, 1H, *J* = 7.1 Hz), 9.58 (s, 1H), 10.96 (s, 1H). LRMS (ESI) m/z calc for $C_{17}H_{12}N_2O_2$ ($[M + H]^+$); 276.1. Found 277.1

3-(2-Methoxyphenyl)pyrazino[1,2-*a*]indol-1(2*H*)-one (5h)

This compound was prepared by the cyclization of **4h** using CH_3COONH_4 (10 eq); *n*-BuOH and AcOH (4:1; 5 mL) as the solvent using conditions as mentioned above yield light yellow solid (120 mg, 70.5%), mp: 193-194 ^{0}C. ^{1}H NMR (300 MHz, DMSO-d_6) δ 3.80 (s, 3H), 7.00 (t, 1H, *J* = 7.4 Hz), 7.10 (d, 1H, *J* = 8.1 Hz), 7.22 (s, 1H), 7.26 (d, 1H, *J* = 7.6 Hz), 7.33 (d, 1H, *J* = 7.4 Hz), 7.42 (t, 2H, *J* = 4.3 Hz), 7.78 (d, 1H, *J* = 7.9 Hz), 7.89 (s, 1H), 8.06 (d, 1H, *J* = 8.3 Hz), 10.96 (s, 1H). LRMS (ESI) m/z calc for $C_{18}H_{14}N_2O_2$ ($[M + H]^+$); 290.1. Found 291.0..

3-(2,4-Dimethoxyphenyl)pyrazino[1,2-*a*]indol-1(2*H*)-one (5i)

This compound was prepared by the cyclization of **4i** using CH_3COONH_4 (10 eq); *n*-BuOH and AcOH (4:1; 5 mL) as the solvent using conditions as mentioned above yield light yellow solid (130 mg, 81.1%). mp: 184-185 ^{0}C. ^{1} H NMR (300 MHz, DMSO-d_6): δ = 3.80 (s, 6H), 6.58 (d, 1H, *J* = 8.3 Hz), 6.60 (s, 1H), 7.20- 7.34 (m, 4H), 7.78 (d, 2H, *J* = 8.1 Hz), 8.04 (d, 1H, *J* = 8.3 Hz), 10.68 (s, 1H). LRMS (ESI) m/z calc for $C_{19}H_{16}N_2O_3$ ([M + H]$^+$); 320.1. Found 321.0.

3-(2,5-Dimethoxyphenyl)pyrazino[1,2-*a*]indol-1(2*H*)-one (5j)

This compound was prepared by the cyclization of **4j** using CH_3COONH_4 (10 eq); *n*-BuOH and AcOH (4:1; 5 mL) as the solvent using conditions as mentioned above yield light yellow solid (120 mg, 75.5%). mp: 178-179 ^{0}C. ^{1} H NMR (300 MHz, $CDCl_3$): δ = 3.83 (s, 3H), 3.87 (s, 3H), 6.90 (s, 2H), 7.04 (s, 1H), 7.29 (t, 1H, *J* = 7.2 Hz), 7.39- 7.43 (m, 2H), 7.51 (s, 1H), 7.68 (d, 1H, *J* = 8.7 Hz), 7.82 (d, 1H, *J* = 7.9 Hz), 8.67 (br, 1H). LRMS (ESI) m/z calc for $C_{19}H_{16}N_2O_3$ ([M + H]$^+$); 320.1. Found 321.0.

3-(4-Hydroxy-3-methoxyphenyl)pyrazino[1,2-*a*]indol-1(2*H*)-one (5k)

This compound was prepared by the cyclization of **4k** using CH_3COONH_4 (10 eq); *n*-BuOH and AcOH (4:1; 5 mL) as the solvent using conditions as mentioned above yield light yellow solid (120 mg, 78.4%). mp: > 250 ^{0}C. ^{1}H NMR (300 MHz, DMSO-d_6): δ = 3.86 (s, 3H), 6.81 (d, 1H, *J* = 7.8 Hz), 7.22-7.40 (m, 4H), 7.80 (d, 1H, *J* = 7.1 Hz), 8.10 (s, 1H), 8.18 (d, 1H, *J* = 7.2 Hz), 9.24 (s, 1H), 10.96 (s, 1H). LRMS (ESI) m/z calc for $C_{18}H_{14}N_2O_3$ ([M + H]$^+$); 306.1. Found 307.0.

3-(3-Hydroxy-4-methoxyphenyl)pyrazino[1,2-*a*]indol-1(2*H*)-one (5l)

This compound was prepared by the cyclization of **4l** using CH_3COONH_4 (10 eq); *n*-BuOH and AcOH (4:1; 5 mL) as the solvent using conditions as mentioned above yield yellow solid (120 mg, 78.4%). mp: > 250 ^{0}C. ^{1} H NMR (300 MHz, DMSO-d_6): δ = 3.80 (s, 3H), 6.97 (d, 1H, *J* = 8.7

Hz), 7.15-7.18 (m, 2H), 7.22 (s, 1H), 7.26 (d, 1H, *J* = 8.2 Hz), 7.37 (s, 1H), 7.77 (d, 1H, *J* = 8.2 Hz), 8.04 (s, 1H), 8.16 (d, 1H, *J* = 8.4 Hz), 9.08 (s, 1H), 10.90 (s, 1H). LRMS (ESI) m/z calc for $C_{18}H_{14}N_2O_3$ ($[M + H]^+$); 306.1. Found 307.0..

9-Methoxy-3-phenylpyrazino[1,2-*a*]indo-1(2*H*)-one (5m)

This compound was prepared by the cyclization of **4m** using CH_3COONH_4 (10 eq); *n*-BuOH and AcOH (4:1; 5 mL) as the solvent using conditions as mentioned above yield yellow solid (120 mg, 78.4%). mp: >250 ^{0}C (78.4%). ^{1}H NMR (DMSO-d_6, 300 MHz): δ = 3.92 (s, 3H), 6.73 (d, 1H, *J* =7.7 Hz), 7.17 (s, 1H), 7.29-7.48 (m, 4H), 7.74-7.78 (m, 3H), 8.15 (s, 1H), 11.03 (s, 1H). LRMS (ESI) m/z calc for $C_{18}H_{14}N_2O_2$ ($[M + H]^+$); 290.1. Found 291.0.

8-Methoxy-3-phenylpyrazino[1,2-*a*]indo-1(2*H*)-one (5n)

This compound was prepared by the cyclization of **4n** using CH_3COONH_4 (10 eq); *n*-BuOH and AcOH (4:1; 5 mL) as the solvent using conditions as mentioned above yield light yellowish solid (120 mg). mp: 188-189 ^{0}C (78.4%). ^{1}H NMR (DMSO-d_6, 300 MHz): δ = 3.80 (s, 3H), 7.01 (s, 1H), 7.06 (d, 1H, *J* = 7.2 Hz), 7.16 (s, 1H), 7.24 (d, 1H), 7.29 (d, 2H, *J* = 7.2 Hz), 7.43 (d, 2H, *J* =7.4Hz), 7.75 (d, 1H, *J* = 8.1 Hz), 8.19 (s, 1H), 11.0 (s, 1H). LRMS (ESI) m/z calc for $C_{18}H_{14}N_2O_2$ ($[M + H]^+$); 290.1. Found 291.0.

6.2 Biological Evaluation

6.2.1 Cholinesterase assay

The *PPI* derivatives were tested using a 96-well plate format using tacrine and rivastigmine as reference compounds. To each wells, 160 µl of 1.5 mM solution of DTNB was added which was prepared using 50 mM Tris-HCl buffer (pH = 8.0; contains 0.1 M NaCl and 0.02 M $MgCl_2.6H_2O$). To this, 50 µL of the cholinesterase enzyme (human AChE/ BuChE) was added which was prepared in a buffer solution of 50 mM Tris-HCl of pH 8.0, containing 0.1% w/v bovine serum albumin. Then, different concentrations of the test compound viz. 1, 2.5, 5, 10, 25, 50 µl (1-50 µM) in DMSO and buffer solution was added to individual wells. The loaded plate was incubated at room temperature for 5 min, and then 30 µl of the substrate (ACh/ BuCh) was added. Measurements were made by observing the absorbance of each well at 405 nm at 0, 1, 2, and 3 min time intervals. The blank control well-contained 80 µL of DTNB stock solution, 25µL of buffer A solution, 4 µL of DMSO and 15 µL of thiocholine solution (ACSh/ BuSh). While, 100% control contained 80 µL of DTNB stock solution, 25 µL of cholinesterase enzymes (AChE/ BuChE), 1 µL of DMSO, 4 µL of Buffer A and 15 µL of thiocholine solution (AChT/ BuhT). Percent inhibition was calculated using the formula:

$$\%\ inhibition = \frac{Abs.of\ 100\%\ wells - Abs.from\ inhibitor\ wells}{Abs.of\ 100\%\ wells}\ X\ 100$$

IC_{50} values were calculated plotting the percent inhibition vs. concentration logarithmically, and the results were expressed as the mean± standard deviation (SD) of three independent experiments (n = 3).

6.2.2 Aβ aggregation inhibition assay

The anti-Aβ aggregation activity of *PPI* derivatives was evaluated using the ThT-based fluorescence assay. The $A\beta_{1-40}$ and $A\beta_{1-42}$ hexafluoro-2-propanol (HFIP) (rPeptide, USA) stock solutions were prepared in 1% ?? NH_4OH solution for $A\beta_{1-40}$ and $A\beta_{1-42}$ respectively, to obtain a 1 mg/mL stock solution, followed by dilution in phosphate buffer (pH 7.4) to 500 μM. Stock solutions of test compounds were prepared in DMSO and diluted in phosphate buffer (pH 7.4). The ThT fluorescent dye stock solution (15 μM) was prepared in 50 mM glycine buffer (pH 7.4). The aggregation kinetics assay was carried out using Corning® 386-well flat, clear bottom black plates. Each compound containing well was charged with 44 μL of ThT, 20 μl of phosphate buffer (pH 7.4), eight μl of test compounds in different concentrations (1, 5, 10 and 50 μM) and eight μl of Aβ (5 μM final concentration). The plate was incubated at 37 ℃ with a plate cover under shaking and fluorescence was measured every 5 min. Using a BioTek Multimode Microplate Reader (excitation = 440 nm and emission = 490 nm) over a period of 24 h. The known Aβ aggregation inhibitor orange G was used as a reference compound. The percentage inhibition was calculated using the equation 100% control – [(IFi – IFo)] where 100% control indicates no inhibitor, IFi and IFo are the fluorescence intensities in the presence and absence of ThT. The results were expressed as percentage inhibition of two separate experiments of triplicate measurements.

6.2.3 Molecular docking

Molecular docking studies were performed using Discovery Studio (DS) Structure-Based-Design, version 4.0 (BIOVIA, San Diego, U.S.A). For performing the docking studies, X-ray crystal

structures of AChE (PDB: 4EY7), BuChE (PDB: 2XQJ), $A\beta_{40}$ (PDB:2LMN) and $A\beta_{42}$ (2NAO) were obtained from the RCSB protein data bank. To the enzyme structure, hydrogens were added. Test compounds were built in 3D using Build Fragment tool, and energy minimization was performed for 1000 iterations using steepest descent and conjugate gradient minimizations respectively. The CDOCKER algorithm in the receptor-ligand interactions was used to dock the molecules with appropriate enzymes after defining a 15 Å sphere radius within the enzyme which covers all the active site amino acids. CHARMm force field was used for the docking studies. The quality of ligand-enzyme complex was evaluated based on CDOCKER Interaction energy and CDOCKER energy in kcal/mol. Also, polar and nonpolar interactions were visualized to assess the critical interactions involved in compound binding with the respective enzyme/ protein.

6.2.4 Antioxidant activity

For the antioxidant property evaluation of selected *PPI* derivatives, the DPPH radical assay method was used, and the results were compared with reference agents Trolox, curcumin, and resveratrol. Compound stock solutions were prepared using anhydrous MeOH at 250 μM and 500 μM concentrations, while, 100mL of DPPH radical stock solution was prepared at 56 μM concentration using MeOH. 96 well clear, flat bottom plate was used for carrying out the experiments. To each of the wells, 90 μL of DPPH solution followed by 10 μL of the compound solution, making the final concentration of the compound as 25 μM and 50 μM in each well. Compound control wells contained 90 μL of MeOH and 10 μL of the compound, while, the DPPH control wells contained 90 μL of DPPH solution and 10μL of MeOH. The readings were taken

after 1h of the incubation using a BioTek Synergy H1 microplate reader. The results were calculated as % DPPH scavenging using the following formula.

$$\%\ DPPH\ scavenging = \frac{\text{Absorbance by DPPH control} - (\text{absorbance by test compounds} - \text{compound control absorbance})}{\text{Absorbance by DPPH control}}\ X\ 100$$

The results were expressed as mean %inhibition ± SD (SD<10%) for two independent experiments (n = 3).

6.2.5 Transmission electron microscopy (TEM)

TEM samples were prepared by incubating the Aβ with appropriate *PPI* derivatives/ control in a Costar® 96 well, black plate with clear bottom. To each of the wells, 80 µL of phosphate buffer (215 mM) solution was added, which was followed by 20 µL of 250 µM test compound solution. 100 µL of a 50 µM solution of $A\beta_{40/42}$ was then added. Control wells were charged with 18 µL of phosphate buffer and 2µL of DMSO. In $A\beta_{40/42}$ loaded wells, the final $A\beta_{40/42}$ to test compound ratio was 1:1 (at 25 µM). The plate was then incubated on the Fisher plate incubator for 24h, set at the temperature of 37^0C.

TEM grids were prepared by adding 20 µL of the incubated solution over a Formvar- coated copper grids (400 mesh). The grids were subjected to overnight air drying, after which, the grids have been submitted to the washing process so as to remove any precipitated buffer salts. This step was done by adding ~30 µL of deionized water on top of the grids and quickly blotting the water droplet using a small piece of filter paper. The washing step was done twice and a drying period of around 2h was given between each drying step. After the grids were completely dried, the contents of the grids were subjected to the staining process which was done using 2% phosphotungstic acid (PTA). PTA stains the grid negatively (i.e. only the aggregates and other undissolved particles get stained

and not the entire grid). ~20 μL of PTA was used to stain the grid which was blotted right after the addition of the drop of PTA using a small piece of filter paper. After the staining step, the grids were air-dried overnight. The TEM screening was done using a Philips CM 10 transmission electron microscope at 60 kV (at the Department of Biology, University of Waterloo) and the images were obtained using 14- megapixel AMT camera.

References:

(1) Prince, M.; Bryce, R.; Albanese, E.; Wimo, A.; Ribeiro, W.; Ferri, C. P. The Global Prevalence of Dementia: A Systematic Review and Metaanalysis. *Alzheimer's Dement.* **2013**, *9* (1), 63–75.

(2) Alzheimer's Association. 2016 Alzheimer's Disease Facts and Figures. *Alzheimer's Dement.* **2016**, *12* (4), 1–80.

(3) Chambers, L.W., Bancej, C., Dowell, I. Prevalence and Monetary Costs of Dementia in Canada: A Report by the Alzheimer Society of Canada. *Alzheimer's Soc. Canada* **2016**.

(4) Eroglu S., Toprak S., Urgan O, MD, Ozge E. Onur, MD, Arzu Denizbasi, MD, Haldun Akoglu, MD, Cigdem Ozpolat, MD, Ebru Akoglu, M. *DSM-IV Diagnostic and Statistical Manual of Mental Disorder*; 2012; Vol. 33.

(5) Tools for Early Identification , Assessment , and Treatment for People with Alzheimer's Disease and Tools for Early Identification , Assessment , and Treatment for People with Alzheimer's Disease and Dementia. *Chronic Care Networks Alzheimer's Dis. Initiat.* **2003**.

(6) Gaugler, J. E.; Ascher-Svanum, H.; Roth, D. L.; Fafowora, T.; Siderowf, A.; Beach, T. G. Characteristics of Patients Misdiagnosed with Alzheimer's Disease and Their Medication Use: An Analysis of the NACC-UDS Database. *BMC Geriatr.* **2013**, *13* (1), 137.

(7) Thompson, L. M. Neurodegeneration:A Question of Balance. *Nature* **2008**, *452*, 707–708.

(8) Palop, J. J.; Chin, J.; Mucke, L. A Network Dysfunction Perspective on Neurodegenerative Diseases. *Nature* **2006**, *443* (7113), 768–773.

(9) Mohamed, T.; P.N. Rao, P. Alzheimer's Disease: Emerging Trends in Small Molecule Therapies. *Curr. Med. Chem.* **2011**, *18* (28), 4299–4320.

(10) Suh, W. H.; Suslick, K. S.; Suh, Y. Therapeutic Agents for Alzheimer's Disease. *Curr. Med. Chem. – Cent. Nerv. Syst. Agents* **2005**, *5* (4), 259–269.

(11) Serrano-Pozo, A.; Frosch, M. P.; Masliah, E.; Hyman, B. T. Neuropathological Alterations in Alzheimer Disease. *Cold Spring Harb. Perspect. Med.* **2011**, *1* (1), 1–23.

(12) Selkoe, D. J. The Molecular Pathology of Alzheimer's Disease. *Neuron* **1991**, *6*, 487–498.

(13) Thompson, P. M.; Hayashi, K. M.; de Zubicaray, G.; Janke, A. L.; Rose, S. E.; Semple, J.; Herman, D.; Hong, M. S.; Dittmer, S. S.; Doddrell, D. M.; Toga, A. W. Dynamics of Gray Matter Loss in Alzheimer's Disease. *J. Neurosci.* **2003**, *23* (3), 994–1005.

(14) Liu, Chia-Chen; Kanekiyo,Takahisa; Xu, Huaxi; Bu, G. Apolipoprotein E and Alzheimer Disease: Risk, Mechanisms, and Therapy. *Nat Rev Neurol 9* (2), 106–118.

(15) Anoop, A.; Singh, P. K.; Jacob, R. S.; Maji, S. K. CSF Biomarkers for Alzheimer's Disease Diagnosis. *Int. J. Alzheimers. Dis.* **2010**, *2010* (Article ID 606802), 1–12.

(16) Blennow, K.; Hampel, H.; Zetterberg, H. Biomarkers in Amyloid-β Immunotherapy Trials in Alzheimer's Disease. *Neuropsychopharmacology* **2014**, *39* (1), 189–201.

(17) Ritter, A.; Cummings, J. Fluid Biomarkers in Clinical Trials of Alzheimer's Disease Therapeutics. *Front. Neurol.* **2015**, *6* (186).

(18) Forsberg, A.; Engler, H.; Almkvist, O.; Blomquist, G.; Hagman, G.; Wall, A.; Ringheim, A.; Långström, B.; Nordberg, A. PET Imaging of Amyloid Deposition in Patients with Mild Cognitive Impairment. *Neurobiol. Aging* **2008**, *29* (10), 1456–1465.

(19) Adlard, P. A.; Tran, B. A.; Finkelstein, D. I.; Desmond, P. M.; Johnston, L. A.; Bush, A. I.; Egan, G. F. A Review of Beta-Amyloid Neuroimaging in Alzheimer's Disease. *Front. Neurosci.* **2014**, *8* (327), 1–23.

(20) Wu, L.; Rosa-Neto, P.; Gauthier, S. Use of Biomarkers in Clinical Trials of Alzheimer Disease. *Mol. Diagn. Ther.* **2012**, *15* (6), 313–325.

(21) Klafki, H.-W.; Staufenbiel, M.; Kornhuber, J.; Wiltfang, J. Therapeutic Approaches to Alzheimer's Disease. *Brain* **2006**, *129* (11), 2840–2855.

(22) Malinow, R. New Developments on the Role of NMDA Receptors in Alzheimer's Disease. *Curr. Opin. Neurobiol.* **2012**, *22* (3), 559–563.

(23) Varga, E.; Juhász, G.; Bozsó, Z.; Penke, B.; Fülöp, L.; Szegedi, V. Abeta(1-42) Enhances Neuronal Excitability in the CA1 via NR2B Subunit-Containing NMDA Receptors. *Neural Plast.* **2014**, *2014*, 584314.

(24) Tucci, P.; Mhillaj, E.; Morgese, M. G.; Colaianna, M.; Zotti, M.; Schiavone, S.; Cicerale, M.; Trezza, V.; Campolongo, P.; Cuomo, V.; Trabace, L. Memantine Prevents Memory Consolidation Failure Induced by Soluble Beta Amyloid in Rats. *Front. Behav. Neurosci.* **2014**, *8*, 332.

(25) Schmitt, B.; Bernhardt, T.; Moeller, H.; Heuser, I. Combination Therapy in Alzheimer's Disease: A Review of Current Evidence. *CNS Drugs* **2004**, *18* (13), 827–844.

(26) Farlow, M. R.; Grossberg, G. T.; Graham, S. M.; Mcdonald, S. Memantine Treatment in Patients With Moderate to Severe Alzheimer Disease. *Am. Med. Assoc.* **2004**, *291* (3), 317–324.

(27) Querfurth, H. W.; Laferla, F. M. Mechanism of Disease: Alzheimer's Disease. *N. Engl. J. Med.* **2010**, No. 362, 329–344.

(28) Francis, P. T.; Palmer, A. M.; Snape, M.; Wilcock, G. K. The Cholinergic Hypothesis of Alzheimer ' S Disease : A Review of Progress. *J. Neurol. Neurosurg. Psychiatry* **1999**, *66*, 137–147.

(29) Selkoe, D. J.; Hardy, J. The Amyloid Hypothesis of Alzheimer's Disease at 25 Years. *EMBO Mol. Med.* **2016**, *8* (6), 595–608.

(30) Maccioni, R. B.; Farías, G.; Morales, I.; Navarrete, L. The Revitalized Tau Hypothesis on Alzheimer's Disease. *Arch. Med. Res.* **2010**, *41* (3), 226–231.

(31) Carrillo-Mora, P.; Luna, R.; Colín-Barenque, L. Amyloid Beta: Multiple Mechanisms of Toxicity and Only Some Protective Effects? *Oxid. Med. Cell. Longev.* **2014**, *2014*, 1–15.

(32) Soreq, H.; Zevin-sonkin, D.; Avni, a D. I.; Hallt, L. M. C.; Spierert, P. Human Acetylcholinesterase Gene Identified by Homology to the Ace Region of Drosophila. *Proc. Natl. Acad. Sci.* **1985**, *82* (6), 1827–1831.

(33) Rosini, M.; Simoni, E.; Bartolini, M.; Cavalli, A.; Ceccarini, L.; Pascu, N.; McClymont, D. W.; Tarozzi, A.; Bolognesi, M. L.; Minarini, A.; Tumiatti, V.; Andrisano, V.; Mellor, I. R.; Melchiorre, C. Inhibition of Acetylcholinesterase, Beta-Amyloid Aggregation, and NMDA Receptors in Alzheimer's Disease: A Promising Direction for the Multi-Target-Directed Ligands Gold Rush. *J. Med. Chem.* **2008**, *51* (15), 4381–4384.

(34) Dave, K. R.; Syal, A. R.; Katyare, S. S. Tissue Cholinesterases. A Comparative Study of Their Kinetic Properties. *Z Naturforsch C* **2000**, *55* (1–2), 100–108.

(35) Bajda, M.; Więckowska, A.; Hebda, M.; Guzior, N.; Sotriffer, C. A.; Malawska, B. Structure-Based Search for New Inhibitors of Cholinesterases. *Int. J. Mol. Sci.* **2013**, *14* (3), 5608–5632.

(36) Tripathi, K. D. *Essentials of Medical Pharmacology*, Sixth Edit.; Tripathi, M., Ed.; Jaypee Brothers Medical Publishers (P) Ltd.: New Delhi, 2008.

(37) Prody, C. a; Zevin-Sonkin, D.; Gnatt, a; Goldberg, O.; Soreq, H. Isolation and Characterization of Full-Length cDNA Clones Coding for Cholinesterase from Fetal Human Tissues. *Proc. Natl. Acad. Sci. U. S. A.* **1987**, *84* (11), 3555–3559.

(38) Cheung, J.; Rudolph, M. J.; Burshteyn, F.; Cassidy, M. S.; Gary, E. N.; Love, J.; Franklin, M. C.; Height, J. J. Structures of Human Acetylcholinesterase in Complex with Pharmacologically Important Ligands. *J. Med. Chem.* **2012**, *55* (22), 10282–10286.

(39) Massoulié, J.; Bon, S.; Perrier, N.; Falasca, C. The C-Terminal Peptides of Acetylcholinesterase: Cellular Trafficking, Oligomerization and Functional Anchoring. *Chem. Biol. Interact.* **2005**, *157–158*, 3–14.

(40) Colovic, M. B.; Krstic, D. Z.; Lazarevic-Pasti, T. D.; Bondzic, A. M.; Vasic, V. M. Acetylcholinesterase Inhibitors: Pharmacology and Toxicology. *Curr. Neuropharmacol.* **2013**, *11* (3), 315–335.

(41) Johnson, J. L.; Cusack, B.; Hughes, T. F.; McCullough, E. H.; Fauq, A.; Romanovskis, P.; Spatola, A. F.; Rosenberry, T. L. Inhibitors Tethered near the Acetylcholinesterase Active Site Serve as Molecular Rulers of the Peripheral and Acylation Sites. *J. Biol. Chem.* **2003**, *278* (40), 38948–38955.

(42) Shafferman, A.; Velan, B.; Ordentlich, A.; Kronman, C.; Grosfeld, H.; Leitner, M.; Flashner, Y.; Cohen, S.; Barak, D.; Ariel, N. Substrate Inhibition of Acetylcholinesterase: Residues Affecting Signal Transduction from the Surface to the Catalytic Center. *EMBO J.* **1992**, *11* (10), 3561–3568.

(43) Darvesh, S.; Hopkins, D. A.; Geula, C. Neurobiology of Butyrylcholinesterase. *Nat. Rev. Neurosci.* **2003**, *4* (2), 131–138.

(44) Yazisma, A. Butyrylcholinesterase: Structure and Physiological Importance. *Turkish J. Biochem.* **2003**, *28* (2), 54–61.

(45) Greig, N. H.; Lahiri, D. K.; Sambamurti, K. Butyrylcholinesterase : An Important New Target in Alzheimer ' S Disease Therapy. *Int. Psychogeriatics* **2002**, *14* (1), 77–91.

(46) Allderdice, P. W.; Gardner, H. a; Galutira, D.; Lockridge, O.; LaDu, B. N.; McAlpine, P. J. The Cloned Butyrylcholinesterase (BCHE) Gene Maps to a Single Chromosome Site, 3q26. *Genomics* **1991**, *11* (2), 452–454.

(47) Saxena, A.; Redman, A. M. G.; Jiang, X.; Lockridge, O.; Doctor, B. P. Differences in Active Site Gorge Dimensions of Cholinesterases Revealed by Binding of Inhibitors to Human Butyrylcholinesterase. *Biochemistry* **1997**, *72* (97), 14642–14651.

(48) Stelzmann, R. A.; Norman Schnitzlein, H.; Reed Murtagh, F. An English Translation of Alzheimer's 1907 paper, "Uber Eine Eigenartige Erkankung Der Hirnrinde." *Clin. Anat.* **1995**, *8* (6), 429–431.

(49) Haass, C.; Selkoe, D. J. Soluble Protein Oligomers in Neurodegeneration: Lessons from the Alzheimer's Amyloid Beta-Peptide. *Nat. Rev. Mol. Cell Biol.* **2007**, *8* (2), 101–112.

(50) Shankar, G. M.; Bloodgood, B. L.; Townsend, M.; Walsh, D. M.; Selkoe, D. J.; Sabatini, B. L. Natural Oligomers of the Alzheimer Amyloid-Beta Protein Induce Reversible Synapse Loss by Modulating an NMDA- Type Glutamate Receptor-Dependent Signaling Pathway. **2007**, *27* (11), 2866–2875.

(51) Lesné, S.; Koh, M. T.; Kotilinek, L.; Kayed, R.; Glabe, C. G.; Yang, A.; Gallagher, M.; Ashe, K. H. A Specific Amyloid-Beta Protein Assembly in the Brain Impairs Memory. *Nature* **2006**, *440* (7082), 352–357.

(52) Jang, H.; Zheng, J.; Lal, R.; Nussinov, R. New Structures Help the Modeling of Toxic Amyloidß Ion Channels. *Trends Biochem. Sci.* **2008**, *33* (2), 91–100.

(53) Xiao, Y.; Ma, B.; McElheny, D.; Parthasarathy, S.; Long, F.; Hoshi, M.; Nussinov, R.; Ishii, Y. Aβ(1-42) Fibril Structure Illuminates Self-Recognition and Replication of Amyloid in Alzheimer's Disease. *Nat. Struct. Mol. Biol.* **2015**, *22* (6), 499–505.

(54) Randall, a. D.; Witton, J.; Booth, C.; Hynes-Allen, a.; Brown, J. T. The Functional Neurophysiology of the Amyloid Precursor Protein (APP) Processing Pathway. *Neuropharmacology* **2010**, *59* (4–5), 243–267.

(55) Mattson, M. P. Pathways towards and Away from Alzheimer's Disease. *Nature* **2004**, *430* (7000), 631–639.

(56) Sadigh-Eteghad, S.; Sabermarouf, B.; Majdi, A.; Talebi, M.; Farhoudi, M.; Mahmoudi, J. Amyloid-Beta: A Crucial Factor in Alzheimer's Disease. *Med. Princ. Pract.* **2015**, *24* (1), 1–10.

(57) Kamenetz, F.; Tomita, T.; Hsieh, H.; Seabrook, G.; Borchelt, D.; Iwatsubo, T.; Sisodia, S.;

Malinow, R. APP Processing and Synaptic Function. *Neuron* **2003**, *37* (6), 925–937.

(58) Lee, R. K.; Wurtman, R. J.; Cox, a J.; Nitsch, R. M. Amyloid Precursor Protein Processing Is Stimulated by Metabotropic Glutamate Receptors. *Proc. Natl. Acad. Sci. U. S. A.* **1995**, *92* (17), 8083–8087.

(59) Endres, K.; Fahrenholz, F. Regulation of Alpha-Secretase ADAM10 Expression and Activity. *Exp. Brain Res.* **2012**, *217* (3–4), 343–352.

(60) Ghosh, A. K.; Osswald, H. L. BACE1 (β-Secretase) Inhibitors for the Treatment of Alzheimer's Disease. *Chem Soc Rev* **2014**, *43* (19), 6765–6813.

(61) Edwards, P. D.; Albert, J. S.; Sylvester, M.; Aharony, D.; Andisik, D.; Callaghan, O.; Campbell, J. B.; Carr, R. a.; Chessari, G.; Congreve, M.; Frederickson, M.; Folmer, R. H. a; Geschwindner, S.; Koether, G.; Kolmodin, K.; Krumrine, J.; Mauger, R. C.; Murray, C. W.; Olsson, L. L.; Patel, S.; Spear, N.; Tian, G. Application of Fragment-Based Lead Generation to the Discovery of Novel, Cyclic Amidine β-Secretase Inhibitors with Nanomolar Potency, Cellular Activity, and High Ligand Efficiency. *J. Med. Chem.* **2007**, *50* (24), 5912–5925.

(62) De Strooper, B.; Iwatsubo, T.; Wolfe, M. S. Presenilins and Gamma-Secretase: Structure, Function, and Role in Alzheimer Disease. *Cold Spring Harb. Perspect. Med.* **2012**, *2* (1), 1–19.

(63) Wolfe, M. S. Inhibition and Modulation of Gamma -Secretase for Alzheimer's Disease. *Neurother. J. Am. Soc. Exp. Neurother.* **2008**, *5* (3), 391–398.

(64) Nakayama, K.; Nagase, H.; Koh, C.; Ohkawara, T. γ-Secretase — Regulated Signaling and

Alzheimer's Disease.

(65) Mazzitelli, S.; Filipello, F.; Rasile, M.; Lauranzano, E.; Starvaggi-Cucuzza, C.; Tamborini, M.; Pozzi, D.; Barajon, I.; Giorgino, T.; Natalello, A.; Matteoli, M.; Mattson, M.; Scheuner, D.; Selkoe, D.; Bitan, G.; Yan, Y.; Wang, C.; Hubin, E.; Kuperstein, I.; Kane, M.; Meyer-Luehmann, M.; Eisele, Y.; Watts, J.; Oberstein, T.; Howell, S.; Nalbantoglu, J.; Crine, P.; Kurochkin, I.; Goto, S.; Eckman, E.; Reed, D.; Eckman, C.; Hu, J.; Backstrom, J.; Zhang, Q.; Yan, P.; Zhang, R.; Frautschy, S.; Saido, T.; Leissring, M.; Hernandez-Guillamon, M.; Deb, S.; Gottschall, P.; Yin, K.; Belli, M.; Ramazzotti, M.; Chiti, F.; Biancalana, M.; Koide, S.; Khurana, R.; Alvarez, A.; Fillit, H.; Ma, S.; Janelsins, M.; Sheng, J.; Terry, R.; DeKosky, S.; Scheff, S.; Hardy, J.; Selkoe, D.; Prut, L.; Belzung, C.; Rodriguiz, R.; Wetsel, W.; Kliethermes, C.; Cronise, K.; Crabbe, J.; Cheng, D.; Chambon, C.; Faucher, P.; Mikros, E.; Walsh, I.; LeVine, H.; Huang, S.; Librizzi, F.; Cerf, E.; Sarroukh, R.; Mancini, S.; Wesson, D.; Heneka, M.; Golenbock, D.; Latz, E.; Wyss-Coray, T.; Rogers, J.; Meda, L.; Bateman, D.; Chakrabartty, A.; Giannakopoulos, P.; Elman, J.; Jack, C.; Duran-Aniotz, C.; McLean, C.; Price, J.; Games, D.; Karran, E.; Mercken, M.; Strooper, B. De; Thal, D.; Mawuenyega, K.; Cecarini, V.; Shibata, M.; Deane, R.; Deane, R.; Cho, S.; Russo, C.; Kumar, S.; Bates, K.; Castano, E.; Schlenzig, D.; Nasica-Labouze, J.; Luhrs, T.; Ahmed, M.; Colletier, J.; Joshi, P.; Edison, P.; Griciuc, A.; Serrano-Pozo, A.; Okello, A.; Jankowsky, J.; Amijee, H.; Tsolis, A.; Tartaglia, G.; Xiao, Y.; Zhao, Z.; Schindelin, J.; Serrano-Pozo, A.; Wilcock, D.; Gordon, M.; Morgan, D.; Paravastu, A. Amyloid-β 1–24 C-Terminal Truncated Fragment Promotes Amyloid-β 1–42 Aggregate Formation in the Healthy Brain. *Acta Neuropathol. Commun.* **2016**, *4* (1), 110.

(66) Kawahara, M.; Kuroda, Y. Molecular Mechanism of Neurodegeneration Induced by

Alzheimer's B-Amyloid Protein: Channel Formation and Disruption of Calcium Homeostasis. *Brain Res. Bull.* **2000**, *53* (4), 389–397.

(67) Maccioni, R. B.; Munoz, J. P.; Barbeito, L. The Molecular Bases of Alzheimer's Disease and Other Neurodegenerative Disorders. *Arch. Med. Res.* **2001**, *32* (5), 367–381.

(68) Rajasekhar, K.; Chakrabarti, M.; Govindaraju, T. Function and Toxicity of Amyloid Beta and Recent Therapeutic Interventions Targeting Amyloid Beta in Alzheimer's Disease. *Chem. Commun.* **2015**, *51* (70), 13434–13450.

(69) Maynard, C. J.; Bush, A. I.; Masters, C. L.; Cappai, R.; Li, Q.-X. Metals and Amyloid-Beta in Alzheimer's Disease. *Int. J. Exp. Pathol.* **2005**, *86* (3), 147–159.

(70) Smith, D. G.; Cappai, R.; Barnham, K. J. The Redox Chemistry of the Alzheimer's Disease Amyloid Beta Peptide. *Biochim. Biophys. Acta - Biomembr.* **2007**, *1768* (8), 1976–1990.

(71) Curtain, C. C.; Ali, F.; Volitakis, I.; Cherny, R. A.; Norton, R. S.; Beyreuther, K.; Barrow, C. J.; Masters, C. L.; Bush, A. I.; Barnham, K. J. Alzheimer's Disease Amyloid-Beta Binds Copper and Zinc to Generate an Allosterically Ordered Membrane-Penetrating Structure Containing Superoxide Dismutase-like Subunits. *J. Biol. Chem.* **2001**, *276* (23), 20466–20473.

(72) Swerdlow, R. H.; Khan, S. M. A "mitochondrial Cascade Hypothesis" for Sporadic Alzheimer's Disease. *Med. Hypotheses* **2004**, *63* (1), 8–20.

(73) Wang, C.; Youle, R. J. The Role of Mitochondria in Apoptosis. *Annu. Rev. Genet.* **2009**, *43* (1), 95–118.

(74) Kirichok, Y.; Krapivinsky, G.; Clapham, D. E. The Mitochondrial Calcium Uniporter Is a

Highly Selective Ion Channel. *Nature* **2004**, *427* (6972), 360–364.

(75) Cadonic, C.; Sabbir, M. G.; Albensi, B. C. Mechanisms of Mitochondrial Dysfunction in Alzheimer's Disease. *Mol. Neurobiol.* **2016**, *53* (9), 6078–6090.

(76) Kroemer, G.; Reed, J. C. Mitochondrial Control of Cell Death. *Nat Med* **2000**, *6* (5), 513–519.

(77) Di Scala, C.; Chahinian, H.; Yahi, N.; Garmy, N.; Fantini, J. Interaction of Alzheimer's β-Amyloid Peptides with Cholesterol: Mechanistic Insights into Amyloid Pore Formation. *Biochemistry* **2014**, *53* (28), 4489–4502.

(78) Scala, C. Di; Yahi, N.; Garmy, N.; Chahinian, H.; Fantini, J. Biochemical Identi Fi Cation of a Linear Cholesterol-Binding Domain within Alzheimer ' S β Amyloid Peptide. *ACS Chem Neurosci* **2013**, *4* (3), 509–517.

(79) Danysz, W.; Parsons, C. G. Alzheimer's Disease, β-Amyloid, Glutamate, NMDA Receptors and Memantine - Searching for the Connections. *Br. J. Pharmacol.* **2012**, *167* (2), 324–352.

(80) Lesne, S. NMDA Receptor Activation Inhibits -Secretase and Promotes Neuronal Amyloid- Production. *J. Neurosci.* **2005**, *25* (41), 9367–9377.

(81) Kessels, H. W.; Nabavi, S.; Malinow, R. Metabotropic NMDA Receptor Function Is Required for -Amyloid-Induced Synaptic Depression. *Proc. Natl. Acad. Sci.* **2013**, *110* (10), 4033–4038.

(82) Snyder, E. M.; Nong, Y.; Almeida, C. G.; Paul, S.; Moran, T.; Choi, E. Y.; Nairn, A. C.; Salter, M. W.; Lombroso, P. J.; Gouras, G. K.; Greengard, P. Regulation of NMDA Receptor Trafficking by Amyloid-β. *Nat. Neurosci.* **2005**, *8* (8), 1051–1058.

(83) Parsons, C. G.; Danysz, W.; Quack, G. Memantine Is a Clinically Well Tolerated N-Methyl-D-Aspartate (NMDA) Receptor Antagonist - A Review of Preclinical Data. *Neuropharmacology* **1999**, *38* (6), 735–767.

(84) Ghosh, A. K.; Osswald, H. L. BACE1 (β-Secretase) Inhibitors for the Treatment of Alzheimer's Disease. *Chem. Soc. Rev.* **2014**, *43* (19), 6765–6813.

(85) Roberds, S. L.; Anderson, J.; Basi, G.; Bienkowski, M. J.; Branstetter, D. G.; Chen, K. S.; Freedman, S. B.; Frigon, N. L.; Games, D.; Hu, K.; Johnson-wood, K.; Kappenman, K. E.; Kawabe, T. T.; Kola, I.; Kuehn, R.; Lee, M.; Liu, W.; Motter, R.; Nichols, N. F.; Power, M.; Robertson, D. W.; Schenk, D.; Schoor, M.; Shopp, G. M.; Shuck, M. E.; Sinha, S.; Svensson, K. A.; Tatsuno, G.; Tintrup, H.; Wijsman, J.; Wright, S.; Mcconlogue, L. BACE Knockout Mice Are Healthy despite Lacking the Primary β -Secretase Activity in Brain : Implications for Alzheimer ' S Disease Therapeutics. **2001**, *10* (12), 1317–1324.

(86) Luo, Y.; Bolon, B.; Kahn, S.; Bennett, B. D.; Babu-Khan, S.; Denis, P.; Fan, W.; Kha, H.; Zhang, J.; Gong, Y.; Martin, L.; Louis, J.-C.; Yan, Q.; Richards, W. G.; Citron, M.; Vassar, R. Mice Deficient in BACE1, the Alzheimer's β-Secretase, Have Normal Phenotype and Abolished β-Amyloid Generation. *Nat. Neurosci.* **2001**, *4* (3), 231–232.

(87) Vassar, R. BACE1 Inhibitor Drugs in Clinical Trials for Alzheimer's Disease. *Alzheimers. Res. Ther.* **2014**, *6* (9), 89.

(88) Yan, R. Targeting the B-Secretase BACE1 for Alzheimer's Disease Therapy. *Lancet Neurol* **2014**, *13* (3), 319–329.

(89) Yan, R. Stepping Closer to Treating Alzheimer's Disease Patients with BACE1 Inhibitor Drugs. *Transl. Neurodegener.* **2016**, *5*, 13.

(90) Mullard, A. Alzheimer Amyloid Hypothesis Lives on. *Nat. Rev. Drug Discov.* **2016**, *16* (1), 3–5.

(91) Tin, G.; Mohamed, T.; Gondora, N.; Beazely, M. A.; Rao, P. P. N. Tricyclic Phenothiazine and Phenoselenazine Derivatives as Potential Multi-Targeting Agents to Treat Alzheimer's Disease. *Med. Chem. Commun.* **2015**, *6* (11), 1930–1941.

(92) Osman, W.; Mohamed, T.; Sit, V. M.; Vasefi, M. S.; Beazely, M. A.; Rao, P. P. N. Structure Activity Relationship Studies of Benzyl-, Phenethyl-, and Pyridyl-Substituted Tetrahydroacridin-9-Amines as Multitargeting Agents to Treat Alzheimer's Disease. *Chem. Biol. Drug Des.* **2016**, *88* (5), 710–723.

(93) Lombardo, J. a; Stern, E. a; McLellan, M. E.; Kajdasz, S. T.; Hickey, G. a; Bacskai, B. J.; Hyman, B. T. Amyloid-Beta Antibody Treatment Leads to Rapid Normalization of Plaque-Induced Neuritic Alterations. *J. Neurosci.* **2003**, *23* (34), 10879–10883.

(94) Oddo, S.; Caccamo, A.; Shepherd, J. D.; Murphy, M. P.; Golde, T. E.; Kayed, R.; Metherate, R.; Mattson, M. P.; Akbari, Y.; LaFerla, F. M. Triple-Transgenic Model of Alzheimer's Disease with Plaques and Tangles: Intracellular Aβ and Synaptic Dysfunction. *Neuron* **2003**, *39* (3), 409–421.

(95) Morgan, D.; Diamond, D. M.; Gottschall, P. E.; Ugen, K. E.; Dickey, C.; Hardy, J.; Duff, K.; Jantzen, P.; DiCarlo, G.; Wilcock, D.; Connor, K.; Hatcher, J.; Hope, C.; Gordon, M.; Arendash, G. W. A Beta Peptide Vaccination Prevents Memory Loss in an Animal Model of Alzheimer's Disease. *Nature* **2000**, *408*, 982–985.

(96) Santacruz, K.; Lewis, J.; Spires, T.; Paulson, J.; Kotilinek, L.; Ingelsson, M.; Guimaraes, A.; DeTure, M.; Ramsden, M.; McGowan, E.; Forster, C.; Yue, M.; Orne, J.; Janus, C.;

Mariash, A.; Kuskowski, M.; Hyman, B.; Hutton, M.; Ashe, K. H. Tau Suppression in a Neurodegenerative Mouse Model Improves Memory Function. *Science* **2005**, *309* (5733), 476–481.

(97) Finder, V. H.; Glockshuber, R. Amyloid-Beta Aggregation. *Neurodegenerative Diseases*. 2007, pp 13–27.

(98) Paul, A.; Nadimpally, K. C.; Mondal, T.; Thalluri, K.; Mandal, B. Inhibition of Alzheimer's Amyloid-β Peptide Aggregation and Its Disruption by a Conformationally Restricted A/β Hybrid Peptide. *Chem. Commun. (Camb).* **2015**, *51* (12), 2245–2248.

(99) Toche, R.; Chavan, S.; Janrao, R. Microwave-Assisted Synthesis of Fused Tricyclic pyrazino[1,2-A]indole Derivatives. *Monatshefte für Chemie - Chem. Mon.* **2014**, *145*, 1507–1512.

(100) Mohamed, T.; Rao, P. P. N. 2,4-Disubstituted Quinazolines as Amyloid-β Aggregation Inhibitors with Dual Cholinesterase Inhibition and Antioxidant Properties: Development and Structure-Activity Relationship (SAR) Studies. *Eur. J. Med. Chem.* **2017**, *126*, 823–843.

(101) Borra, S. K.; Gurumurthy, P.; Mahendra, J. Antioxidant and Free Radical Scavenging Activity of Curcumin Determined by Using Different in Vitro and Ex Vivo Models. *J. Med. Plant Res.* **2013**, *7* (39), 2680–2690.

(102) Bhatt, S.; Nayak, S. K. Copper(II) Bromide: A Simple and Selective Monobromination Reagent for Electron- Rich Aromatic Compounds. *Synth. Commun.* **2007**, *37* (8), 1381–1388.

(103) Ellman, G. L.; Courtney, K. D.; Andres, V.; Featherstone, R. M. A New and Rapid Colorimetric Determination of Acetylcholinesterase Activity. *Biochem. Pharmacol.* **1961**, *7* (2), 88–95.

(104) Komersová, A.; Komers, K.; Čegan, A. New Findings about Ellman's Method to Determine Cholinesterase Activity. *Zeitschrift fur Naturforsch. - Sect. C J. Biosci.* **2007**, *62* (1–2), 150–154.

(105) Yang, W.; Wong, Y.; Ng, O. T. W.; Bai, L. P.; Kwong, D. W. J.; Ke, Y.; Jiang, Z. H.; Li, H. W.; Yung, K. K. L.; Wong, M. S. Inhibition of Beta-Amyloid Peptide Aggregation by Multifunctional Carbazole-Based Fluorophores. *Angew. Chemie - Int. Ed.* **2012**, *51* (8), 1804–1810.

(106) Zhao, D.; Chen, Y.; Liu, Q.; Zhao, Y.; Li, Y. Exploring the Binding Mechanism of Thioflavin-T to the Beta-Amyloid Peptide by Blind Docking Method. *Sci. China Chem.* **2012**, *55* (1), 112–117.

(107) Shimamura, T.; Sumikura, Y.; Yamazaki, T.; Tada, A.; Kashiwagi, T.; Ishikawa, H.; Matsui, T.; Sugimoto, N.; Akiyama, H.; Ukeda, H. Applicability of the DPPH Assay for Evaluating the Antioxidant Capacity of Food Additives - Inter-Laboratory Evaluation Study -. *Anal. Sci.* **2014**, *30* (7), 717–721.

(108) Garcia, E. J.; Cadorin Oldoni, T. L.; de Alencar, S. M.; Reis, A.; Loguercio, A. D.; Miranda Grande, R. H. Antioxidant Activity by DPPH Assay of Potential Solutions to Be Applied on Bleached Teeth. *Braz. Dent. J.* **2012**, *23* (1), 22–27.

(109) Nimse, S. B.; Pal, D. Free Radicals, Natural Antioxidants, and Their Reaction Mechanisms. *RSC Adv.* **2015**, *5*, 27986–28006.

(110) Goldsbury, C.; Baxa, U.; Simon, M. N.; Steven, A. C.; Engel, A.; Wall, J. S.; Aebi, U.; Müller, S. A. Amyloid Structure and Assembly: Insights from Scanning Transmission Electron Microscopy. *J. Struct. Biol.* **2011**, *173* (1), 1–13.

(111) Mohamed, T.; Hoang, T.; Jelokhani-Niaraki, M.; Rao, P. P. N. Tau-Derived-Hexapeptide 306VQIVYK311 Aggregation Inhibitors: Nitrocatechol Moiety as a Pharmacophore in Drug Design. *ACS Chem. Neurosci.* **2013**, *4*, 1559–1570.

(112) Wang, R.; Yan, H.; Tang, X. Progress in Studies of Huperzine A , a Natural Cholinesterase Inhibitor from Chinese Herbal Medicine 1. **2006**, *27* (1), 1–26.

(113) Hoyer, W.; Gronwall, C.; Jonsson, A.; Stahl, S.; Hard, T. Stabilization of a β-Hairpin in Monomeric Alzheimer's Amyloid-β Peptide Inhibits Amyloid Formation. *Proc Natl Acad Sci U S A* **2008**, *105* (13), 5099–5104.

Appendix

Sample ^{1}H NMR spectra of compounds

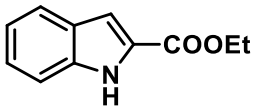

Compound **2a**- ^{1}H NMR (in $CDCl_3$)

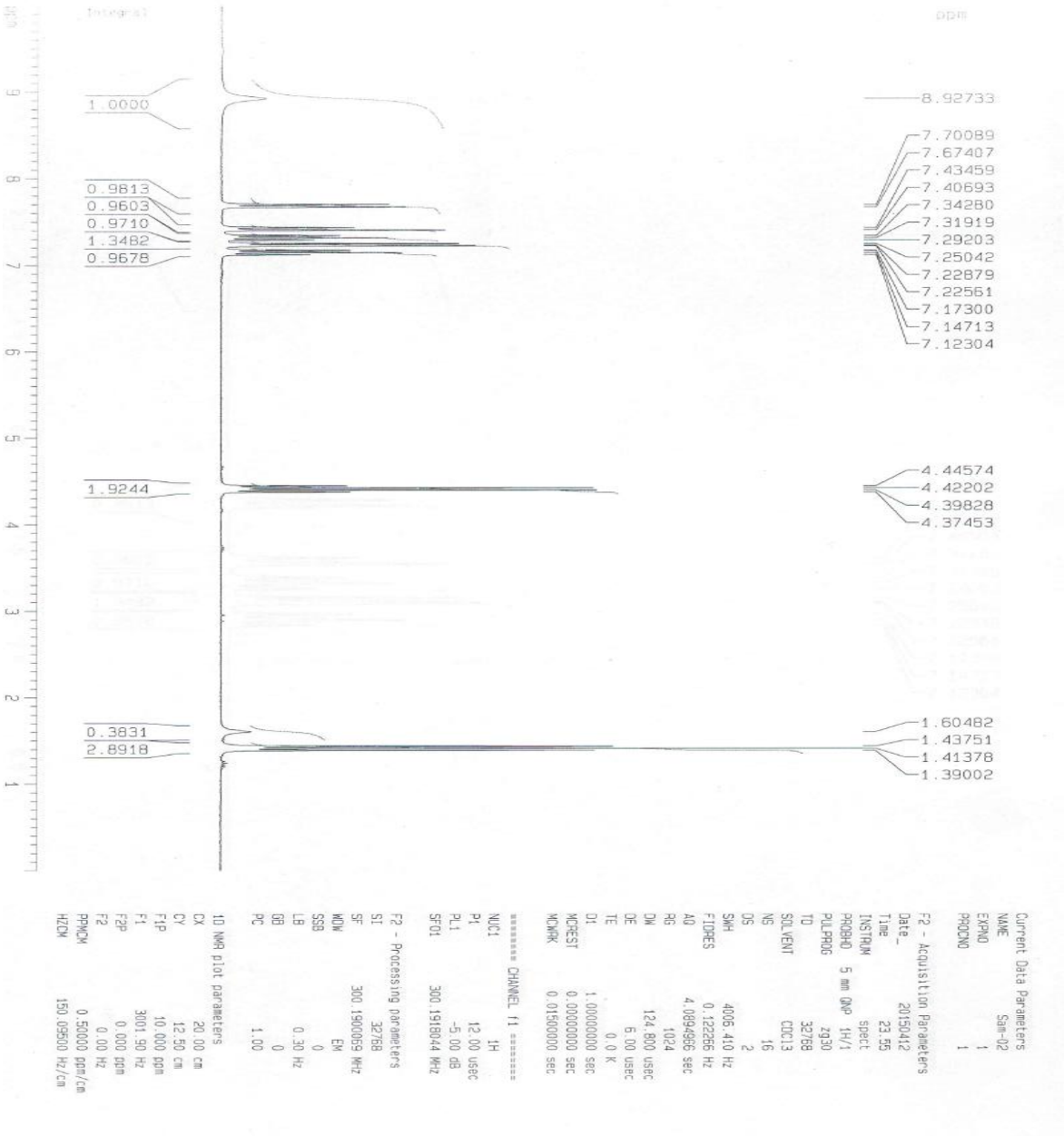

Compound **4a** ^{1}H NMR (in $CDCl_3$)

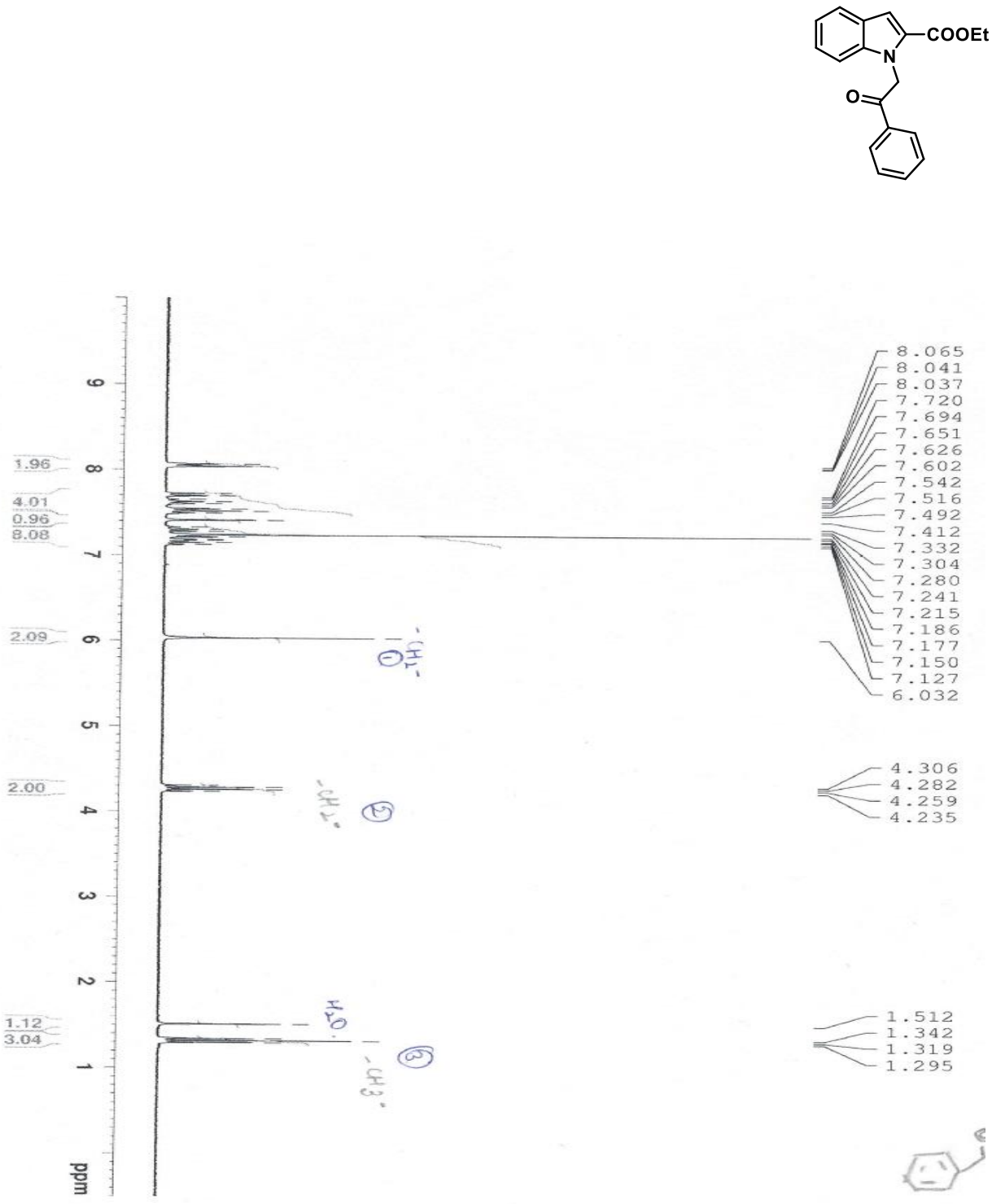

Compound **4c**- ^{1}H NMR (in $CDCl_3$)

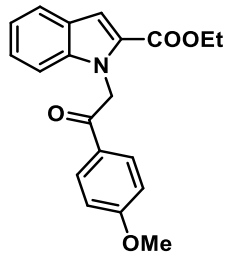

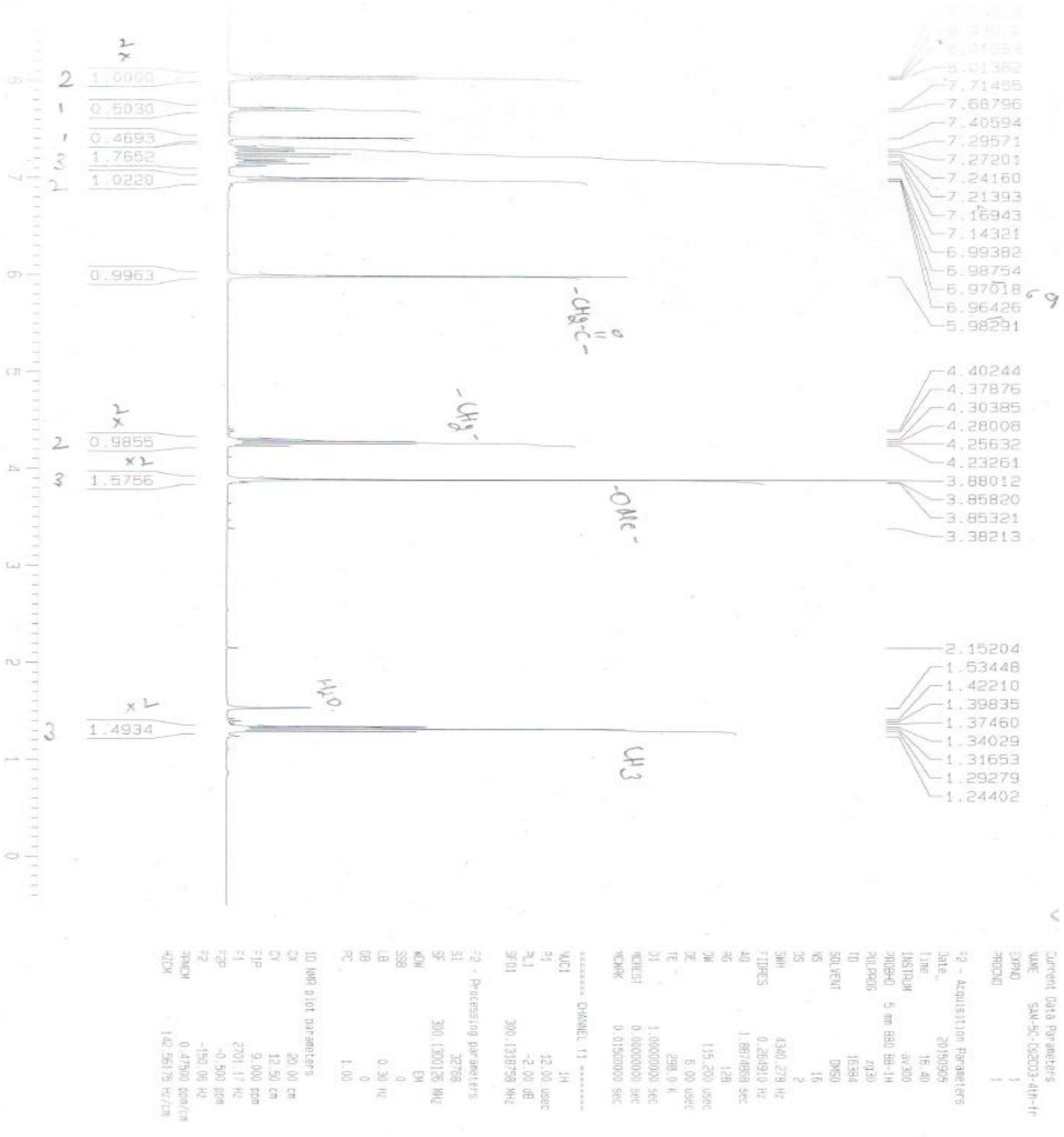

Compound **5a**- ^{1}H NMR (in $CDCl_3$)

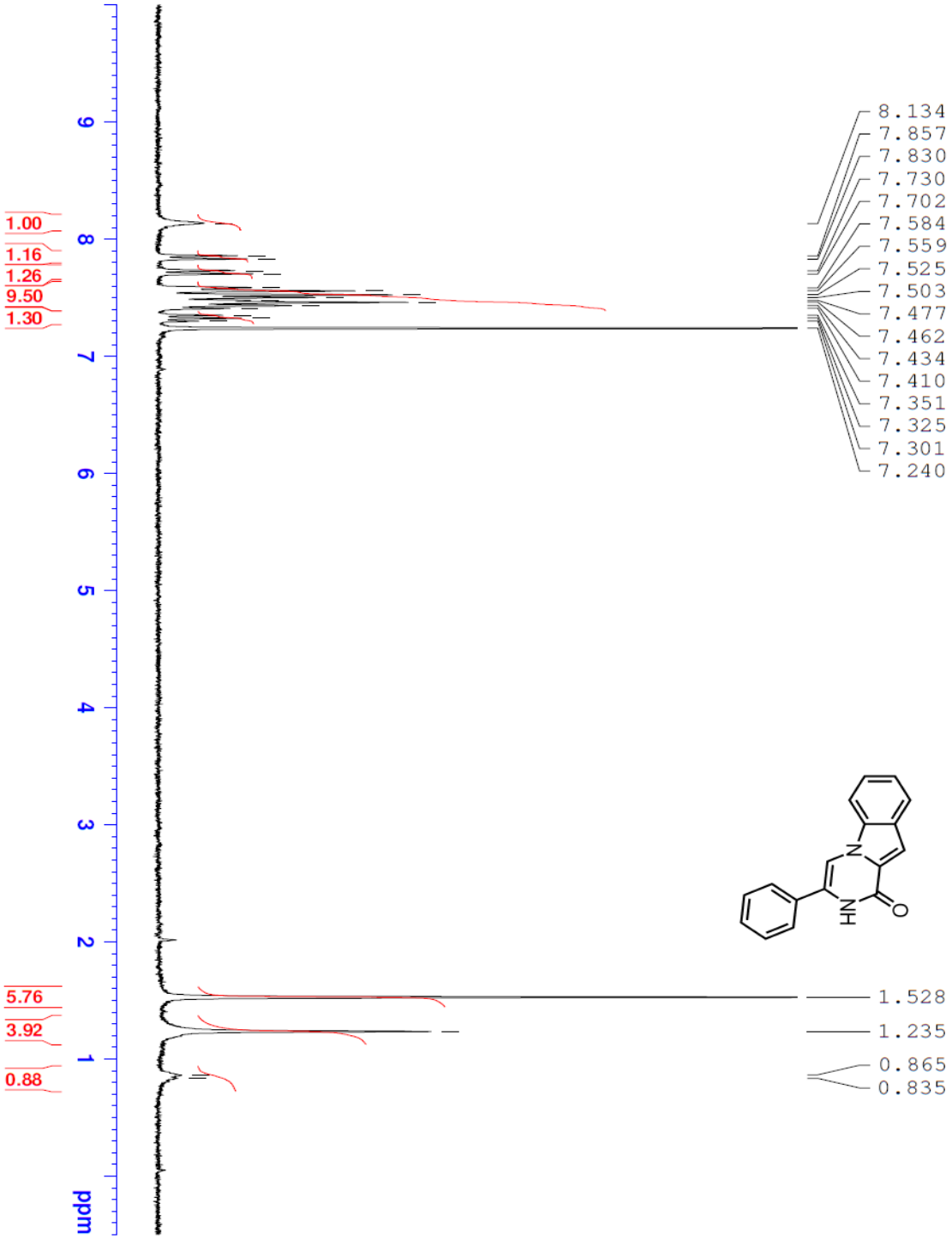

Compound **5d**- ^{1}H NMR (in $CDCl_3$)

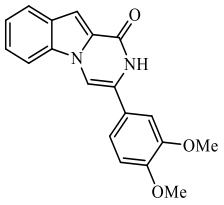

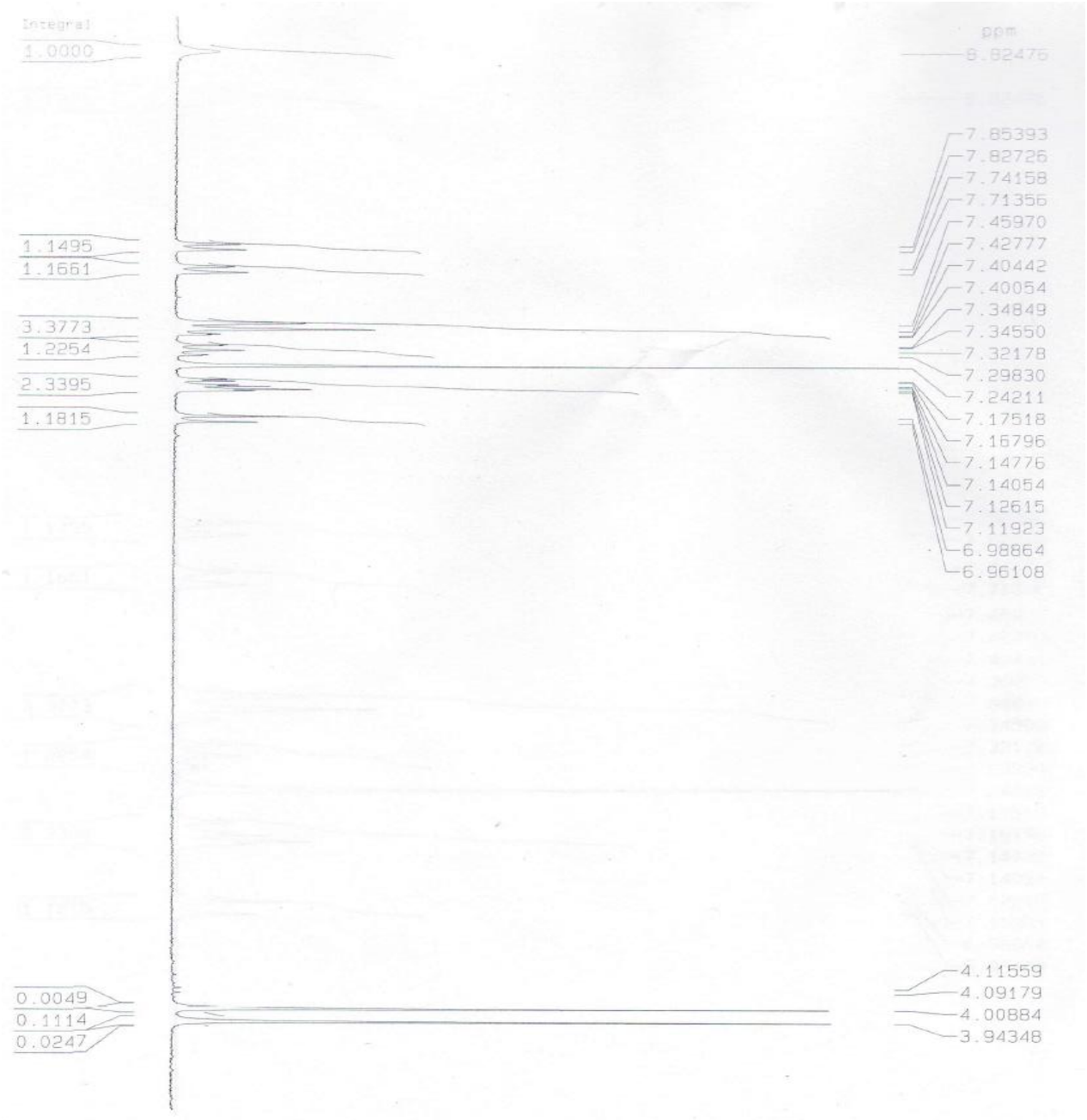

Compound **5e**- ^{1}H NMR (in $CDCl_3$)

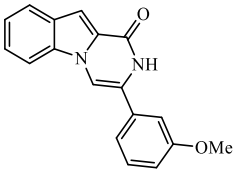

Compound **5f**- ^{1}H NMR (in $CDCl_3$)

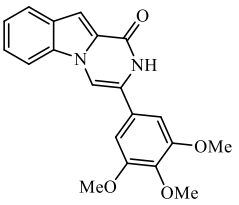

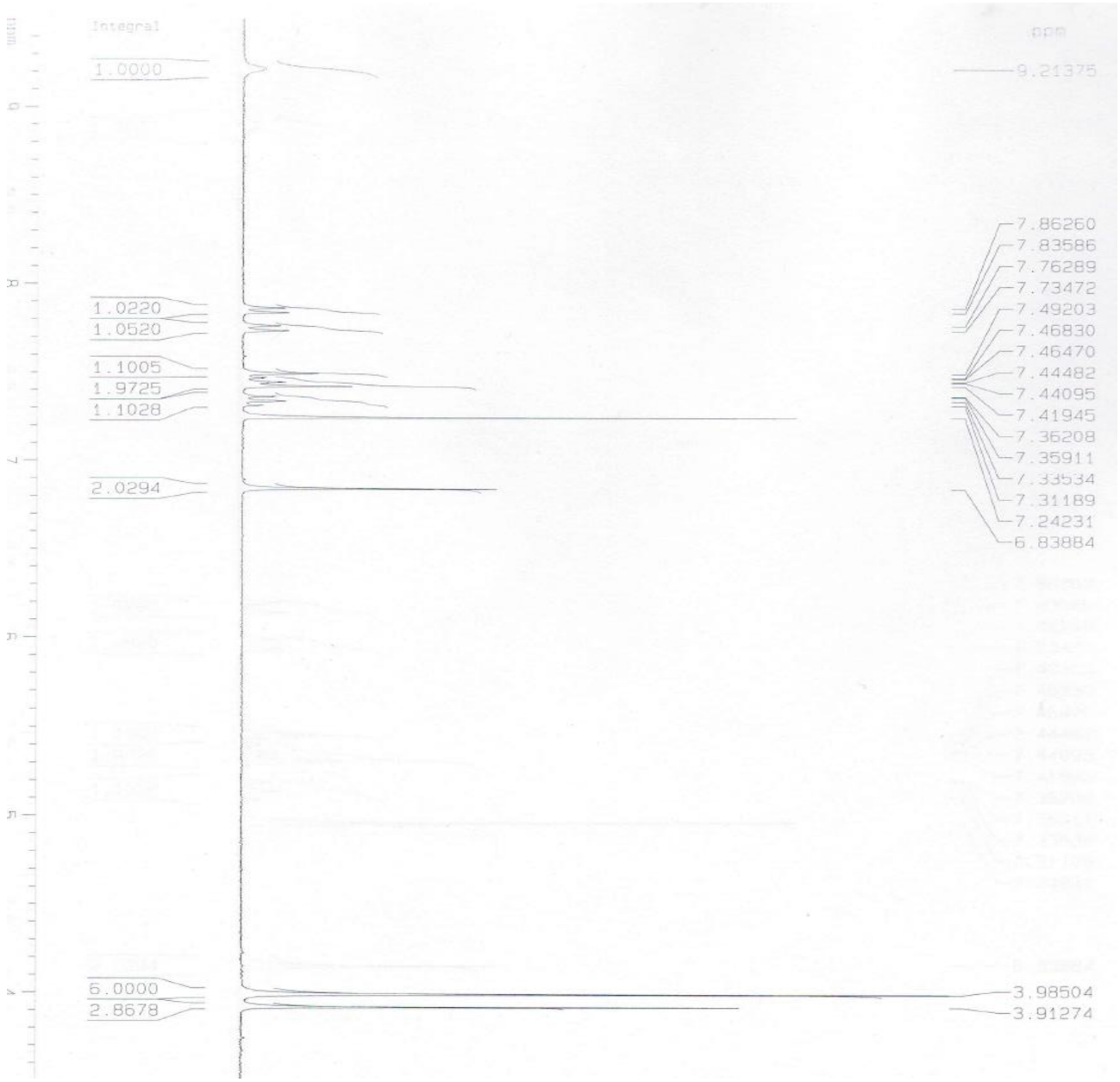

Compound **5h**- ^{1}H NMR (in DMSO-d_6)

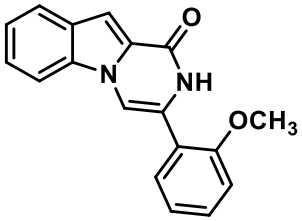

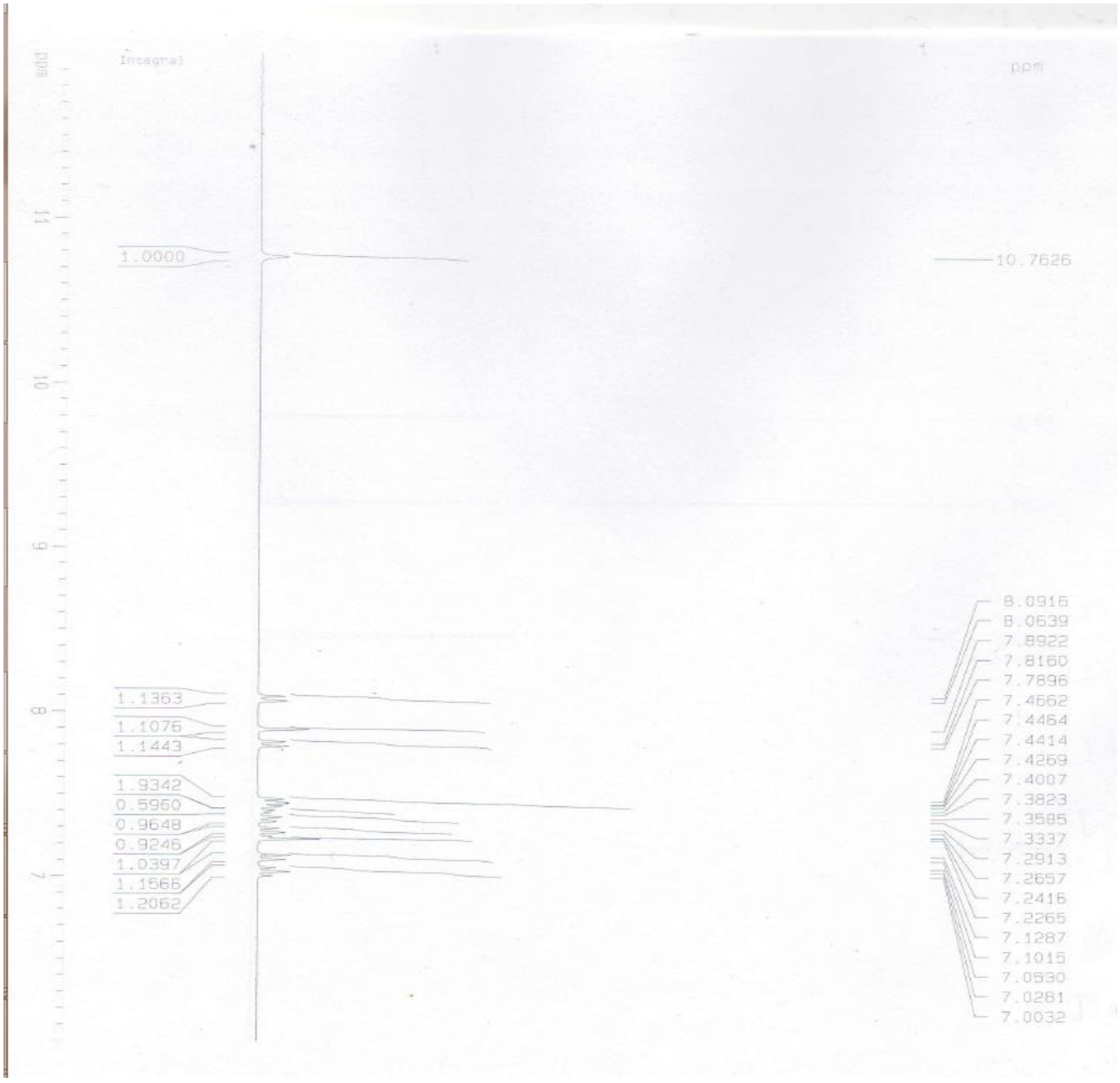

Compound **5i**- ^{1}H NMR (in $CDCl_3$)

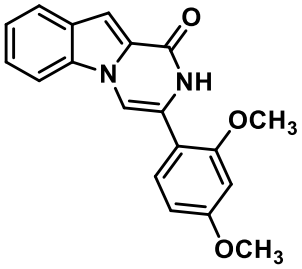

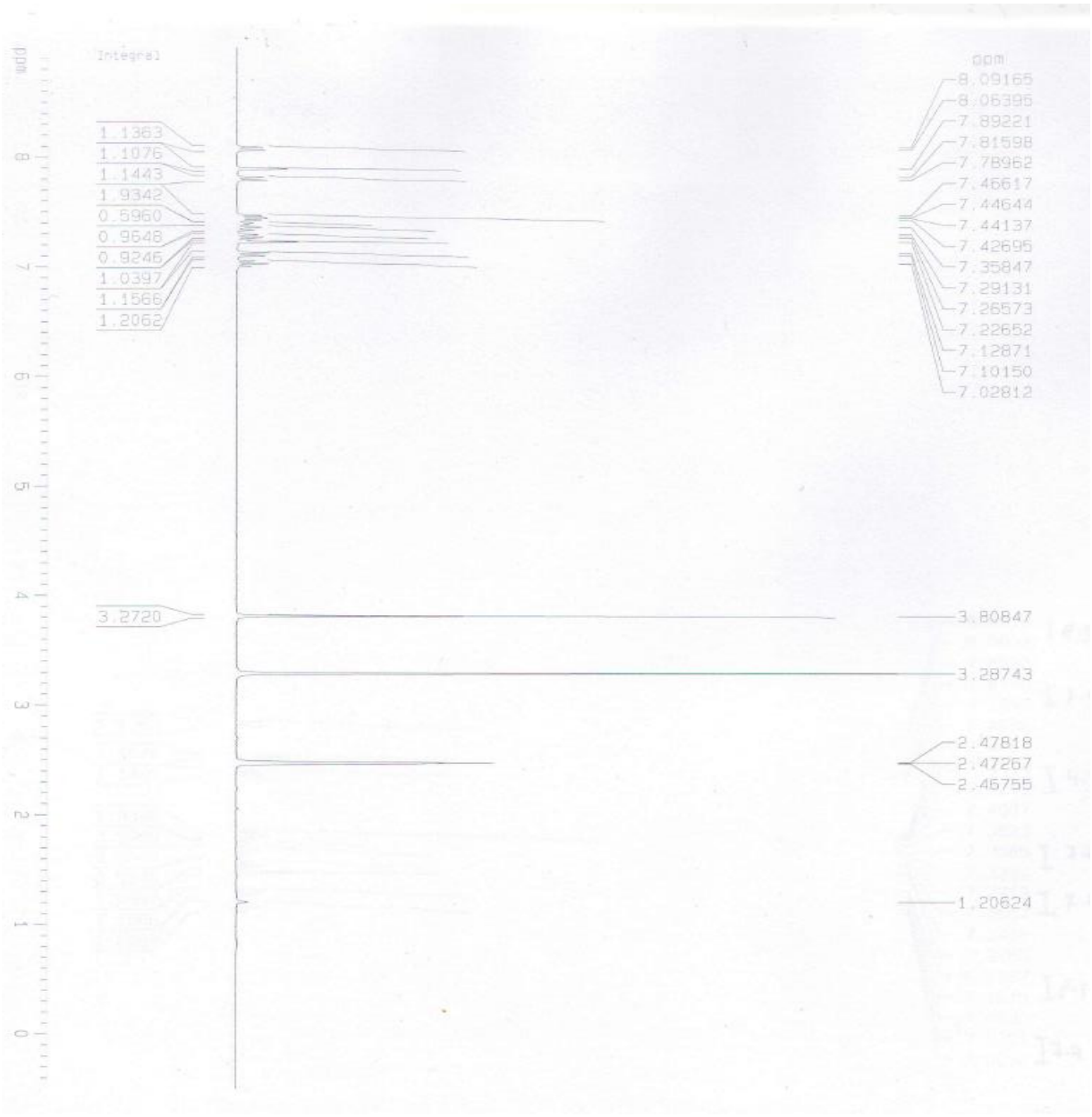

LC-MS data

5a

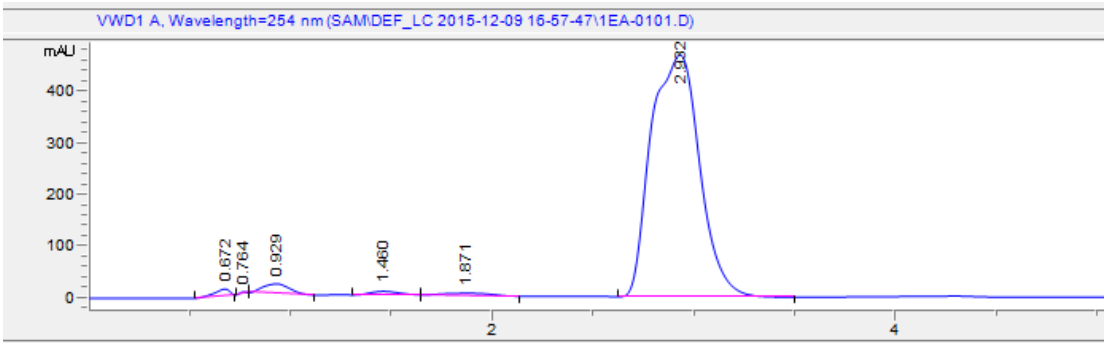

Signal 2: VWD1 A, Wavelength=254 nm

Peak #	RetTime [min]	Type	Width [min]	Area [mAU*s]	Height [mAU]	Area %
1	0.672	BB	0.0786	70.54003	13.36085	0.8575
2	0.764	BB	0.0349	7.21040	3.37960	0.0877
3	0.929	BB	0.1570	176.68272	19.08584	2.1478
4	1.460	BB	0.1528	66.30499	6.91906	0.8060
5	1.871	BB	0.2475	68.25594	4.22521	0.8297
6	2.932	BB	0.2332	7837.21436	468.51965	95.2713
Totals :				8226.20844	515.49022	

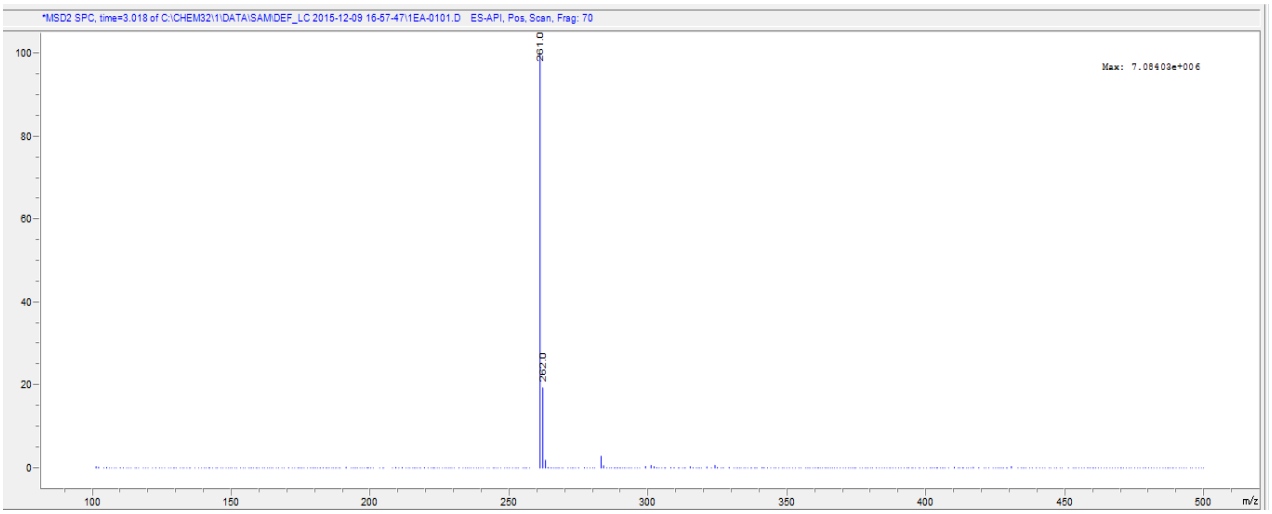

5d

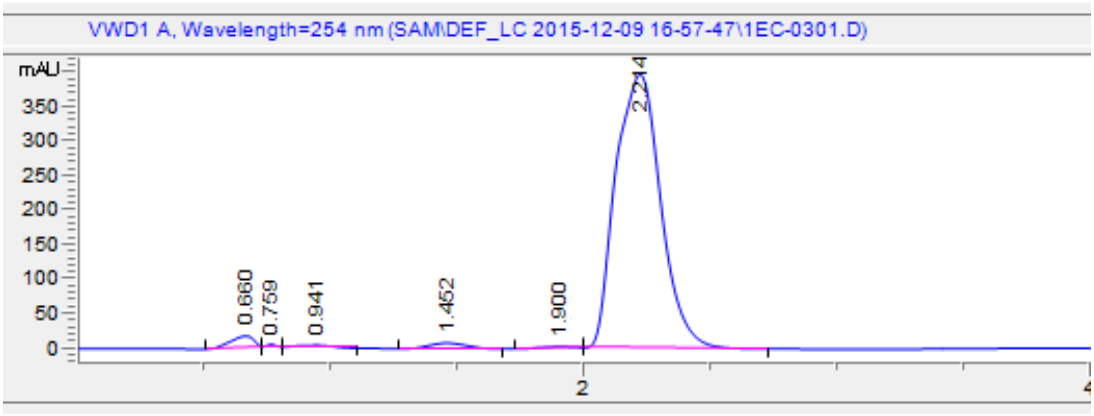

Signal 2: VWD1 A, Wavelength=254 nm

Peak #	RetTime [min]	Type	Width [min]	Area [mAU*s]	Height [mAU]	Area %
1	0.660	BB	0.1032	105.98787	16.66867	2.0485
2	0.759	BB	0.0360	7.50941	3.37493	0.1451
3	0.941	BB	0.1403	30.68026	3.21552	0.5930
4	1.452	BB	0.1674	86.44474	8.37571	1.6707
5	1.900	BB	0.1465	16.05177	1.92087	0.3102
6	2.214	BB	0.1768	4927.37109	399.77563	95.2325
Totals :				5174.04514	433.33134	

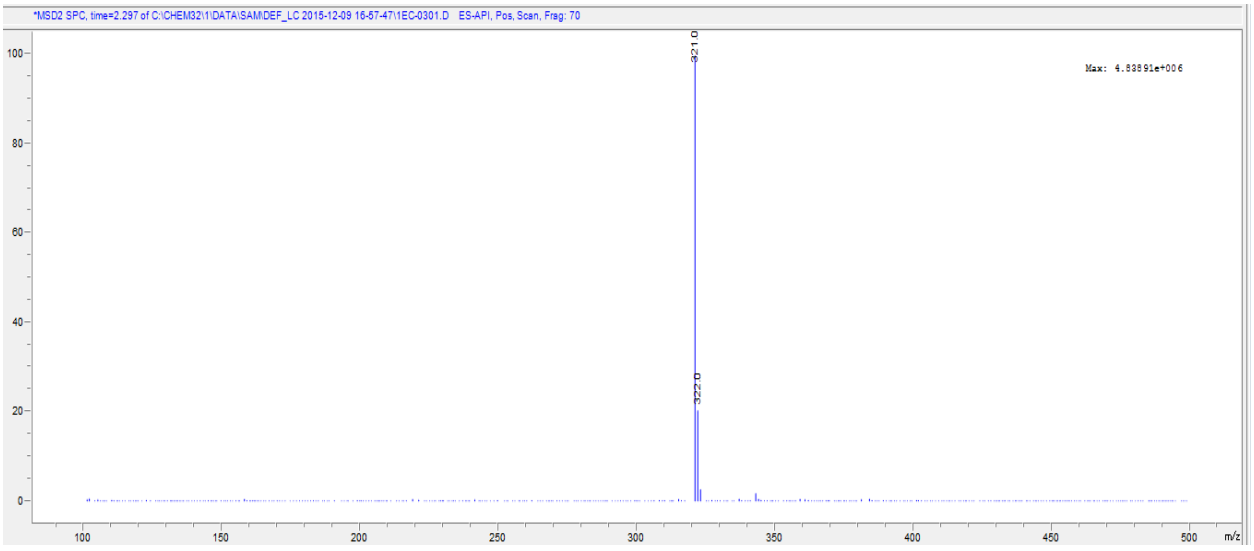

5h

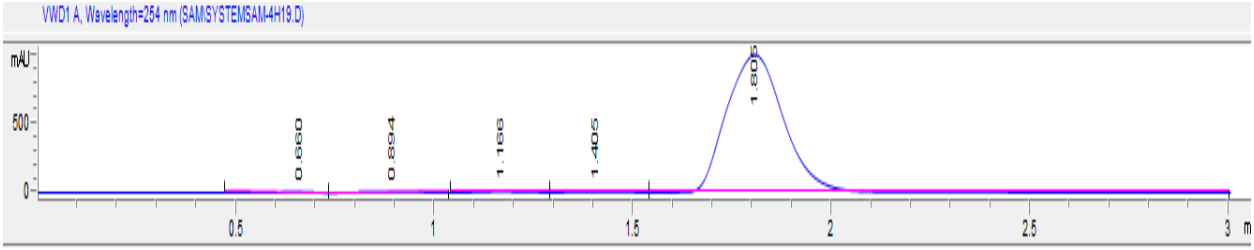

Signal 3: VWD1 A, Wavelength=254 nm

Peak #	RetTime [min]	Type	Width [min]	Area [mAU*s]	Height [mAU]	Area %
1	0.660	BB	0.0986	52.31675	8.29557	0.5096
2	0.894	BB	0.1766	66.46624	6.32754	0.6474
3	1.166	BB	0.1140	45.15237	6.42779	0.4398
4	1.405	BB	0.1169	19.18100	2.69893	0.1868
5	1.805	BBA	0.1627	1.00835e4	1007.99188	98.2164
Totals :				1.02667e4	1031.74172	

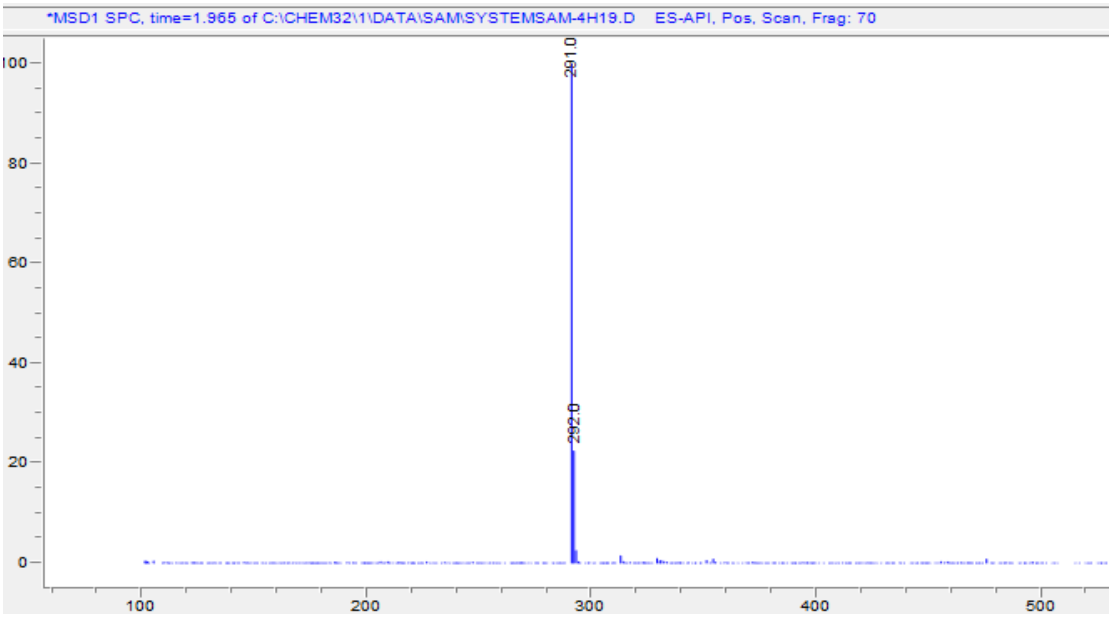

5k

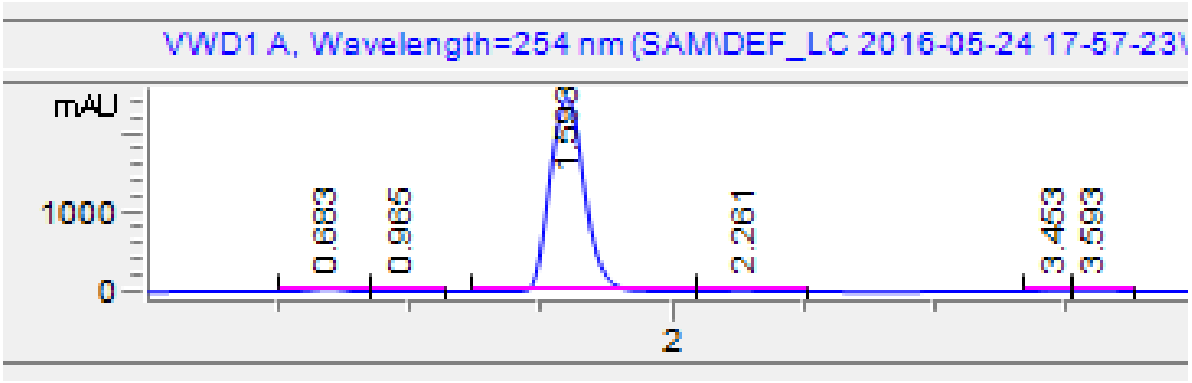

Signal 3: VWD1 A, Wavelength=254 nm

Peak #	RetTime [min]	Type	Width [min]	Area [mAU*s]	Height [mAU]	Area %
1	0.683	BB	0.1315	296.43677	35.47549	1.3031
2	0.965	BB	0.1215	25.01483	2.84780	0.1100
3	1.593	BB	0.1446	2.22379e4	2456.78247	97.7544
4	2.261	BB	0.1894	83.48943	7.35861	0.3670
5	3.453	BB	0.1020	53.40955	8.53033	0.2348
6	3.593	BB	0.1049	52.48896	7.85678	0.2307
Totals :				2.27487e4	2518.85148